REPUBLIC OF TURKEY

ADANA ALPARSLAN TÜRKEŞ SCIENCE AND TECHNOLOGY UNIVERSITY

GRADUATE SCHOOL OF NATURAL AND APPLIED SCIENCES

DEPARTMENT OF MECHANICAL ENGINEERING

INVESTIGATION ON THE FLOW STRUCTURE IN THE AORTIC VESSEL FOR PATIENTS HAVING AN AORTIC ANEURYSM AND HAVING COVID-19

ONUR MİRAN ÖZTEKİN

MASTER OF SCIENCE

ADANA 2022

REPUBLIC OF TURKEY
ADANA ALPARSLAN TÜRKEŞ SCIENCE AND TECHNOLOGY UNIVERSITY

GRADUATE SCHOOL OF NATURAL AND APPLIED SCIENCES
DEPARTMENT OF MECHANICAL ENGINEERING

INVESTIGATION ON THE FLOW STRUCTURE IN THE AORTIC VESSEL FOR PATIENTS HAVING AN AORTIC ANEURYSM AND HAVING COVID-19

ONUR MİRAN ÖZTEKİN
MASTER OF SCIENCE

SUPERVISOR
ASSOC. PROF. DR. NAİME FİLİZ ÖZDİL

ADANA 2022

ABSTRACT

Investigation On The Flow Structure In The Aortic Vessel For Patients Having An Aortic Aneurysm And Having Covid-19

Onur Miran ÖZTEKİN

Department of Mechanical Engineering

Supervisor: Assoc. Prof. Dr. Naime Filiz ÖZDİL

January 2022, 77 pages

When medical imaging software and engineering programs are used in cooperation with each other, they will play an essential role in patients' treatments. This thesis is an investigation on the flow structure of the aorta, the main artery originating from the heart, in patients who have undergone thoracic aortic surgery with a diagnosis of thoracic aortic aneurysm and patients diagnosed with covid-19 as a fundamental effort to assess the adequacy of numerical simulation for this area of research. The deformation on aorta walls and velocity profiles at different times in the vessels have been modeled using the ANSYS-Fluent which is a computational fluid dynamic program (CFD). The highest velocity value has been acquired as 0.86 m/s where the vessel is repaired for the patient that undergone the surgery whereas it has been 1.135 m/s at the entrance and exit part of the covid-affected patient's aorta. The maximum pressure has been found at 13380 Pa in the repaired aorta while 14430 Pa in the aorta affected by the covid-19. On the other hand, wall shear stress results are found to be around 20 Pa for the patient affected by covid-19 but a maximum of 6.02 Pa for the patient having repaired vessel. In addition, it is observed that the change in cell volume is not at a level that would cause a problem for the two vessels examined, it occurred between 1.3% and 3%. When the analysis results of these 2 vessels were investigated in general, it was seen that most of the hemodynamic values were higher in the covid-19 infected patient.

Keywords: Aorta, Medical Imaging, Ansys-Fluent, Non-Newtonian Flow

ÖZET

Aort Anevrizması ve Covid 19 Olan Hastaların Aort Damarlarındaki Akış Yapılarının İncelenmesi

Onur Miran ÖZTEKİN

Makina Mühendisliği Anabilim Dalı

Danışman: Doç. Dr. Naime Filiz ÖZDİL

Ocak 2022, 77 sayfa

Tıbbi görüntüleme yazılımları ve mühendislik programları beraber kullanıldığında hastaların tedavilerinde önemli bir rol oynayacaktır. Bu tezde sayısal simülasyonun yeterliliğini değerlendirmek için temel bir çaba olarak torasik aort anevrizması tanısı ile göğüs aort cerrahisi geçiren hastalarda ve covid-19 tanısı konan hastalarda kalpten çıkan ana arter olan aortun akış yapısı incelenmiştir. ANSYS-Fluent programı kullanılarak damarlarda farklı zamanlarda aort duvarları ve hız profilleri modellenmiştir. En yüksek hız değeri ameliyat olan hastada damarın tamir edildiği bölgede 0.86 m/s olarak elde edilirken, covidli hastanın aortunun giriş ve çıkış kısmında 1.135 m/s olarak elde edilmiştir. Onarılan aortta maksimum basınç 13380 Pa ve Covid 19'dan etkilenen aortta 14430 Pa olarak bulunmuştur. Öte yandan, Covid 19'dan etkilenen hasta için duvar kesme stresi sonuçları 20 Pa civarında bulunurken damarı tamir edilen hasta için maksimum stres 6,02 Pa civarında elde edilmiştir. Ayrıca hücre hacmindeki değişimin incelenen iki damar için sorun yaratacak düzeyde olmadığı, %1,3 ile %3 arasında gerçekleştiği gözlemlenmiştir. Bu 2 damarın genel olarak analiz sonuçları incelendiğinde hemodinamik değerlerin çoğunun covid-19 bulaşmış hastada daha yüksek olduğu görüldü.

Anahtar Kelimeler: Aort, Medikal Görüntüleme, Ansys-Fluent, Newtonyen Olmayan Akış

TABLE OF CONTENTS

LIST OF FIGURES

LIST OF TABLES

ABBREVIATIONS

AD	: Aorta Dissection
ATAA	: Ascending Thoracic Aortic Aneurysm
CFD	: Computational Fluid Dynamics
CoA	: Aorta Coarctation
CTA	: Computed Tomographic Angiography
DM	: Modeler Module
FE	: Finite Element
FFR	: Fractional Flow Reserve
FSI	: Fluid-Solid Interaction
G&R	: Growth and Remodeling
LV	: Left Ventricle
LVAD	: Left Ventricular Assist Device
PSD	: Post Stenotic Dilatation
RBF	: Radial Basis Functions
RRT	: Related Residency Time
STL	: Unstructured Triangulated Format
TKE	: Turbulence Kinetic Energy
UDF	: User Defined Function
VFI	: Vector Flow Imaging
VOF	: Fluid Volume
WSS	: Wall Shear Stress
CT	: Computed Tomography
MRI	: Magnetic Resonance Imaging
Echo	: Echocardiogram
TEE	: Transesophageal Echocardiogram

NOMENCLATURE

μ_∞	: Maximum value of viscosity
μ_0	: Minimum value of viscosity
a	: Independent variable
γ	: Shear rate
$\overline{V}$	: Mean velocity
D	: Diameter of the vessel
ρ	: Density of blood
η	: Blood viscosity / Dynamic viscosity
$\vec{\tau}$	: Wall shear stress
$\dot{\varepsilon}$	: Deformation rate
$\vec{n}$	: Orthogonal vessel wall vector
$\dot{m}$	: Entry mass stream
t	: Time

1. INTRODUCTION

1.1. Specification of Need

Most diseases expose themselves through changes in the speed of the blood, the pressure applied by the blood, and and the shear stress of the walls which is called WSS. For this reason, understanding the effects of these variables based on the results obtained from the correct calculation and examination of their changes is a very important issue. There are some studies regarding this issue which has been shown in the literature review section. However, no study has been conducted utilizing scientific discipline (CFD) for the investigation of the outcomes of the Covid-19 virus (which has emerged in recent years and caused deaths of people in the later stages of the disease) on the aorta, which is the main artery originating from the heart, and the effect of thoracic aortic surgery on aorta hemodynamics caused by certain diseases. For this reason, the need to accelerate clinical studies for new diseases such as Covid, to make the treatment processes of patients more effectively, and to minimize the risk of death by examining the effects of diseases on the flow structure in the aorta has emerged.

1.2. Objectives

The aim of this thesis can be listed in four categories:

- To support the treatment of patients by examining the changes occurred by the Covid-19 virus, which has emerged in recent years in our age, in parameters such as wall shear stress, blood flow velocity, pressure difference, and cell volume change in the aorta, which is one of the most important vessels of humans.

- To better investigate the hemodynamic changes in the vessel after surgery in patients with aortic aneurysms.

- Maximizing computational fluid dynamics results' accuracy by creating as real boundary conditions as possible.

- To embody the results of the disease effects by comparing the vascular conditions after the analysis results.

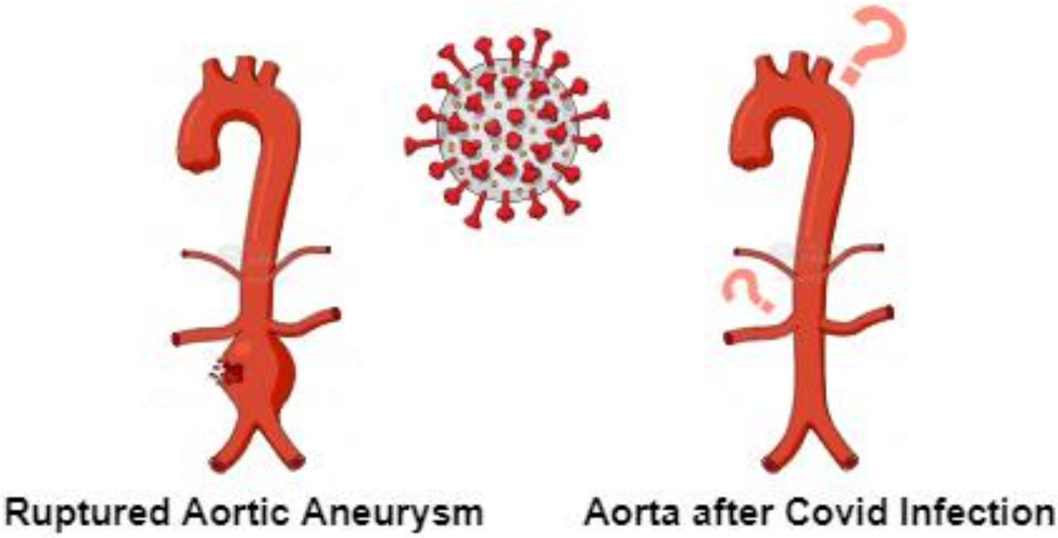

Figure 1. Schematic representation of aortic aneurysm and the effect of covid on the aorta

2. BACKGROUND

An aneurysm occurrence is a dangerous situation caused by the weakening of artery walls forming an unusual big bulge. Rupture and internal bleeding might start as a result of this bulge, leading to the death of many people. Aneurysms can happen in any part of the body but are mostly seen in people's aorta, legs, or brains. Despite the fact that the reasons to form an aneurysm are still unclear, some diseases that harm the artery walls and result in weak vessel walls in time, high blood pressure which is called hypertension, and fatty plaque formation in vessels named atherosclerosis can be count as the main causes. When there happens to be an aneurysm in the aorta, a bloated, debilitated zone appears on the walls of the vein. This area escalates in time creating a risk of dissection or rupture. On the grounds of this, bleeding that is dangerous enough to result in death can occur. A thoracic aortic aneurysm example is demonstrated in Figure 2. It can be diagnosed through the computed tomography scan method (CT), magnetic resonance technique (MRI), image created by an echocardiograph (echo), transesophageal echocardiogram (TEE), using electromagnetic waves for the chest, or arteriogram (angiogram).

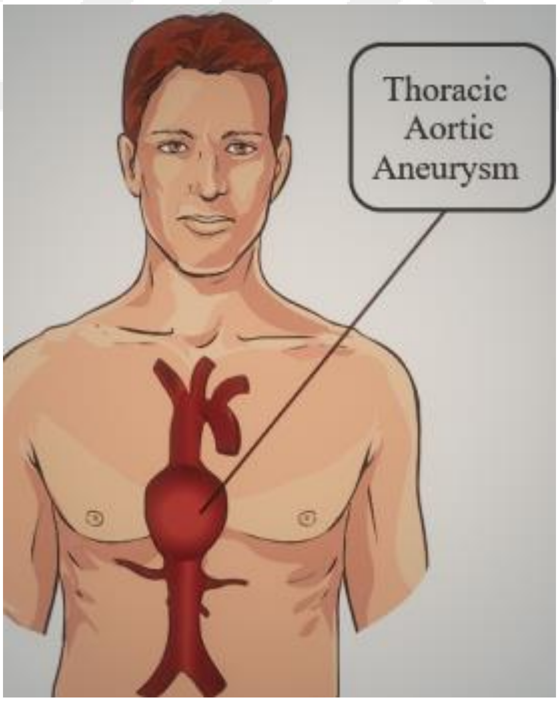

Figure 2. Thoracic Aortic Aneurysm [7]

In addition to these, the Covid virus has also been found to be one the most dangerous viruses causing life-threatening diseases. The virus has mostly been known to have an effect on the respiratory system but also affects the aorta negatively causing aortic bursts. The virus has popped out at the Wuhan region of China then propagated worldwide creating a pandemic still going on. The appearance of the virus is shown in Figure 3. Fever, coughing a lot, and having breath shortness might be count as the beginning symptoms of covid.

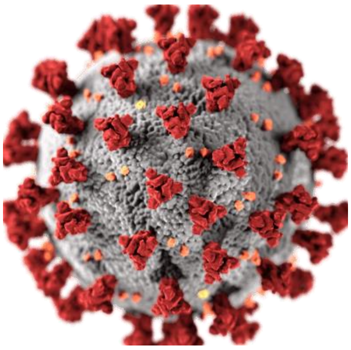

Figure 3. The detailed appearance of the virus [63]

2.1. The Aorta

The biggest artery of the body is the Aorta, which starts from the top of the strong supplying compartment vessel called the left ventricle. Its wideness is around an inch at the beginning and goes up in time. The aorta takes the oxygen-rich blood coming out of the left ventricle and pumps it into the organs via the valve of the aorta. It consists of 4 main zones, namely, the ascending aorta, the descending thoracic aorta which is over the diaphragm, the abdominal aorta that is located beneath the diaphragm, and the aortic arch. Huge and flexible artery terms can also be used for the aorta. Its anatomy is indicated in Figure 4.

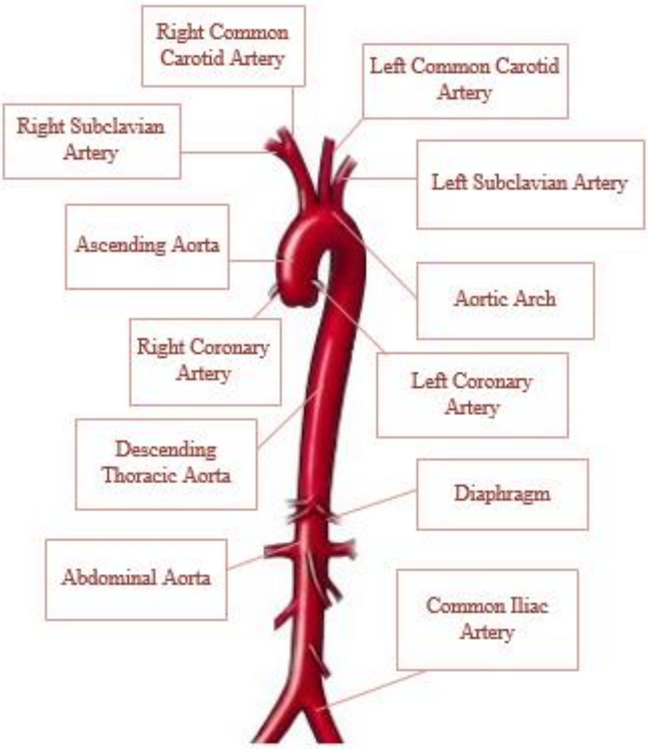

Figure 4. The anatomy of the aorta [29]

2.1.1. Aortic Arch

It is the area starting from the ascending aorta and ending in descending aorta (Figure 6). It is also the portion of the aorta which is responsible for sending blood to the head and other parts of the body through the vessels arising on it. The aortic arch has nerve endings in the walls that are responsive to the changes that occur in blood pressure.

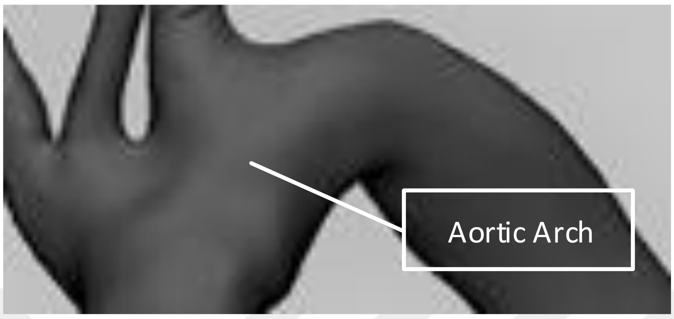

Figure 5. A closer look at the aortic arch zone

2.1.2. Ascending Aorta

It is the beginning segment of the aorta arising from the left ventricle connecting with the aortic arch (Figure 7). The aortic valve is originated at the ascending aorta. This valve permits blood to discharge in one trajectory; on the outside of the chamber of the left ventricle and in the direction of the aorta. It yields a path that has less exertion for blood to follow when it is taken from the left ventricle.

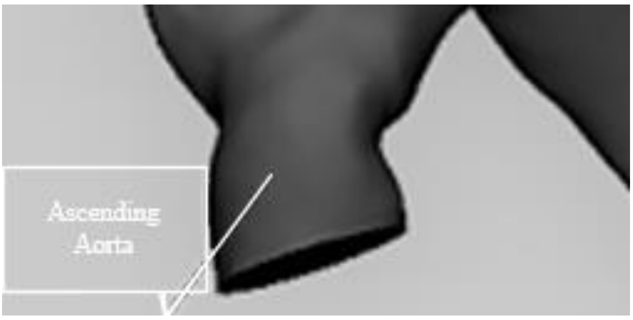

Figure 6. The ascending aorta

2.1.3. Descending Aorta

It is within the confines of the aortic arch and the diaphragm tissue, which is located under the ribs (Figure 8). The descending aorta is the portion of the aorta that gets through the lower part of the arch of the aorta towards the chest. It is identified as the descending thoracic aorta, as well. Descending the aorta consists of a lot of small arteries that provide blood throughout the body.

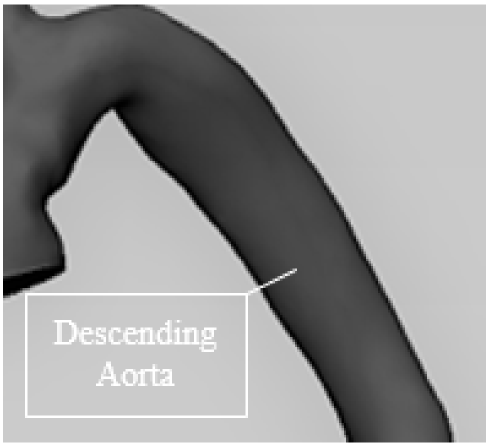

Figure 7. Descending thoracic aorta

2.1.4. Abdominal Aorta

The final portion of the aorta is called the abdominal aorta (Figure 9). It begins at the area of the diaphragm and finishes at the starting zone of the iliac arteries, which is connected to the legs. It provides blood to many parts of the body. The stomach, intestines, and pancreas can be given as an instance to the body organs that obtained blood from the abdominal aorta.

Figure 8. Abdominal aorta

2.2. Aorta Histology

Aorta walls are made up of tunica media, intima, and adventitia layers (Figure 10). An individual layer of endothelial cells creates the inner layer of the aorta called the intima. The biggest elements in the aorta walls can be found in the tunica media area since muscle cells and the matrix outside the hive are formed there. These muscle cells improve the stiffness of the vessel walls when the activation of them is completed and adjust the pressure of the blood and flow. The matrix is responsible for controlling the aorta's biomechanical characteristics. Lamellae are created by the matrix including flexible filaments, proteins, proteoglycan, and glycosaminoglycan. Besides, the adventitia is the exterior conjunctive tissue covering the aortic walls. Little blood vessels and lengthwise arrayed collagen fibers produce the adventitia. More elastic fibers are seen in the thoracic aorta than the abdominal one. Thus, the thoracic aorta is more dilatable. The expandability of the aorta decreases when the person gets older or has a wider diameter of the aorta.

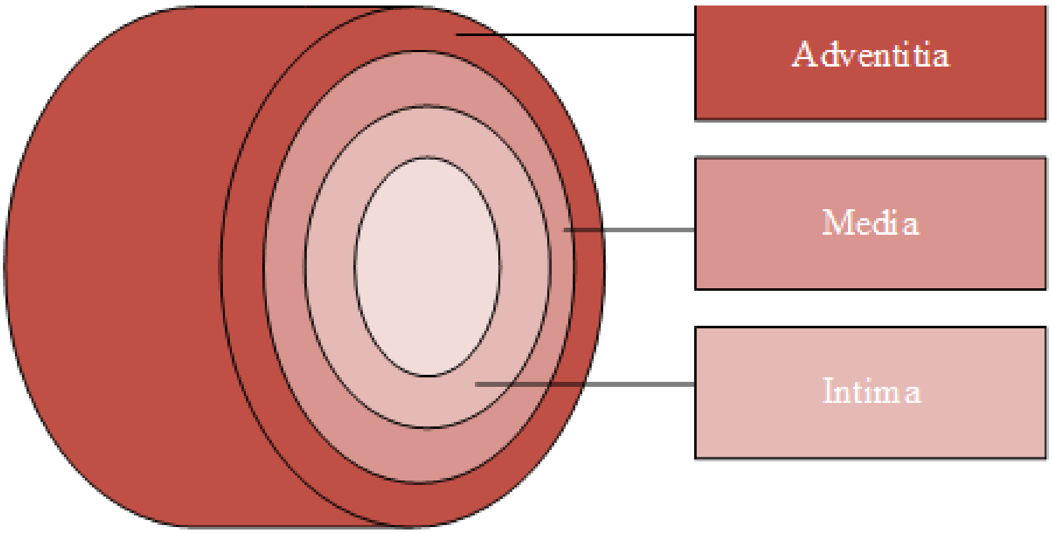

Figure 9. The layers of the aorta

2.3. Aorta Aging

The procedure of growing older is complex for organs as it affects their natural functions in some ways and may even give rise to gradual differences in organ malfunction. Disruption risk in the normal functioning of organs, and particularly coronary illnesses might arise when age increases. When the studies in the literature are examined, it is seen that the diameter of the aorta rises with age regardless the person is a female or male. The growth rate of the aorta occurs up to 0,2 mm per year.

2.4. Aortic Aneurysms

Expansion of the aorta walls is called an aortic aneurysm. The aorta usually gets around 1,5 times bigger than its normal size (Medicana, n.d.). The aortic aneurysms are mostly encountered at the abdominal or thoracic part of the aorta. Therefore, dissection formation or ruptures primarily happen in these areas. Statistical consequences have shown that thoracic aortic aneurysms are largely formed in men between the age of 60 to 70 rather than women. The aneurysms around 5,5 centimeters are accepted as large. Although aortic aneurysms are very rare at young ages, they can also be seen in young people if there is a family history of similar diseases. The reasons for aortic aneurysms can be listed as below:

1) Degradation caused by a high rate of the pressure of the blood: This factor can't be mentioned as the only effective factor for the formation of an aneurysm. A lot of people

experiencing high blood pressure do not have an aneurysm. But, the results of scientific data collected by the government indicate that this factor has a great effect on the formation of aneurysms.

2) Swelling: Anatomical counteraction happens in the walls of the vessel.
3) Inherited disarray caused by cardiac wall delicacy: Structural diseases caused by connective tissue disorders.
4) Cigarette Usage: A scientifically-known truth is the cigarette usage causes the development of aneurysms. Vessels in the kidneys are known to be the most affected by this action.
5) Aging: It is one of the factors that have a great effect on the formation of aneurysms especially for patients above 65 years old if the person does not have any connective tissue disease

2.4.1. Thoracic Aortic Aneurysm

Balloon formation or enlargement of the aorta is called a thoracic aortic aneurysm or thoracic aneurysm (Figure 10). For the reason that the aortic vessel is the body's primary vessel that the blood is carried to vital organs in the body, the risk of the aorta bursting increases when the aneurysm enlarges, causing extensive damage to the vessel walls and unstoppable bleeding, resulting in death. A thoracic aortic aneurysm can occur as a result of damage to the aortic vessel wall by various diseases, as well as genetic reasons, and age can be listed among the important reasons. Patients with thoracic aortic aneurysms usually have uncontrolled hypertension. Back pain, difficulty in swallowing, and shortness of breath can be counted as the symptoms that occur with a thoracic aortic aneurysm. (Johns Hopkins Medicine, n.d.)

The causes of thoracic aortic aneurysm, in general, can be listed as follows (Koksoy, n.d.);

1) Atherosclerosis, which occurs due to aging and increases over time, causes weakening of the vessel wall and constitutes a risk factor for the aneurysm.
2) Genetic predisposition is a major risk factor for people with an aneurysm in their family or relatives. However, the risk of aneurysm formation increases in people with genetic disorders in the vascular structure.
3) Thoracic aortic aneurysm and rupture can occur as a result of certain diseases such as connective tissue diseases, Marfan syndrome, Behçet disease, tuberculosis and syphilis, and traumas such as falling from a height, although it is rarely encountered.
4) With increasing age, the risk of enlargement and rupture of the aneurysm increases.

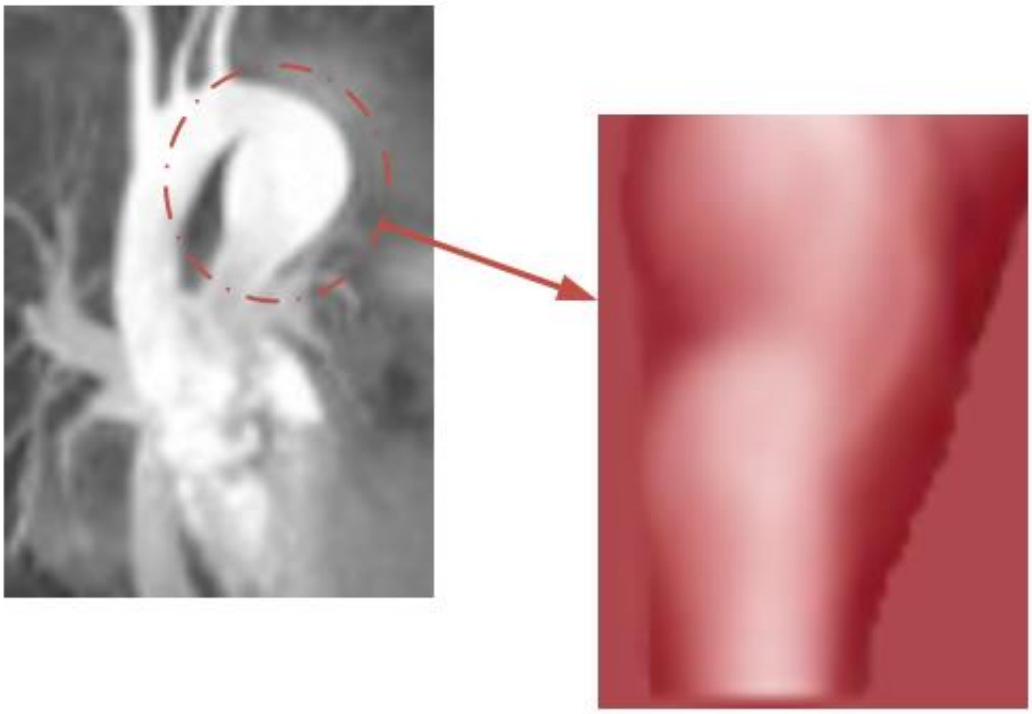

Figure 10. Thoracic aortic aneurysm formation [24]

2.4.2 Abdominal Aortic Aneurysm

It is the abdomen region of aortic vessel's extraordinary growth. The most dangerous aspect of this aneurysm is that it may continue to expand and cause a rupture (Figure 11). In this case, the blood in the aorta fills the abdominal cavity fast and death occurs in a short time depending on the size of the tear (Alpman, n.d). The mortality rate in ruptured aneurysms is between 70-90% due to the statistical results. In the United States, 15,000 people die from abdominal aortic aneurysms ruptures every year. Therefore, the diagnosis of aortic aneurysms is vital for their treatment without rupture. To give an example, it was an abdominal aortic aneurysm rupture that caused Albert Einstein's death in 1955 at the age of 76. (Fitzgerald, 2018). Although the exact cause of abdominal aortic aneurysms (AAA) is not recognised, there are some serious threatening characteristics:

1) Due to its negative effects on the human body, smoking plays a leading role as in most aneurysms.
2) AAA can also be seen frequently in patients with atherosclerosis.
3) Hypertension and hereditary determinants also are the reasons for the abdominal aortic aneurysm. In people over 65 years of age, if siblings have AAA, the risk of developing an aneurysm in the person increases up to eighteen percent. Those with cardiovascular disease or peripheral artery disease (leg artery disease) have a higher AAA rate.

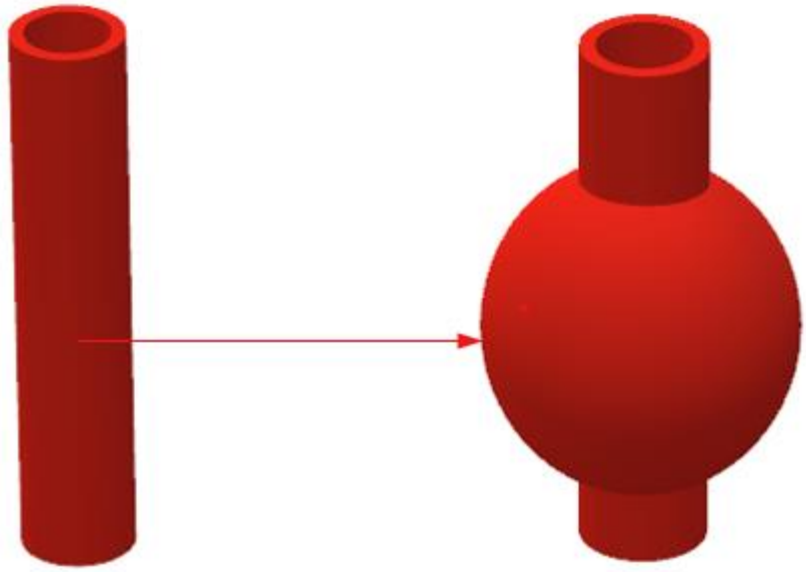

Figure 11. Representative picture of abdominal aortic aneurysm

2.5. Aortic Imaging Methods

2.5.1. Computed tomography (CT)

Images of human body areas from a variety of angles are formed by the radiation in this technique (Figure 12). In computed tomography, the patient is in a supine position. A stretcher is placed inside the device. The section thickness is adjusted from the computer (Benli, 2020). The patient is positioned according to the area to be displayed. Then, the engine of the device is started and regional images of x-ray beams are created. If the imaging is to be performed using medicines (contrast), the intravenous line is opened, the medicine is given and sections are taken. CT can be used for detailed examination of different body parts. It is used to determine the presence if any, location, and size of stenosis or occlusion in the heart vessels by administering medication from the arm. In addition to helping the diagnosis, computed tomography is also used as a guide in the evaluation of treatment and intervention in the correct area in interventional procedures.

Examples of these situations are;

- Evaluation of internal organs in terms of condition and bleeding in severe injuries,

- Bone line and general condition evaluation of bone in fractures in bones, diagnosis of bone tumors,

- Evaluation of patients preparing for surgery and radiation therapy.

Computed tomography angiography images have been used in this thesis to reconstruct the aorta arteries of people for the analyses.

Figure 12. A preview of the aorta construction using CT images [26]

2.5.2. Trans Esophageal Echocardiography (TEE)

This measurement method is used when the patient's chest structure (due to lung disease, deformity, etc.) does not provide an adequate quality echocardiographic image or when it is necessary to evaluate intracardiac formations more closely (Klomp W.W.J., 2016). Trans Esophageal Echocardiography is an endoscopic examination. TEE is also known as cardiac ultrasound, cardiac endoscopy. With a thin tube (probe) that is lowered into the esophagus through the mouth, the posterior neighborhood of the heart is accessed and a very clear and detailed image is obtained (Memorial Tıbbi Yayın Kurulu, 2021). At the point reached by the technology used today, with the help of its device, the structures adjacent to the heart in the heart and chest cavity can be examined in much more detail, intensive care patients and critical patients can be examined in detail in terms of heart diseases, and treatment can be directed as a result of more reliable images. It is a method used to investigate clots or infections in the heart, evaluate prosthetic valve functions, diagnose ruptures of the main artery, namely aorta, examine heart holes, determine the status of heart valve insufficiency, and evaluate the success of heart valve surgeries or surgeries for heart holes. It is also used for the identification and theraphy purposes. TEE is a useful examination method for the heart.

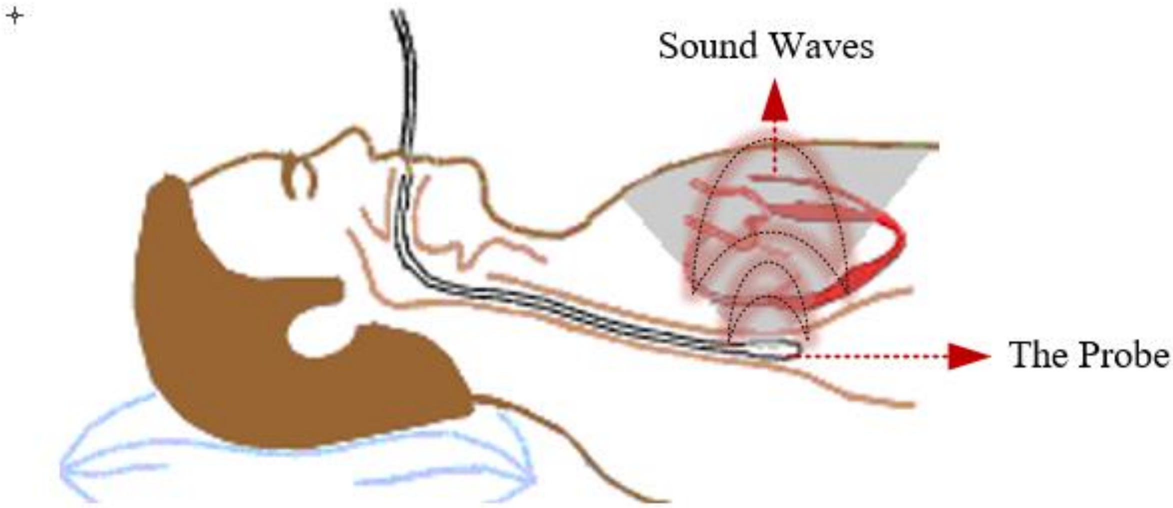

Figure 13. The method of TEE [1]

2.5.3. Magnetic resonance imaging (MRI)

A comprehensive analysis of the systems in the human body can be done by the technique of medical imaging (MR) (Bulut, 2020). 2-D or 3-D images are formed by this method. This method is mostly employed to distinguish illnesses sending non-harmful rays. MR results help diagnose, plan treatments and evaluate how effective previous treatment has been. An MRI scan produces a much clearer image than regular X-rays and computed tomography (CT). The organs inside of the body can be imaged by this method. Focusing on the heart or blood vessels, MRI can evaluate:

1) The size and functions of the chambers of the heart.
2) How thick the heart walls are.
3) How extensive damage of a heart illness.
4) Constructional issues.
5) Inflammation or blockage of blood vessels.

The MRI machine is shown in Figure 14.

2.5.4. Intravascular Ultrasound

Intravascular ultrasonography has entered the field of cardiovascular medicine as an important method for imaging the coronary vessel wall. (UCLA Health, n.d.) In the evaluation of coronary artery disease, new methods have begun to be used (Gören, 2005). Insights into the arterial wall structure and stenosed flow characteristics of the vessel can be obtained with this method. An atherosclerosis example under the view of intravascular imaging is shown in Figure 15.

Figure 14. The MRI machine [33]

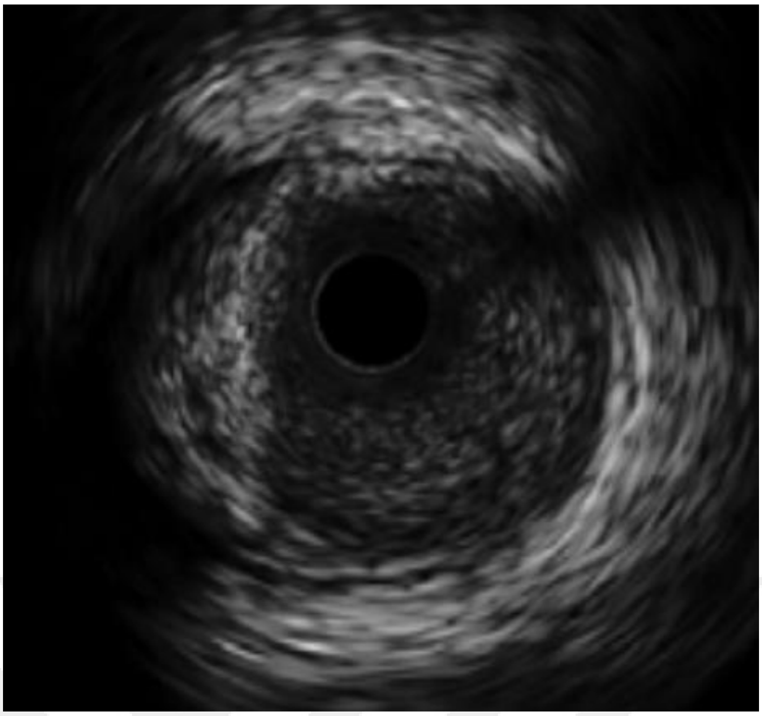

Figure 15. A view of coronary atherosclerosis gathered from intravascular ultrasound [44]

2.6. Blood Vessel Segmentation Programs

The importance of vessel segmentation has increased especially in recent years with the advancement of technology. The reason for this increase in importance can be shown as supporting doctors and other healthcare professionals with the images provided by the programs, thanks to fully or semi-automatic vessel segmentations. Besides, more detailed analyzes can be made with the support of various engineering programs employing these segmentations. In this thesis, 3D-Slicer which is one of the vessel segmentation programs, and Ansys which is an engineering program, have been used together, and analyses have been performed on hemodynamic parameters.

2.7. The ANSYS Software

A variety of examinations and computer modeling can be performed related to many fields in Ansys (Cadsay, n.d.). The finite element is one of the most employed methods in the ANSYS program. With the finite element method, objects with complex geometry such as vessels, that are not possible to be analyzed as a full-body directly because of the complex structure, are divided in little parts and analyzed separately. A single and consistent analysis result is obtained by combining the results obtained with the analysis results of a finite number of elements. In engineering simulations, the properties of the material from which the analyzed model is made are of great importance. The ANSYS program allows the 3D model of the object to be exactly matched with the material properties to be used in reality. Different types of material properties such as ductility or flexibility can be arranged or chosen from the catalogs of Ansys earlier than the beginning time of the simulations. Some ANSYS modules and their usage areas can be listed as follows (Akıncı, 2020):

1) Static Structural: Static structural module is a preferred module if the object is not a moving mechanism. The deformation of the object under force is examined. In this

module, the strength of a bridge can be calculated as well as stress values occurring in materials can be observed in interlocking mechanisms.

2) Transient Structural: This module is used when it is desired to calculate the stresses that occur in the interconnected limbs during operation as well as the position, velocity, and acceleration analysis of the mechanism in moving mechanisms. It is one of the modules used in vessel analysis.
3) Steady-State Thermal: It is the module in which the thermal changes that occur with convection, radiation, and conduction are analyzed in the material that is not dependent on time.
4) Transient Thermal: It is the module in which thermal changes in the material due to convection, radiation, and conduction are analyzed over time.

Different analyzes can be performed by associating some modules with each other. The calculation of deformations that may occur in the vessel can be found with the 2-way FSI method, which is created by using several modules together. The steps that take place during the vessel analysis can be briefly mentioned as follows:

The Fluid Flow (Fluent) module must be used and the workflow differs in this module. Unlike other modules, no material definition is made in the engineering data section. Material properties are defined in the program at a later stage. First of all, geometry is imported, mesh analysis is completed and definitions are made on the geometry. The inlet, outlet, walls regions where the flow will take place are defined by selecting named selection on the geometry. In the setup tab, certain settings are selected in Fluent Launcher and the fluent solver is opened. First, the choice of the solvent must be made. It is decided whether the solver type will depend on pressure or density. The solvent which depends on the pressure is employed for low velocity not-compressible or slightly compressible flows. The resolver that is based on density is used for high velocity and flows that can be compressed. The density-related resolver provides greater accuracy than the pressure-related one. Moreover, it is expected to select steady or transient under the time expression. Here steady means that the solution will continue until the flow becomes stable in an unlimited time. Transient, on the other hand, expresses how many steps are defined without waiting for the equilibrium state to be reached, the further it will be. The answers to these steps are important for the accuracy of the analysis. In the Setup-models section, the problem is introduced to the Ansys. For instance, the statement is asked whether the energy equations will work. Energy equations should be opened if heat transfer is also in question in the flow analysis. Fluid-material definitions are made in the materials section. After the mesh analysis in boundary conditions, the necessary questions are answered in the momentum and thermal tabs for the regions where we define named selections. Reference value, solution method/controls, initialize steps are followed. In the run calculation section, the number of iterations is entered and the solution is expected to converge. In the graph followed during the solution, upward movement in the vertical will mean that the error has increased and this is an undesirable situation.

2.8. Source Limitations

During the execution of this thesis, the number of networks to be created on vessel walls, which have a very complex structure, or how much RAM the computer should have to perform the analysis, have created restrictions. It has been observed that the number of meshes created on computers with low RAM cannot be kept high, and even if the analysis starts, the analysis is performed very slowly, causing a crash in the computer. However, keeping the amount of mesh in excess is an important criterion for high accuracy analysis. Therefore, computers with good technical features should be used to perform these analyses. In addition to these, vessel segmentation should be done with great care. Here, the quality of the images taken from the hospital is also important. If the quality of images in MR or similar formats is not good enough, vessel segmentations can take a very long time. In addition, the usability of the employed segmentation program is crucial, too. If the program has a complex interface, the segmentation and editing process will slow down. Furthermore, the very high usage fees of some programs create a negative factor, as well.

2.9. The Covid-19 Virus

Before giving general information about coronavirus, it would be useful to briefly talk about viruses. The basic self-replicating species are viruses. It is made up of a protein molecule that covers the DNA or RNA which exclusively conveys hereditary data. An envelope is a coating of fat that few viruses possess, as in the coronavirus. Such a simple organism has no ability to reproduce on its own. Viruses are hidden parasitic organisms that can reproduce when they penetrate a region called a host, that they have selected in a certain way Viruses are hidden parasitic organisms that can reproduce when they penetrate a region called a host, that they have selected in a certain way. Viruses are hidden parasitic organisms that can reproduce when they penetrate a region called a host, that they have selected in a certain way. Viruses are hidden parasitic organisms that can reproduce when they penetrate a region called a host, that they have selected in a certain way. Viruses are hidden parasitic organisms that can reproduce when they penetrate a region called a host, that they have selected in a certain way. Viruses are hidden parasitic organisms that can reproduce when they penetrate a region called a host, that they have selected in a certain way. Viruses are hidden parasitic organisms that can reproduce when they penetrate a region called a host, that they have selected in a certain way. This situation can be compared to that of computer viruses. They can also be referred as very small programs; They can not operate a computer by themselves. In order to reproduce itself, it aims to enter the computer program and use the operating system there and send copies of itself to other computers. Just as a computer program reproduces and spreads itself, the analogy of viruses to these programs is an example similar to that in nature. Viruses prefer healthy cells; for instance, the novel coronavirus is spread to other people via droplets since it favours the mucosa of the respiratory system. When the virus infects the pulmonary nasal passages, it requires a specific period of time for the virus to multiply and harm the body. This period is known as the incubation period. The new coronavirus, sometimes described as the unauthorized Wuhan coronavirus, was initially discovered by authorities in the Wuhan region of China during beginning of December 2019 and is a deadly pathogen causing serious infection and can be spread to other areas. The World Health Organization (WHO) has named the virus SARS-CoV-2 as its official name (Severe Acute Respiratory Syndrome - Coronavirus-2). The sickness caused by the virus is referred to as COVID-19 by the World Health Organization. The World Health Organization classified CoViD-19 as a worldwide health crisis on January 30, 2020. The virus was labeled a pandemic, or worldwide outbreak, on March 11, 2020. The unusual coronavirus sickness (Covid-19) is a viral disease with a respiratory infection and difficulty breathing that was initially found on January 13, 2020. The disease is known to be propagated by droplets and touch. Because of the global viral scenario it causes, it is classified as a pandemic. The newfound coronavirus is a coronavirus variant that can infect all living creatures. In history, it is evident that several group of viruses cause severe respiratory infections such as MERS (Middle East Respiratory Syndrome) and SARS (Severe Acute Respiratory Syndrome) (Severe Acute Respiratory Syndrome). Coronaviruses are titled from the Latin word corona, which means crown, since they form a circular, projecting crown when examined under an electron microscope. Coronaviruses have been around for a long time in our civilization. The common cold is the simplest and most common of these. A coronavirus is a family of 20 various types of pathogen that causes respiratory system illness and a stuffy nose. Plenty of other pathogens in the group cause lesser severe infections with fewer indicators than the newest coronavirus. As a result, when it refers to conditions such as the cold or flu, coronaviruses haven't generated any concern. Coronaviruses can be spread among living creatures at times. Viruses have different genetic information due to RNA mutations. It bypasses the immune system that has previously formed through sticking towards the tissue, especially in the surface proteins, and changing the proteins it requires to get through. It could also grow quicker and inflict far more harm to the cells by changing the proteins it needs to get inside. The virus, which was formerly known as SARS, caused an illness that was quite similar to the current coronavirus. The coronavirus, which is of the issues to consider, is analogized to the second SARS virus. Aside from that, other highly pathogenic viruses made headlines around the world due to their capability to cause devastating infections and outbreaks. MERS, or Middle East Respiratory Syndrome, is a disease caused by a coronavirus that is spread from camels to individuals and has been causing an epidemic in the Middle East for some time. MERS wasn't classified as an epidemic because the virus's impacts were not seen throughout the world. MERS cases are still being reported in Middle Eastern countries regularly. Since it was originally identified in 2019, the coronavirus infection that we are presently encountering has been known as CoViD-19.

2.9.1. Coronavirus Symptoms

Flu, coughing, chest pain, with breathing problems, are the most common side effects of a new coronavirus diagnosis. The disease can cause fever, respiratory distress collapse, kidney problems, or even deaths in more serious forms. High body temperature, migraine, and a persistent cough that lasts numerous days are by far the most frequent signs of coronavirus. Other symptoms can be listed as;

- Breathing problems
- Coughing up
- Sore throat
- Aches
- Stuffy nose
- Migraine
- Chronic insufficiency
- Conditions such as kidney failure can be among the symptoms of coronavirus.

Before going to the relevant health institutions, people who show symptoms of coronavirus should take precautions by wearing a mask in order not to infect the people around them. There are also a number of types of masks to be used. The N95 mask is designed to be relatively non-porous and a tight fit to protect from 95 percent of airborne particles. N95 masks are only recommended for people who will be close to patients with suspected viruses and healthcare workers. An example of an N95 mask is shown in Figure 16.

Figure 16. An N95 mask [35]

Face masks are appropriate for usage in places with a low potential virus concentration. These masks prevent the spread of respiratory secretions in the case of coughing and sneezing. This type of mask is recommended for caregivers and sick people. An image of this type of mask is given in Figure 17.

Figure 17. A surgical mask [20]

Homemade masks are also used by people during the pandemic. However, the protection of masks made of fabric varies according to the type of material used. It is recommended to use these masks when a medical face mask is not available. An example of such masks is given in Figure 18.

Figure 18. A hand-made mask [23]

Although the coronavirus influences young people and kids with minor symptoms, it also impacts those over 65 and those with chronic illnesses which including lungs, and hypertension.

Despite the fact that data from many authoritative sources differs, fatality rates by segments of the population are consistently;

- 3.6 % for those aged 60 to 69.
- 1.3 % for those aged 50 to 59
- 0.4 % for those aged 40 to 49.
- For those aged 39 and under, the rate is 0.2 %.

According to the statistics given, it is observed that the mortality rates due to coronavirus in children and young people (in the 10 to 39 age group) are the lowest.

2.9.2 Covid effects in patients experiencing heart illnesses

Covid-19 is similar to other known influenza viruses. However, it differs from influenza in its effects since more organs are affected. One of these vital organs is the heart. The effects of the virus are more severe especially in elderly people and milder in young people. The older the organs, the harder they protect themselves against the coronavirus**.** Covid-19 is more dangerous and long-lasting in those with chronic heart disease. The degree of heart disease of people may increase. The heart problem of people with second-degree cardiac insufficiency can progress to the third and fourth degree. Blood pressure can get out of control and cause rhythm disturbances. Furthermore, some people infected with the coronavirus may experience a cytokine storm. Cytokines are molecules that regulate biological functions such as immune response formation. In cases where the body encounters an infection, a certain amount of cytokine release is necessary for the immune system to fight the infection. However, since high amounts of cytokines are released into the blood very quickly, a cytokine storm occurs. Cytokine storms can lead to multi-organ failure.

Cytokine storms can cause inflammation (inflammation) of the heart muscle. This condition, called myocarditis, causes the heart to contract and pump blood. Myocarditis can result in heart failure. As an addition to Covid 19 myocarditis; It can cause arrhythmia, acute coronary syndrome, and thromboembolism.

The following criteria are important for patients with heart disease to be protected from coronavirus:

1) Especially people over the age of 60-65 should not enter crowded environments.
2) The distance between people should not be closer than 5 meters.
3) Plenty of water should be drunk.
4) Excessive physical and psychological fatigue of the body should be prevented.
5) Immunity should be kept strong, additional supplements should be used if necessary.
6) Crowded environments should not be entered unless necessary.
7) Disposable gloves and masks should be used outside.

In addition to all these, cardiovascular patients should comply with social isolation the most. It has been observed that especially patients over 60 years of age are at very high risk. In this period, even with individuals who are thought to be healthy, contact should be reduced by considering the possibility of being carriers and great attention to personal hygiene should be given. There are some exercises that cardiovascular patients or people in the risk group should do regularly. Staying still, especially under home isolation, can have negative consequences. It is more beneficial for health to apply exercise programs for patients who are at risk for cardiovascular health under social isolation. However, the exercise equipment used should be cleaned with surface disinfectants each time and the working room should be regularly ventilated. However, there are some important points to consider about exercising which are:

1) Exercise programs should be planned according to the disease and risk status.
2) The immune system may be adversely affected as excessive strenuous exercise can reduce the secretion of some protective antibodies in the respiratory tract. Exercising after an extremely tiring period is also not suitable as it may increase the risk of infection.

2.10. Medical Treatments of Aortic Aneurysms and Covid

In some aortic diseases, regular medical follow-up can be done by reducing the risk factors, as well as angiographic interventions with a closed method and open surgical intervention in necessary cases.

2.10.1. Small Cases

Small aneurysms that do not cause any complaints in the patient are followed up before surgical intervention. The patient is examined with tests such as computed tomography and ultrasonography every 6 months on average. The size and shape of the aneurysm and the patient's complaints are evaluated. Data obtained in 6-month periods are compared. Follow-up continues until the aneurysm exceeds 5,5 cm. In the meantime, patients are kept under control in terms of problems such as high blood pressure and smoking that will cause the aneurysm to grow. When the aneurysm is large or causes symptoms, an operation must be performed to prevent it from bursting. When some patients have risk factors, their aneurysms can be operated on even when they are small. When thoracic aortic aneurysms are treated surgically, On that the left shoulder of the rib cage, a scratch is created. If the aneurysm has advanced into the abdomen, the incision is extended to the abdomen. In the surgery, a pump or shunt is used for the blood supply of the vessels coming out of the aorta and feeding the vital organs. An artificial vein is used in the area where the aneurysm is formed. Through the windows opened in this vein, a connection is made to the veins going to the organs. The parts of the veins that go to the intestines, liver, and kidneys from the aorta are also sutured to the artificial vein. Then, the artificial vascular graft is attached under the aorta and the pump, shunt, and clamps used are removed.

2.10.2. Open surgical repair

Based on the area of the aneurysm, a cut is made inside the chest or belly for half-closed surgery. Throughout the operation, a primed synthetic graft is sewn into the diseased area of the aorta that has ballooned and is anchored in place, thus connecting the defective area with the normal aorta on both sides (Figure 19). The fresh, fabricated part of the coronary artery starts to behave like a regular and healthy aorta once the treatment is completed. The treatment lasts three to five hours, with a five to ten-day stay in the hospital afterward. Many individuals require a brief stay in a rehab institution to finish their recovery. In six to twelve weeks, the majority of people are back to usual. Open surgical treatment is a tried-and-true procedure with excellent long-term benefits.

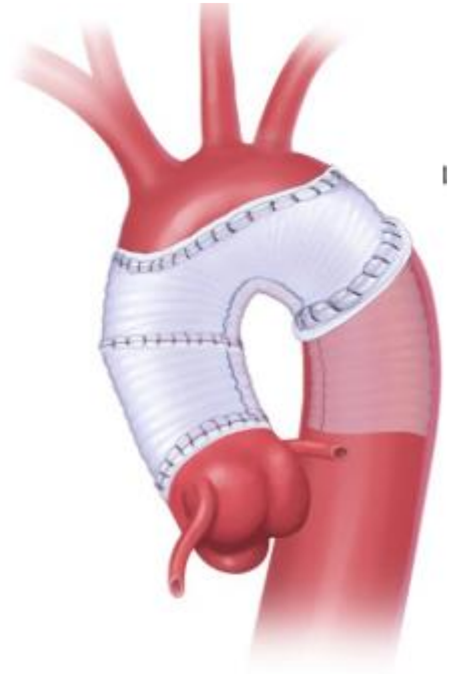

Figure 19. The look of the aorta after an open surgery [79]

2.10.3. Endovascular Repair

Endovascular repair is rapidly progressing to become the treatment of choice for abdominal aortic aneurysms and is increasingly being used in the treatment of thoracic aortic aneurysms. The doctor inserts small cuts in the inguinal region to reach the vessels which lead to the aortic arch during the endovascular recovery process. A guidewire is pushed into the damaged section of the aorta after passing through the veins. The doctor puts the stents grafts over the guidewire into a canal underneath X-ray monitoring (a long thin tube). A stent graft is a fabric-like tube used to strengthen the aorta's weakest section and is combined with metal wire stents (also called a frame). The surgeon then advances the stent graft into the aneurysm area by moving it along the guidewire inside the catheter (Figure 20). The catheter is removed, as well as the sealant graft on both sides of the aneurysm extends like a piston. The catheter transplant, once in position, functions as a new channel for blood to pass forward without pulling the aneurysm up. Since there is no pressure exerted on the aneurysm, the aneurysm shrinks over time. The endovascular repair offers the following benefits:

- It usually takes one to three hours to complete the process.
- Individuals can head back after the surgery within a couple of days.
- Compared to open surgical techniques, the incisions are smaller and there is less trauma.
- Around two to five weeks, the majority of the population are back to normal.

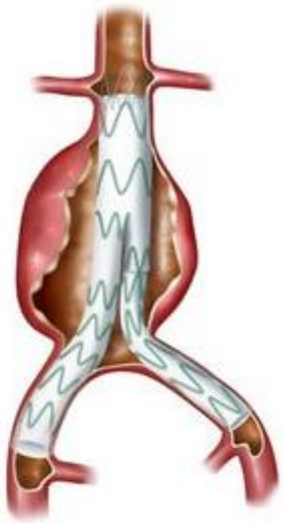

Figure 20. A view of the endovascular repair [19]

3. LITERATURE REVIEW

Ong et al. (2020) pointed out that the analysis between aortic pathology and blood flow using computational flow dynamics was promising to guide the treatments of patients. Nevertheless, they emphasized that there was not an extensive review of the literature about the usage of computational fluid dynamics (CFD) on aorta diseases. 136 articles had been checked to complete the literature survey in their study. As a result, they observed that twenty-one percent of the studies performed used clinical imaging to confirm computational fluid dynamics results. Botar-Jid et al. (2009) mentioned that the requirements to calculate the blood flow correctly were as follows. Acquisition of the geometry, the depiction of blood flow behavior and its relation with vascular tissues, influx, and effluence states. In addition, the flow speed of blood, pressure, and stress on vessel walls and the representation of mesh are counted as important parameters. SOLIDEDGEV20 was used to create the vessel of the patient virtually in their study. Moreover, a program called GAMBIT is used to smoothen the surface of the vessel and to design and mesh for geometry purposes. It was also said that the best model for complex flows was the CFD-Reynold Stress model, hence this model was selected. The dynamic mesh was chosen to complete the analysis and the vessels were considered elastic. The vessel they worked on was assumed to be rigid and elastic. Subsequently, a comparison was made depending on the results. Brown et al. (2012) utilized the full FSI method to analyze vessels. The particular reason for the circumstance is that along with the flow, the change in vessel walls also be examined with this method. Windkessel model of Ansys was used for calculations and the aorta was taken by the ShIRT program. Mesh number was chosen 500,000 and the thickness of the aorta wall was taken 0,8 mm. Hope et al. (2008) gave details about an implementation of a 4D flow and its techniques for arterial blood vessel pathologies. EnSight and GtFlow programs were introduced for that purpose. Biglarian et al. (2020) focused on the investigation of wall shear stresses along the vessel. To achieve this objective, computational fluid dynamics was based on the finite element method. In this method, the boundary conditions were divided into two categories. inflow and outflow. Outflow conditions were based on some acceptances such as zero surface tension and fixed boundaries whereas blood flow rate and distribution of mass flux at the inlet were important factors for inflow conditions. The fluid model was preferred as Newtonian and incompressible. Mesh type was selected dynamic and laminar flow including more than 3 cycles was included in the analysis. All things considered, the effect of wall shear stress on the flow and diseases were checked out. Liang et al. (2020) took a different approach and estimated the constant pressure and velocity distributions on many different aorta geometries by the deep learning method. In this way, the aorta of 729 people was inspected and the error rate was found 1,5 percent. Accordingly, it was proven that neural network usage was suitable for this aim. Investigation of the correctness of a 2-D plane wave vector flow imaging method under streamline and multiplex blood flow conditions in healthy carotid arteries was completed by Jensen et al. (2018). The carotid artery of 10 people was examined with some assumptions including no-slip condition and zero outlet pressure. Furthermore, fluid was assumed to be Newtonian. Womersley-Evans model was chosen to construct the inlet condition and the analysis was completed employing the Navier-Stroke equation. Healthy 36 volunteers with either physiologically shaped sinus prostheses or conventional tube grafts participated in a study that aimed to compare aortic flow patterns against the David-valve-sparing aortic root replacement in the study of Oechtering et al (2016). They have made use of the 4D Flow MRI method and concluded that the secondary flow pattern number has increased in patients that had the operation. Karimi et al. (2014) compared nine non-newtonian and Newtonian models to indicate wall shear stresses and non-newtonian effect factors for the aorta. The vessel was created virtually via 3D Slicer V4.0. Along with it, the constructed body was exported to GAMBIT and CATIA V5 to prepare it for analysis. The Finite Volume method was preferred and the flow was assumed to be time-dependent and incompressible. Then, the Navier-Strokes equation was utilized together with the supposition of the rigid artery wall. The advantages of models were discussed depending on the results of the analysis. Many analyses were made to explore the effects of different boundary conditions on fractional flow reserve (FFR) etymology by Lo et al. (2020). In this regard, the aorta of 10 people was modeled and meshed in Simpleware SCAN IP. The flow was presumed to be laminar and incompressible while the modeling of blood was completed as Newtonian and homogeneous. Navier-Strokes equation was operated in the CFX module of Ansys. Besides, the presupposition of rigid vessel walls and no-slip conditions were taken into account. 2 element Windkessel model was associated with outflow conditions whereas the inflow inside the aortic vessel was adjusted as steady. It was proclaimed that the outlet conditions which were more representative for every patient be an efficient way to improve FFR calculations. The impacts of gender and age on the thoracic aorta were studied by Tawfik et al. (2019). Hence, aortic length calculations of 182 people were examined with Volume Viewer software and it was found that the tortuousness of the aorta increases with age regardless of gender. Wu et al. (2017) draw attention to the importance of the angle between the SMA and distal aorta artery when performing SISMAD through various analysis processes. The aorta of 37 patients was created and edited virtually in Mimics and Materialise HQ programs. Ansys-ICEM was used for meshing and a 1 mm artery wall thickness was chosen before analyzations. Boundary conditions of velocities were measured with velocimetry. They concluded that higher artery wall stresses caused larger angles. Zhang et al. (2020) dissected the mechanics of post-stenotic dilatation (PSD). Carreau-Yasuda model simulations were executed through cardiac cycles and the geometry of PSD was rebuilt from the scans of tomography. They concluded that an increase in the degree of coarctation increases the risk of developing a PSD. Cilla et al. (2020) stated that factors such as the size of the aorta, flowing patterns, blood pressure, and blood flow rate were effective factors in the emergence of diseases. They conducted a parametric study using computational fluid dynamics to provide information on aortic disease. The aorta was created in Solidworks and then the work continued in the ICEM module of Ansys. The acceptations of the rigid model and no-slip condition were made in the study. It was seen that their study could be helpful for the evaluation of aorta hemodynamics. Zhang et al. (2017) carried on mathematical studies to see the effects of the location of LVAD outflow on thrombi distribution in the aorta. The aortic model was created in Mimics. The surface quality of the model was improved in Geomagic. Ansys-ICEM was used for meshing. As a result of the analysis, the distribution of the thrombi was observed to be highly affected by the LVAD output location. Analysis and evaluation of a pre-aneurysmal and post-aneurysmal aorta were completed by Tse et al. (2011) Mimics and HyperMesh was employed for modeling and meshing. They found that high wall shear stress could be the reason for tear formation. Barber et al. (2007) presented a fast and effective method to derive mesh from medical images. Two examples of utilization of their algorithm were provided. They showed that their algorithm was suitable for high-accuracy meshing. Mojarab and Kamali

(2020) et al. investigated the outcomes of different microsensor locations on blood flow properties in the aorta. After extracting the geometry of the aorta from medical images, inlet and outlet conditions were applied and parameters of the blood flow were checked out. After the designing stage of the microsensor was completed, they added it to the analysis and the numerical blood flow characteristics were examined. As a result, it was seen that the maximum blood flow rate increased up to 10 percent at the point where the microsensor is located. Su et al. (2020) demonstrated that machine learning algorithms could be implemented instead of computational fluid dynamics (CFD) to save time when generating hemodynamic parameters. For that purpose, Python OpenFOAM and TensorFlow 2.0 programs were used to gather the wall shear stress values. The outcomes showed that the percentage error of the algorithm was around 2,5 percent. Changes in the hemodynamic properties of the thoracic aorta before and after the replacement of the aortic valve were investigated by Kamada et al. (2020) They executed Thoracic 4D-flow MRI on 10 patients before and after the operation. Volume flow rates and helicity densities were investigated. It was observed from the results that volume flow rates were increased after the operation. Mendez et al. made use of finite element analysis (FEA), fluid-solid interaction (FSI), and computational fluid dynamics (CFD) to decide on the clinically important parameters such as wall shear stress and aneurysmal wall elasticity for ascending thoracic aortic aneurysm (ATAA). To enhance the higher cognitive process and quantify the danger of complications in terms of prognosticative principles, simulation of the ATAA has been created. The consequence of the usage of feasible boundary conditions taking into account the scratching and twisting of the aorta has been discussed. Although the internal and shear stress distributions have been obtained to be inconsistent for the given ATAA, 2-way FSI outcomes have been compared with the FEA and CFD results. Expectancies of the CFD-based and FEA-based analyses are a match for the complex 2-way FSI modeling. It has been concluded that these results have probably been caused by the rigid aneurysmal wall that experiences fewer diameter changes during the heartbeat. Lee et al. mentioned that the reason behind the considerable discrepancy that occurred in the aorta valve leaflets has not been fully discovered yet. That being the case, the connection between the patterns of the blood flow through the aorta valve and the calcification's dimensional positioning on the aorta cusps has been investigated. A mathematical examination including the reconstructed Left Ventricular (LV) models of seven people has been carried out. Body Section Roentgenography images have been attained to create the models. No-slip conditions on the vessel walls and transitory volume flow rate at the bicuspid inlet and the outlet of the aorta during the cardiac cycle have been chosen for the computational fluid dynamics (CFD) analysis. The turbulence kinetic energy (TKE) impact in conjunction with shear stress has been taken into consideration for the CFD analysis. Simulation results have been used to determine the probability of calcification in aortic valves by showing consideration for LV hemodynamic properties. As a consequence, wall shear stresses in the zone of the aortic valve are much higher as compared to the border area between right and left cusps. Furthermore, it has been found that TKE has been avoided by the calcium in the aortic valves. König et al. calculated wall shear stress changes in the endothelial layer using Computational Fluid Dynamics (CFD) for different vessel thicknesses. They added that the forecasted WSS values might not refer to the real force affecting the endothelial cells (ECs) as a consequence of roughness. Altogether, wall shear stress variations inside the limits of top ECs (Mmax) and joint zones (Mmin) may be further considered for lower diameters. On the grounds of this, numerous bidimensional axisymmetric models with different vessel diameters have been generated. Dimensional analysis has been implemented to complete scaling intolerable limits to obtain high-grade convergence. Reynolds number has been assumed as unchanging for mesh tests. CFX-4 code has been employed in the computational fluid dynamics solver. They have observed depending on the results that wall shear stresses have increased by the decreased diameter of the vessels. Fukui et al. stated that blood flow and motion of the walls are the primary reasons for the distribution of wall shear stress (WSS). However, many studies have assumed that the artery wall is rigid, and wall motion is ignored. Taking that into consideration, they have utilized 2 different artery models including a stenosed and non-stenosed area in the model tubes to explore the effects of wall motion. Fluid and solid correlations have been solved by an approved code of Radioss. Two waves have been produced by the pulse applied to the entrance in the smooth tube; radial motion wave and axial wave which is 3 times faster than the radial wave. The end of the vessels has been assumed as fixed so that the waves have been reflected. It has been observed for the uniform tube that the blood speed is reduced by the axial wall motion resulting in decreasing the wall shear stresses by 15%. The biggest effect of wall motion is reached when both waves have occurred simultaneously which causes a 30% decrease in WSS. In the tube with stenosis, it has been figured out that the flow has occurred faster towards the stenosis and created recirculation zones at the end of it. The relationship between the inlet pulse and flow is found complex and the stenosed area has been seen as the reason for the very complicated wall shear stress distribution. Nakamura et al. conducted a study to better understand the flow characteristics in the aorta and left ventricle. So, computational fluid dynamics (CFD) and phase-contrast magnetic resonance images (PC-MRI) have been incorporated. They added that the reason for using PC-MRI is to create realistic aorta geometry for CFD calculations so that the necessary velocity data could have been obtained for boundary conditions. As a consequence, it has been demonstrated that the blood has been redistributed under the aortic valve and discharging flow to the aorta. This discharged flow has been found to have unbalanced velocity profiles, accelerating throughout the mitral valve. CFD outcomes have indicated that the aorta has 2 different flow structures, a helical right-handed structure in the ascending zone and left-handed in the descending part. It has also been observed that the flow at intersection areas has been situated without a proper direction. Kostic et al. intended to invent a simple stent that has common flow characteristics of other mostly-used stents. On the grounds of this, computational fluid dynamics have been employed to design a stent that required fewer materials. So, a basic 2D aorta model has been created. Their investigation results have shown that a simpler stent usage could be also effective on pressure drop by 70%. Tse et al. performed a study on the initiation and progress of the severing aneurysm since clinical examinations have shown that the aneurysm could be related to the hemodynamic parameters. To build more understanding of the relationship between the hemodynamic parameters and aneurysm, computational fluid dynamics (CFD) has been utilized. Distribution of the velocity along the vessel, patterns of the flow, pressure change, and wall shear stress that is hard to obtain results in in vivo measurements, have been investigated through simulations. Changes in the blood flow parameters of the patient-specified aortas have been inspected under two conditions, namely, pre and post aneurysms using CFD. Feasible boundary conditions that are time-sensitive have been set for the fully reconstructed aorta geometries. It has been suggested that the helical flow that causes the revelation of the false lumen might have a relation with the hemodynamic nature of the aorta. Contraction of the aorta has been the reason for huge recirculation occurring in the area of poststenosis. 0.21 kPa has come as the result of the difference in pressure values and the area that this value has been obtained has been found as the region of the possible lumenal aneurysm. Furthermore, high wall shear stresses have been associated with the occurrence of tears along the walls. Perinajova et al. stated that wall shear stresses (WSS) and abnormal flow of the blood are the reasons for aorta aneurisms. These aneurisms might be examined when the computational fluid dynamics (CFD) and magnetic resonance images are coupled together. Therefore, a study has been accomplished driving benefit from the CFD simulations for the aorta geometries taken by 10 patients and WSS positioning along the walls has been shown. Segmentation of the aorta for each patient has been completed 4 times employing the identical boundary condition. Following that, the simulations have been carried out based upon magnetic resonance images at the maximum point of systole. A comparison of the average and maximum values of WSS has shown a high success rate for rescanning. The ability to reproduce results is slightly less, but still comparable to, the ability to rescan sections of the thoracic artery. Voxel-to-voxel comparison has resulted in higher rates of geometric differences. The ability for wall shear stress rescan and the ability to reproduce results has been significantly less than the average/maximum comparison method. A study has been performed by Canè et al. to have a sight at the diagnosis progress earlier. Computational fluid dynamics that are specified for each patient separately based on magnetic resonance or other medical images have been put to use. Left ventricle (LV) shapes have been recreated to evaluate the biomarkers that are based upon hemodynamic parameters to provide help to clinicians on the initial diagnosis, progression, and healing process of ill people. Chimera technique with unfixed boundary conditions has been employed to get rid of the problems of convergency caused by the Arbitrarian Lagrangian-Eulerian approach. The CFD model of the left ventricle of each patient has been built to offer progress. The effects of torsional motion on hemodynamic properties of left ventricles have also been examined during the progress testing stage. CFD simulations of a volunteer in good physical condition have been performed using the magnetic resonance images of the person. Three left ventricle models that have undergone 3 different torsion states have been created and the simulations for 6 cardiac cycles have been performed. The Chimera technique is resilient in balancing the move of impulses coming from the left ventricle letting the variations be seen in each case of the simulations. It has been observed that the torsion affects the blood flow velocity, curling of the velocity field, and wall shear stresses. Energy losses have not been affected by torsion. A two-sided effect has been created in connection with occupancy time: movement of the particles in LV has only been affected by high torsion rates while the injected particles have decreased in a beat. It has shown that the torsion effects might be neglected during operations. Begic et al. researched the differences in the design of stents and abdominal aorta's size-changing (getting smaller in size) utilizing developed methods and outcomes. They also have visualized the progress that the aorta goes through when the stent design has been changed in 3D simulations. A decrease in the pressure that might be useful on less material usage and lowering the cost of the process has been indicated. 3D examination computational fluid dynamics methods have been utilized in the study. The models have been constructed via the student version of Ansys. The balance of the outcomes has been compared with the two-dimensional fluid dynamics results. The greater part of the pressure has been perceived at the center of the aneurysm. 3D simulations have shown that the reduced size of the stents indicates better results. Jayendiran et al. carried out scientific research on the wall shear stress (WSS) and strain profiles at the layers of the aorta vessel as well as the Dacron graft which is a special kind of fabric that placed in the dissected aorta section for treatment to prevent the death of the patient on aorta properties as well as the layers of the aorta. They have looked over to the comeback of the aorta segment when Dacroc graft is exposed to the blood flow making use of the 3D fluid-solid interaction (FSI) method in a program called Abaqus. WSS and strain profiles have been created for each layer of the aorta together with the Dacron graft. Flexible and very elastic models have been adopted to make a comparison on the results when isotropy/anisotropy is presumed. Some assumptions have also been made in their study. The flow is regarded as Newtonian, not compressible, pulsating, and swirling. The consequences have demonstrated that stress distribution at the crossing point of the aorta and Dacron graft was lower considering the aorta's ultimate strength for all of the cases. Plus, no considerable difference has occurred in the radial substitution at the boundaries of the materials. It has been mentioned in Caimi et al.'s study that coronary stents have been mostly used to cure the aorta coarctation (CoA) among people of a wide age range. The reason for that has been told as the preclusion ability with the low probability of side effects of coronary stents. They added that the method has been successful in the short term, the risk of hypertension still has remained. In consideration of that, they have developed a new protocol that is a finite element (FE) to evaluate the results of simulations for patients. Their stent protocol has been tested using 3 different patients' CoA anatomies after remeshing of the geometries have been completed to cope with the CoA challenges. Their new protocol has provided the results for the wall shear stresses on the aorta walls and swelling. In addition to that, the statistical outcomes of the stress and deformation that occur on stents have been yielded. The feedback of the simulations has been obtained to be relatable with the previous studies' results in the literature and their approximation has been suggested to comprehend the patient specified coarctation of the aorta. Zakaria et al. proceeded with an investigation on developing a brand new method to figure out how flows occur in complex geometries like an aorta. It follows that a new grid cartesian method that doesn't require any boundaries (NBF) has been developed. The algorithm of the method has been established on the fluid volume (VOF) color function towards the open-source stage (OpenFOAM). The solid model has been made to treat as a fluid that has a great degree of viscosity to lower its deformation capability hypothetically. The no-slip condition has been assumed at the boundaries. A new simulated term of color function that has a big effect on the occurrence of deformation in the solid area has been described in the mathematical system as the authenticity of their study. Their improved solving program has been confirmed performing a wide range of statistical and empirical results found in the literature. On the grounds of that, they have indicated that their code is very practical since the problem doesn't require a mesh generation to work in complex geometries, unlike other methods. Capellini et al. performed a study comparing various methods used in determining arterial flow and volume. They found that, while the methods of computational fluid dynamic (CFD) and fluid-structure interaction (FSI) are the two preferred methods to determine the volume of blood passing through the aortic vessel, they both have some limitations in the data they represent. Because CFD relies on fixed structures within the aortic vessel, the method is unable to account for variable deformities which might skew the results. FSI relies on presupposed hypotheses to determine the properties of vessel construction and is expensive to compute. To overcome these flaws, a new method is being tested to utilize short-term simulations and Radial Basis Functions (RBF) mesh morphing, a method that can be applied to specific patient needs and dissimilarities during all the stages of the cardiac cycle. During testing, the aorta is cumulatively mapped using the RBF technique, including accurately gauged aortic deformities during the cardiac cycle. When compared to the average fluid volume determined during the CFD process, this new method accounts more accurately for fluid volume and includes variable flow increases and reductions on a patient-to-patient basis. In comparison to the FSI method, this new process is more accurate and accounts for variations in the shape of the vessel, while being less costly to compute. Chi et al. made mention of the number of patients that experienced aorta dissection (AD) has increased over time although cardiovascular illnesses have reduced due to the improvements in medical care and added that there have been two types of aorta dissections, namely, type A and type B. When these dissections are compared with each other, it has been seen that type A is the most health-threatening one and requires an operation to be treated. Accordingly, they have aimed to examine the connection between the wall shear stress (WSS) and the possible tear areas utilizing computational fluid dynamics. 2 healthy aortic vessel geometries and 5 dissected aorta models have been contained. Besides that, shear stresses at elevated levels have also been in conjunction with the reversed flows. The uppermost WSS in clients with dissected aortas has been found as twice as the ones in the control group. It has been observed from the computation fluid dynamics outcomes that the wall shear stresses have been reduced in the aorta that has no dilatation whereas the differences in the blood pressure have been much higher as compared to the aortas with dilatation. There have been considerable changes in bending degrees of the AD conditions between the normal and dissected aortas. As a result of this, dilatation has been found as a key factor that causes type A dissection. Hansen et al. applied the vector flow imaging (VFI) method which is useful to evaluate the flows in complex geometries ultrasonically to the ascending aorta of patients who experienced different stenosis types in their aorta regions and underwent a treatment process. 30 patients with tricuspid, bicuspid aortic valve stenosis, and healthy aortic valves have been scanned via VFI and a machine called conventional spectral doppler that yields illustrated profiles of flow speed. An overcomplicated flow has been observed in the tricuspid aortic valve as compared to the bicuspid AS but the flow speed has been much higher for two of the situations in comparison with the healthy aortic valves. In the end, the outcomes have demonstrated that the method of vector flow imaging can generate novel parameters for flows and implant evaluation. Lopes et al. carried out a study on the behavior of blood flow in carotid arteries to find out the difference in parameters on elastic and rigid walls. On that account, geometries of arteries have been constructed for each person employing transient boundary conditions. Computational fluid dynamics has been used to examine only the blood flow behavior when the properties of rigid walls have been checked. fluid-solid interaction between the arteries and blood flow has been investigated for the elastic walls. Subsequently, a study of fluid-structure interaction has been performed. In addition to what has been said, the impact of atherosclerosis on blood flow has been found to have a stiffing effect on the artery's mechanical properties as the uniqueness of their study as compared to other works in the same field. The outcomes have demonstrated that wall shear stresses in the carotid sinus have been small, which has made it a preferable area to evaluate atherosclerosis. In the same manner, it has been observed that arterial walls can be considered elastic since the rigid model in the study has forecasted the wall shear stresses and flow speed. For other mechanical properties of the examined vessel, the influence of atherosclerosis has been obtained to be small, in the profiles of wall shear stress. Despite what proceeded, dissipation and blood flow velocity profiles should be considered for the arteries that have undergone stenosis. Neidlin et al. mentioned in their study that subclavian arteries provide an alternative area for left ventricular assist device (LVAD) as a consequence of having easy surgical entry and implementation in risky patients. Since the clinical results have been strongly affected by the blood flow characteristics, dissimilar inserting zones can be evaluated through the length and breadth of LVAD support. The workability of right and left subclavian arteries (SA) has been researched for the ventricular assist device HeartWare HVAD with the employment of a statistical multi-scaled model. 3D model of the aorta has been constructed and linked to a plodded model placed in the cardiovascular system in the process of LVAD assistance. 3 disparate angles have been used in the graftings of right and left subclavian arteries. In addition to this, modeling of the typical graftings for the descending and ascending aortas has been completed. Analysis of full land half supportive LVAD processes has been accomplished in the beating and anti-beating modes. The positioning of the grafts has been examined for the brainal and coronary passage of the blood. The effect of crosssection angle between the two blood vessels on wall shear stress distribution has been assessed. When usual cannula positions have been taken into consideration, it has been seen that left and right SA graftings had similar hemodynamic undertakings. The results have demonstrated that the difference in angles of graft anastomosis while going from ninety degrees to thirty degrees can increase the blood flow speed up to nine degrees starting from six degrees reducing the wall shear stresses thirty-five percent. Plus, the insertion of the cannula of subclavian arteries is found to be a suitable anastomosis area for the research vessel that is supported by LVAD. Usage of a channel to produce picture-based statistical simulations for the hemodynamics inside of the heart is researched by This et al. Data of 12 people has been used to compute the capacity of the pipeline. The whole prescribed processes have been completed by automated action of the system in fifty-five minutes and low errors have been obtained in comparison with the spatial resolution processes. Following that, the pipeline has been utilized to investigate the hemodynamics of the mitral valve that experienced diseases. It has been observed that the inconsistency in the vicinity of computer-generated cases is principally caused by the shape of the valve and restating specifics. The surroundings of the PISA method has been decided by the statistical simulation outcomes taking into consideration the various type of MR. Although the PISA method is useful to give reasonable results for simple spherical regurgitation cases, it has also been gained from the results that inconclusive estimations are acquired for the not spherical case outflows. Over and above that, it has been illustrated that the preference for a higher degree aliasing speed might give rise to complexities in evaluating MR. Zhuo et al. presented a study about the shape of the vessel, stream pattern, wall shear stresses, and velocities of flows since these parameters create great importance in constitutional heart improvement. In such a manner, a wild mouse has been subjected to analysis. Micro ultrasound method has been used for tiny animals to observe the boundary conditions of blood and flow speed properties in bigger arteries. The boundary conditions of blood flow have been employed to create the biggest artery and arc of the aorta at a subsequent time. Speed of blood flow has been used as an input for computational fluid dynamics simulations to illustrate hemodynamical properties. Ultrasound measurements have shown that blood flow speed in the biggest artery and arc of the aorta had had a powerful relationship with the vessel sizes whereas the pressure of the blood hasn't been affected by the size. Wall shear stresses have been found to increase towards the vessel branches the magnitude of these stresses has decreased towards the root of the aorta. The values obtained for the descending aorta have been observed to have a relation with fluid mechanics to some degree. Hameed et al. applied computational fluid dynamics to find out the hemodynamic differences in a reconstructed aorta. They have exerted multiple scales computational fluid dynamics analysis of a patient-specified anatomical structure along with the assumption of a non-newtonian model and unstable smooth fluid motion cases. The constructed three-dimensional model has been connected to a zero-dimensional model to conclude the boundaries of the condition. It has been mentioned after the results are obtained that the discharge at the respiratory exit has caused an area where the flow is under the normal speed. Likewise, the changes that occurred in the hemodynamic parameters are convenient. Bruening et al. proposed a study about the investigation of hemodynamic parameters after a valve replacement process utilizing a patient-specified model since their importance in the cardiology area has increased due to their forecast ability. In consideration of the fact that the flow profile in the left ventricle can't be known earlier than the medication happens, the hemodynamic properties have been investigated after the valve renewal. The properties have been computed based upon independent inlet profiles, namely, a common stopping profile and a profile originating from four-dimensional magnetic resonance images. Tolerable parameters haven't been affected using these profiles. An all-encompassing profile has been attained to be enough for forecasting the hemodynamics avoiding having a comply with the difficulty in estimating patient-specified boundary conditions. Hochstuhl et al. aimed to verify the computational fluid dynamics simulations of left ventricular assist devices (LVAD) quantifying the blood flow in three-dimensional reproduced aorta geometries of the patients since usage of LVAD for a long time needs a superior comprehension of differences in hemodynamic parameters further on transplanting. It has also been stated that these computational fluid dynamics simulations are useful to see the patient-specified hemodynamic parameter changes that especially occur in wall shear stresses and pressures. They have created a circuit of a combination of left ventricular assist device and aorta and the outcomes have been contrasted with the computational fluid dynamics simulations. Deriving from the computed tomography angiographies of 5 people with LVAD, the aorta anatomies have been constructed and copies have been imprinted. A fluid of consisting glycerol and water has been used instead of blood for the LVAD machine. The flow that occurred in the circuits has been examined utilizing magnetic resonance imaging. In addition to this, computational fluid dynamics simulations of the patients with left ventricular assist devices have been executed. When the variance of these 2 methods has been checked, it has been seen that there have been no big differences. The results have been attained similar to each other in terms of flow patterns and volumetric flow rates. A study about avoiding the ascending thoracic aortic aneurysm (ATAA) which is responsible for the weakening of the wall of the aorta has been performed by Mousavi et al. It has been added that ill people that have premolar aortic valves found to have a high relation with ATAA occurrence. Therefore, a statistical computational fluid dynamics and four-dimensional magnetic resonance imaging connected with finite element (FE) method has been suggested to make a simulation on the hemodynamic changes and growth and remodeling (G&R) that occur in the aorta of each patient. Four-dimensional magnetic resonance images that contain the information of geometries of the aortas and blood flow speed have been used to decide the boundary conditions. Wall shear stress evaluation and related residency time (RRT) along the walls have been yielded by the computational fluid dynamics simulations. A low blow has been put to use afterward on the finite element model undertaking the volume of the blow would associate with the related residency time acquired from the computational fluid dynamics simulations. Moreover, simulations of the G&R have been accomplished. The component compartments in the finite element models have been improved repeatedly. Data of 2 well and 2 ill people have been utilized. The frameworks of the G&R have been regulated taking cognizance of the earlier created mathematical models of the ATAA increase proportion. Simulation outcomes have demonstrated that the stiffness of the walls plays a great role in the progression of ascending thoracic aortic aneurysms. In addition, cells that are sensitive to mechanical stimuli have been observed to be of great importance in ATAA.

As discussed in the literature survey above, there is still a huge gap in the utilization of computational fluid dynamics on aorta diseases. In this thesis, unlike the above-mentioned studies, a comparison has been made on the change of parameters between the repaired and covid-affected aorta. Furthermore, some parameters such as blood flow, stress on the vessel walls, and volume change occurred have been examined. The outcomes obtained are promising when compared with the results of healthy vessel analysis in the literature. It has also been concluded that the method used to obtain these results could be used in future studies.

4. MATERIALS AND METHODS

With the developing technology of our age, new technologies and techniques are emerging in many fields every day. One of these new techniques is the utilization of medical imaging programs and engineering programs together. In this way, it is possible to analyze the effect of diseases that endanger human health in some engineering programs after their construction are taken from the visualization programs so that their effects can be examined in detail. In this thesis, 3D Slicer, in which organs can be visualized and reconstructed, and Ansys, in which a wide range of analyzations are possible from the littlest to the most complex components, are cooperated. The change in hemodynamic parameters of an aorta that has undergone thoracic surgery and the aorta of a patient that is affected by the Covid virus have been investigated.

4.1. 3D Slicer

3D Slicer software is used for the visualization and analysis of bones, vessels, and similar structures in 2D, 3D, or 4D formats in the healthcare field (Fedorov, 2018.). Vessel segmentation, surfaces of organs, and vessels can be reconstructed with this program. The analysis section in the program includes many functions related to segmentation, recording, and analysis. This program also provides great benefits for researchers to develop and evaluate new methods quickly. All the features in the program are equivalent to those in Python and C++ programs. In addition to all these, it plays a great role in quickly creating product prototypes and presenting these products to potential users. In this way, it is easy to focus on developing new features. The fact that the program has an uncomplicated interface and is completely free to use also provides a big advantage for users. An aorta segmentation example is given in Figure 21.

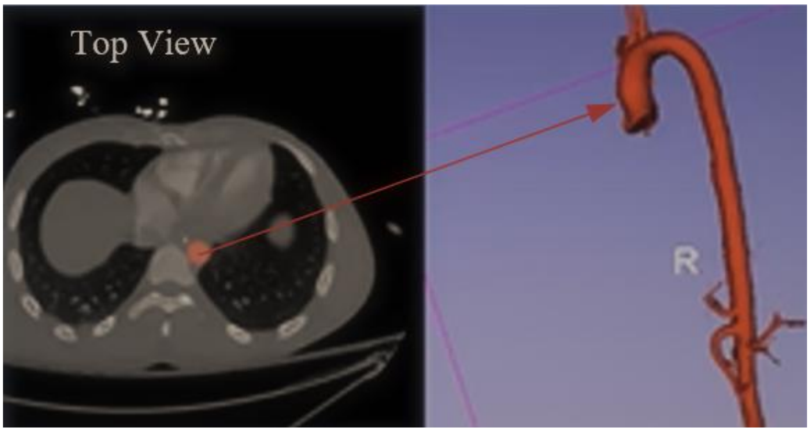

Figure 21. Aorta segmentation in 3D Slicer [26]

4.2. General CFD Procedure

CFD is a method that solves flow analyses with a large number of numerical equations and is frequently used in engineering applications. While performing flow analysis with CFD, different algorithms are used in addition to mathematical methods and equations. The result of these is transferred as a simulation. CFD is a method used in analysis programs such as ANSYS. Transferring the problems in fluid behavior to the computer environment using certain algorithms and analyzing them through simulation can be defined as CFD. Some special software is used for CFD analysis. Certain steps must be followed for the analysis to take place correctly. The steps that can be followed and the CFD analysis are generally as follows (Opal Mühendislik, n.d.):

1) The 3D model of the part to be analyzed is prepared with CAD or a suitable program and the prepared model is transferred to ANSYS SpaceClaim software.
2) Flow volume is created via the ANSYS SpaceClaim program.
3) After the flow volume, mesh, that is, a finite element network is created.
4) CFD modeling is done and the process is completed with solution settings, taking the solution, obtaining and reporting the results.

4.2.1. Features of the CFD Method

1) Applications of Flow Control: More advanced designs are provided when enhanced flow distributions are needed.
2) Thermal formation of prototypes: Effects of all types of heat transfer can be investigated.
3) Structural applications: More optimization designs are possible.
4) Free exterior design: Boundaries between liquids and gases or solids can be simulated.
5) Specific equation usage: Any equation related to the interest area can be defined in the system for the analysis.
6) Smart mesh optimization: Mesh automation can be applied to all surfaces.

4.2.1.1. Dimensional Modeling

Reconstruction of vessels, bones or any part in 3D can be reconstructed by many programs. Programs such as ANSYS, 3D Slicer, Mimics Innovation Suite, 3-Matic, Meshmixer, SolidWorks, Catia, Autocad are among the most used programs for creating, editing, and analyzing these reconstructed geometries. In this thesis, after the computerized angiographic tomography images were taken, aorta segmentations were completed using the 3D slicer program. Afterward, the Meshmixer program was utilized to prepare the vessels for the analyses. The reason for that is to perform analysis in Ansys, the surfaces must be smooth and this can be easily done with the meshmixer program. An instance of a reconstructed vessel used in this thesis is indicated in Figure 22.

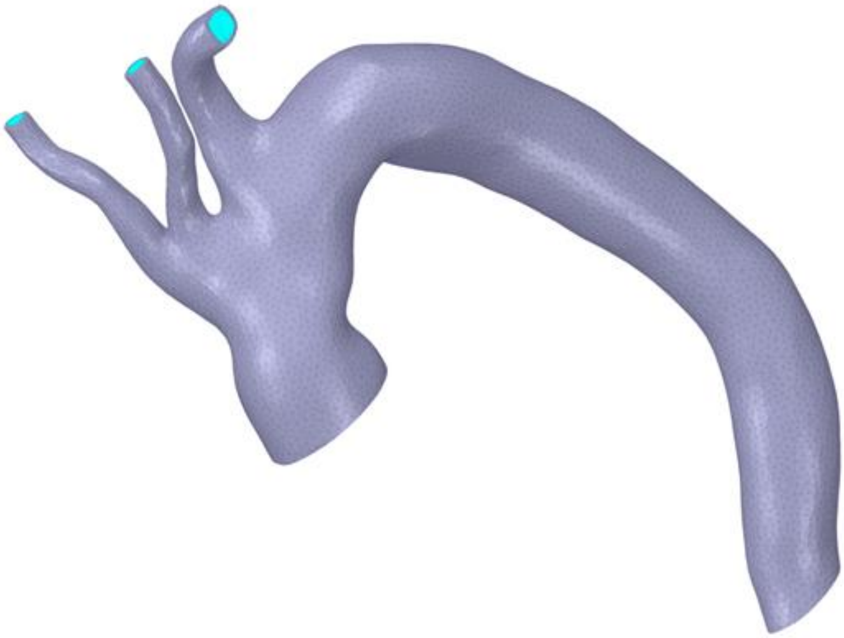

Figure 22. A repaired reconstructed aorta [26]

4.2.1.2. Clustering

Clustering aims to separate the necessary place where the flow will occur in each geometric element named grid cells that equations are utilized. For that purpose, the ICEM module of ANSYS is employed. Complex geometries and a wide range of mesh types and generations can be created in this module. The kinds of elements that can be formed with this module are demonstrated in Figure 23.

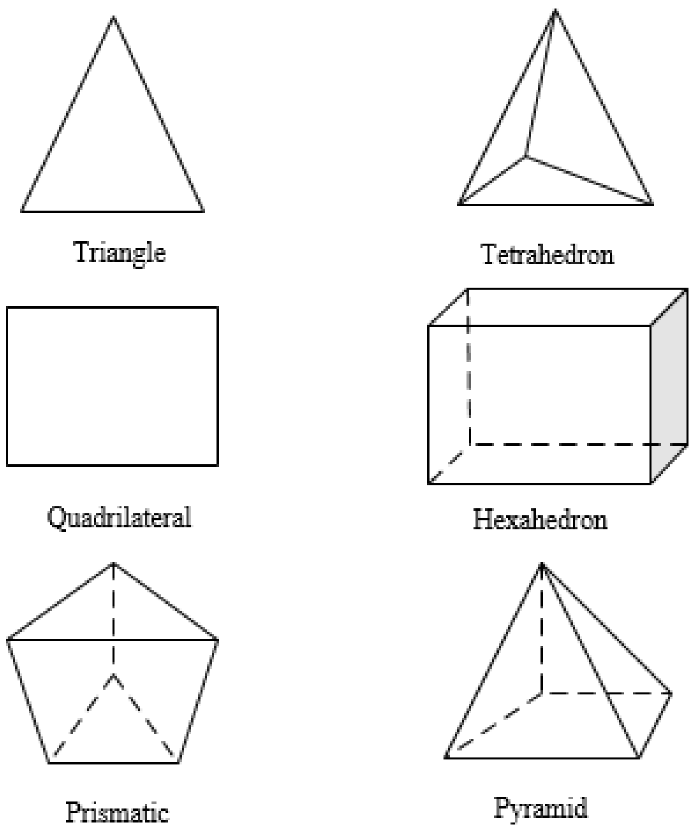

Figure 23. Element types in ANSYS-ICEM [3]

4.2.1.2.1. Type of Mesh

There are mainly 2 kinds of mesh structures, namely, structured and unstructured. Structured mesh is based on a standard connection which is usually specified by 2D or 3D arrays. These arrays lower the requirements of storage and create effective solving algorithms. There is a restriction in the utilization of a structured mesh. When there is a need for a mesh formation on surfaces, a quadrilateral structure needs to be used whereas a hexahedral structure is used for volumes. An instance of a structured mesh is indicated in Figure 24. The reason for this mesh type to be chosen is that it provides solutions with great accuracy although the creation of these structured grids takes a long time.

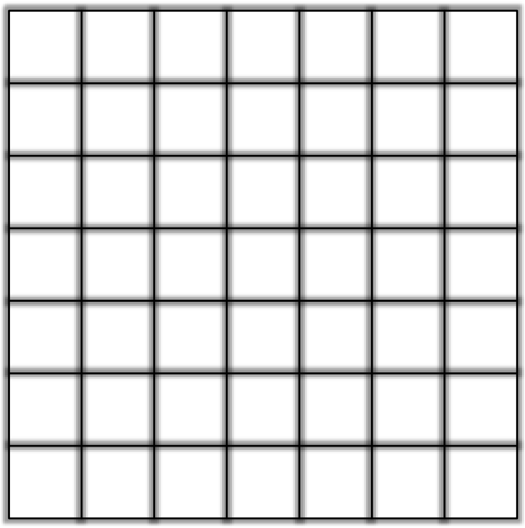

Figure 24. A structured mesh example [3]

An unstructured mesh may consist of whole element types shown in Figure 23. In these types of situations, they are mostly called mixed or hybrid mesh. Triangular shapes are generally formed on the surface of bodies and tetrahedron type is created on volumes. The order of the elements in this mesh type is random, as demonstrated in Figure 25. It is the most preferred mesh type in commercial solving systems at present. Local connection between the dissimilar cells caused by the non-uniformity of the mesh structure has to be stored as more space is needed as compared to structured mesh. One of the advantages of employing unstructured mesh is the operation of automation so that the mesh is distributed without changing the shape of the geometry to a great degree. When these pluses and minuses of the mesh structures are taken into consideration, the unstructured mesh type is chosen for the complex vessel geometries.

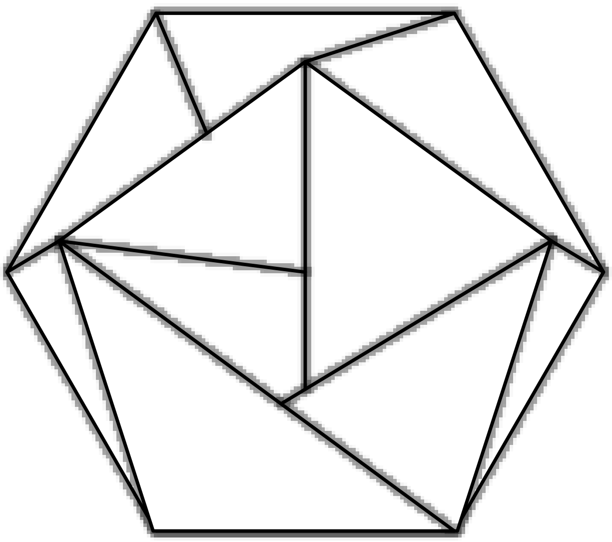

Figure 25. An unstructured mesh example. [3]

4.2.1.2.2. Mesh Selection Criteria

Some points to consider when choosing mesh are as follows:

1) Deciding on Element Type and Size: It is critical to select the proper component shape and utilize it in the requisite quantity is limited components to achieve a realistic result. The size of the elements employed should ideally be minimal enough to examine differences in the computational domain. Using a big number of needless pieces is likewise unacceptable. In this situation, there is an excessive amount of calculation time required, and the likelihood of a statistical inference overestimation. Element sizes should be reduced in parts that affect the result more, such as in regions where stresses are intense. A view of a cubic geometry with different mesh numbers and sizes is shown in Figure 26.
2) Attention should be paid to the allowable deformities in the geometries: In cases where the shape is complex when knitting with geometric shape elements, or when the appropriate element mesh cannot be formed, the elements are extremely deformed in some regions. In such places, care should be taken to ensure that the deformation of the elements is within acceptable limits. While meshing (while the element mesh is being knitted), leaving the control completely to the program can sometimes give this result. For this reason, before meshing, which edges will be divided into how many parts, or what element sizes to be used in those regions are decided by the user.

A view of a cubic geometry with different mesh numbers is shown in Figure 26.

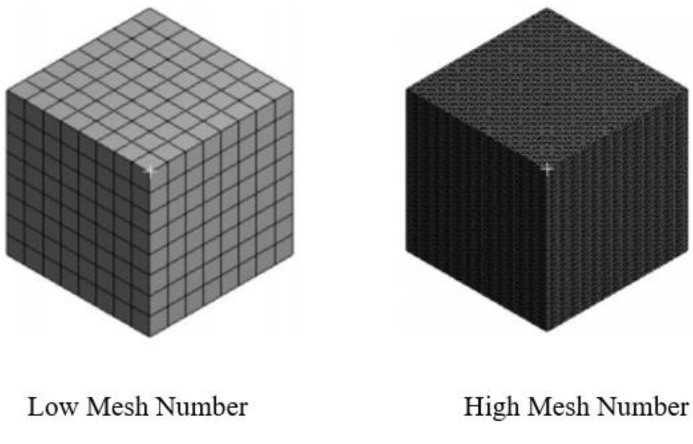

Figure 26. Comparison of mesh number and size on the same geometry [21]

4.2.1.2.3. Meshing Methods

There are many mesh creation methods in Ansys and choosing the right method for the part to be analyzed is important. These methods are automatic, tetrahedrons, hex-dominant, multizone, cartesian, and sweep and you can select the division number of elements, respectively. Figure 27 shows an example of each method on the same element.

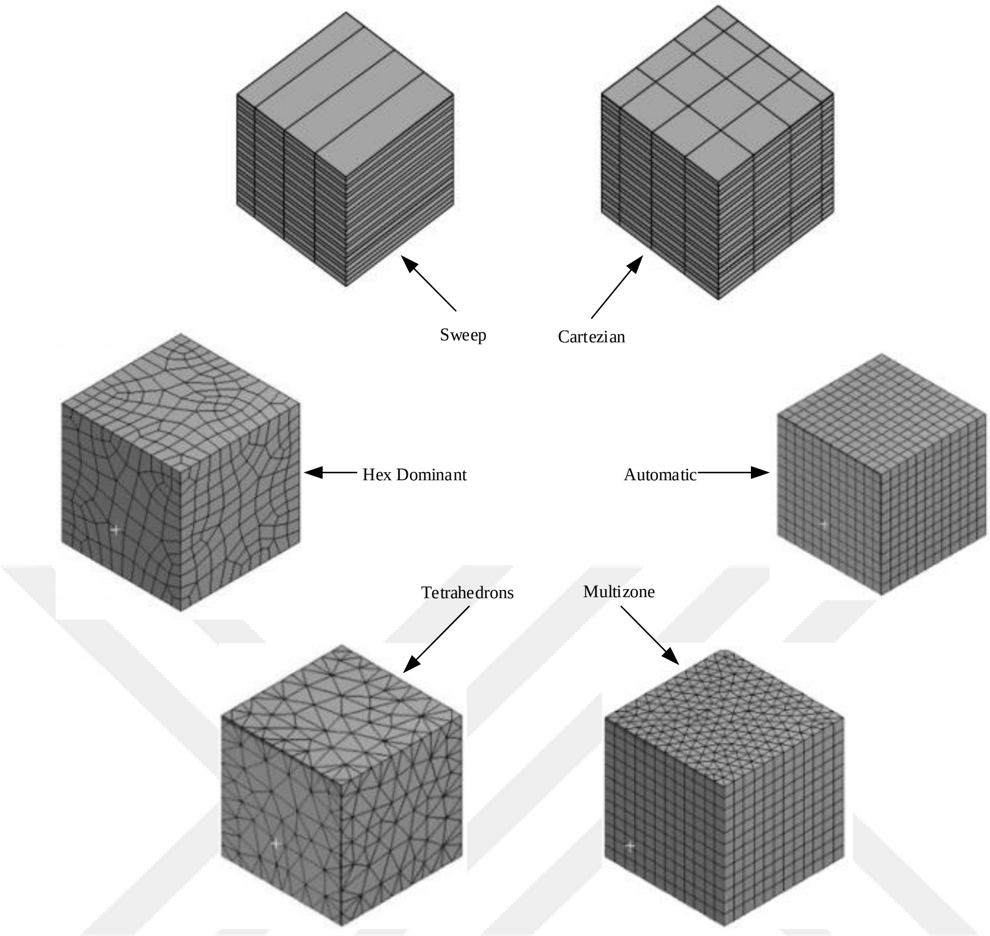

Figure 27. Meshing methods [21]

In this thesis, the hex dominant method was used for aortic vessels and smaller meshes were used at the borders.

4.2.1.2.4. Mesh Quality

Quality of the mesh has a significant impact on the accuracy of the results. Following are the main four major parameters that influence mesh quality (Dassault Systemes, n.d.). These are growth rate, aspect ratio, jacobian ratio, and skewness. A mesh with uniform regular tetrahedral elements with equal length sides achieves the maximum numerical accuracy for a solid mesh. A mesh of regular tetrahedral elements cannot be created for a general geometry. Due to small edges, curved geometry, thin features, and sharp corners, some edges of certain rendered elements may be much longer than others. When the edge lengths of an element are very different from each other, the accuracy of the results decreases. The aspect ratio of a regular tetrahedral element is the basis for calculating the aspect ratios of the other elements. The aspect ratio of an element is defined as the ratio between the longest side and the shortest side drawn from a vertex to the opposite face below, normalized to a regular tetrahedron. A uniform tetrahedral component has a ratio of one by definition. The aspect ratio verification implies that linear sides link the four-sided elements. The application uses image resolution control to direct and manage grid size. Hyperbolic components are substantially more precise at mapping curved shapes than linear elements with the same length. The model's exact topology is placed on the semi nodes of an entity's border edges. Putting semi nodes over the real shape at excessively sharp or curved borders might result in deformed parts with infrastructure to meet. A minus Jacobian value is found in a strongly deformed element. The analysis software will stop working if an element has a negative Jacobian dot.

The main factors affecting the mesh quality and their numerical meanings can be defined as (İpci, n.d.):

Growth rate: It refers to the gradual growth of the mesh. The more this ratio can be kept close to 1, the higher the quality of the mesh will be. The effect of growth rate on the mesh is shown visually in Figure 28.

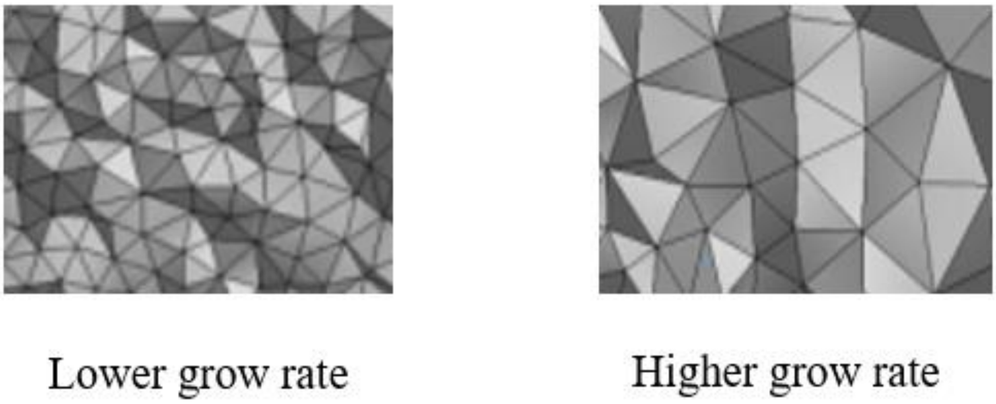

Figure 28. Different growth rates of mesh on the same geometry [62]

Aspect Ratio: It is the ratio of the largest edge to the smallest edge of the mesh. The numerical explanation of the numbers in terms of mesh in the aspect ratio topic is shown in Table 1. Values greater than 10 starts to give incorrect results.

Table 1. The relationship between the aspect ratios and mesh conditions. [25]

Aspect Ratio (AR)		Mesh Condition
AR = 1	→	Perfect
1 < AR < 3	→	Good
3 < AR < 10	→	Acceptable
AR > 10	→	Unacceptable

Jacobian Ratio: It is related to the curvature of the elements. Jacobian points are used for quality elements. Table 2 shows the connection between jacobian ratios and element states.

Table 2. The connection between jacobian ratios and element conditions. [25]

Jacobian Ratio (JR)		Element Condition
JR = 1	→	Perfect
1 < JR < 40	→	Acceptable
40 < AR < …	→	Unacceptable
0 < JR < 1	→	Can never be accepted

Skewness: Compares the current mesh structure with the optimum mesh structure. It is applied only to triangles and tetrahedra according to the current volume deviation, and to all cell and face shapes according to the normalized angle deviation. The relation between the meaning of numerical skewness values and the quality of the mesh is shown in Table 3.

Table 3. The effect of skewness on the mesh quality [25]

Skewness (S)		Mesh Quality
0 < S < 0,25	→	Excellent
0,25 < S < 0,50	→	Very good
0,50 < S < 0,80	→	Good
0,80 < S < 0,95	→	Acceptable
0,95 < S < 0,98	→	Bad
0,98 < S < 1	→	Unacceptable

4.3. The Steps Followed to Complete the Aorta Analyses

	Explanation of the Steps
1) Obtaining necessary computed tomographic angiography (CTA) files from the doctor has been completed.	This is the initial step of beginning a vessel analysis. To analyze the vessels, their geometries have to be reconstructed. This construction is possible via computed tomography or magnetic resonance image files that are taken from hospitals.
2) CTA files have been transferred to the 3D Slicer program	In order to make these CT files usable, the free 3D Slicer program, which fulfills the function of viewing the files and recreating the vessels, has been used. Plus, the quality of the images has been checked.
3) Hearts of the patients have been created virtually and the separation of the aortas from other vessels has been accomplished.	The visualization process of the hearts is an important step because it facilitates the detection of the aorta and its separation from other vessels. This visualization process also needs to be done meticulously, otherwise, the analysis will not yield realistic results.
4) Surfaces of the reconstructed models have been smoothed and solidified.	To be able to perform an analysis in Ansys, the surfaces of the parts must be both smooth and solidified. Therefore, after the surfaces are cleared of surface defects, solidification must be applied and saved in solid format to start the analysis.
5) Each analysis has been started accordingly after the solidified models have been imported to the Ansys workbench.	After the necessary arrangements have been made on the reconstructed vessels in the Ansys workbench, vessel analyzes have been started, respectively.
6) The consistency of the outcomes has been compared with the results of different vessel analyses in the Literature and the consequences have been saved into the computer.	The consistency of the results has been checked by comparing the results of some vascular studies in the literature providing the advantage of commenting on the accuracy rates

4.4. Reconstruction of the Aorta Geometries

The creation processes after the tomography images of the aortic geometries are transferred to the system are given below, respectively.

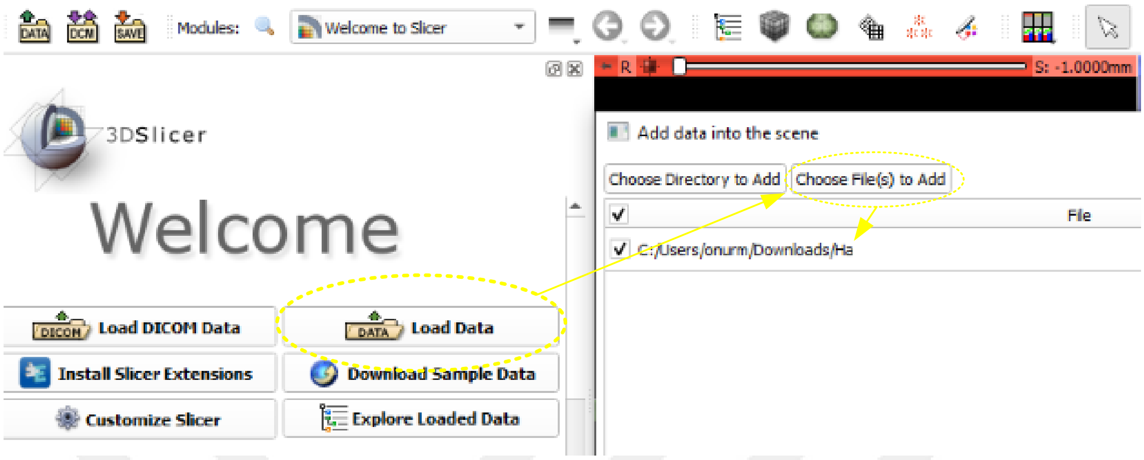

Figure 29. Introducing aorta files to the system [26]

After the 3D Slicer program is opened as a starting step, the files obtained from the doctor were introduced to the system since a certain geometry is needed for analysis (Figure 30). Then the Crop Volume command was chosen since the system must focus on the region of interest (Figure 31). Otherwise, many organs and bones will be included in the created image in addition to the aorta. If more details are desired in the images, the spacing scale can be increased in this section. In this thesis, it is adjusted as 3 times more of the normal value.

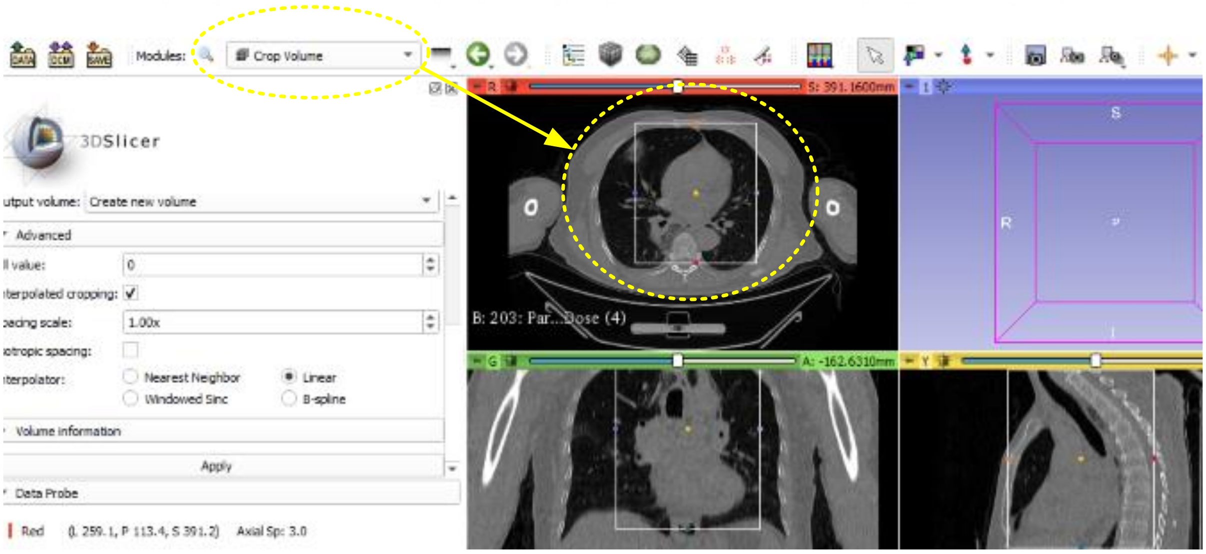

Figure 30. Crop Volume command [26]

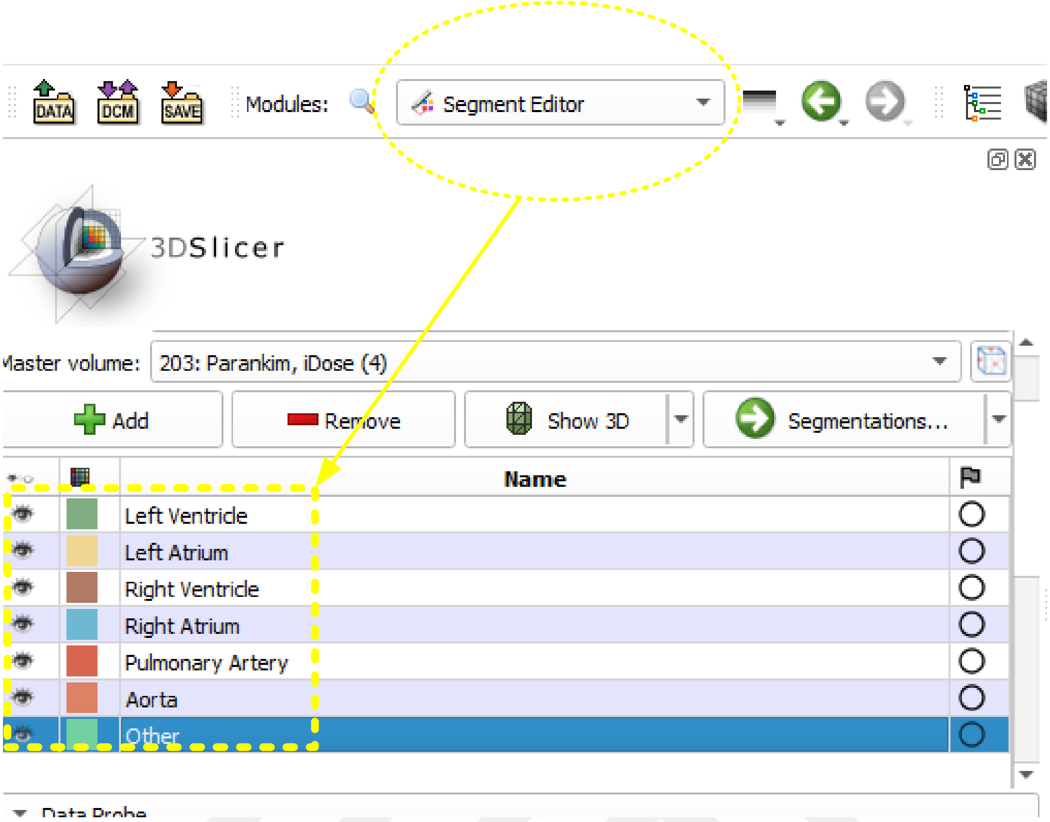

Figure 31. Segment Editor Command [26]

As the next step, the segmenting module is opened. This module is important for determining the boundaries of the aorta and its surrounding vessels. Otherwise, many unwanted vessels and bone structures will be formed. Boundary conditions were created from the left ventricle, left atrium, right ventricle, right atrium, and pulmonary artery. These veins are the veins that originate from the heart and are the most suitable veins to form a border to the aorta. Although boundaries are created, a section named other is also formed to crop the unwanted areas. After the locations of the relevant veins are introduced to the system, the regeneration of the heart is completed with the grow from seeds command. Figure 33 shows the grow from seeds and other auxiliary commands.

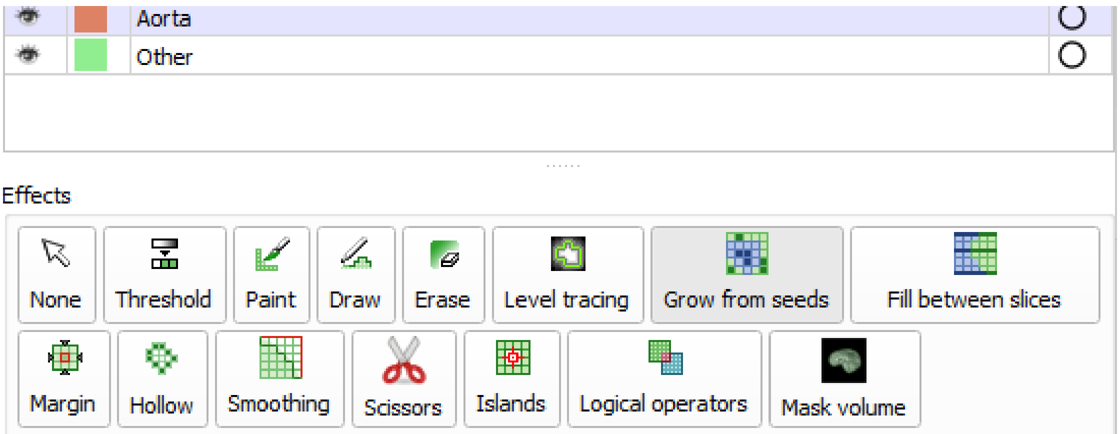

Figure 32. Other helpful commands in the system [26]

The heart sample created after completing all these steps is shown in Figure 33. Now sequentially non-aorta vessels can be closed in the system and saved in other formats for further editing.

Figure 33. An example of a heart created using 3D Slicer [65]

4.5. Analysis

The steps taken by the reconstructed aortic vessels until the analysis is started in ANSYS are given below in order.

First, Ansys Workbench was opened. Under analysis systems, Fluid flow (Fluent) was found and dragged into the project schematic (Figure 35) and given a name depending on the case. The names of aortic vessels 1 & 2 are given to the projects in this thesis. The next step is to open the Geometry section and import the solid model. Geometry is created with the Generate command (Figure 36). In this way, the geometries are introduced in Ansys and ready to be processed on them. It should be noted that the imported geometry consists of a single surface and body. If there are many surface parts in the geometry, the results are negatively affected both during meshing and in other steps, considerably slowing down the preparation of the analysis process. Therefore, all surfaces should be merged as one piece and transferred to the system as one-piece solid. The next steps continued with the preparation of the aorta models for mesh. After the part was generated, virtual topology was applied to the model. The next steps continued with the preparation of the aorta models for mesh. After the part was generated, virtual topology was applied to the model. Virtual topology is a feature used to stick surfaces on the geometry together and make it easier for the program to recognize the geometry. Thus, it would help with the meshing. A simple example of virtual topology is shown in Figure 36. Because of the very complex structure of the aortic vessels, a whole virtual cell couldn't be created. There were some surfaces where the curvatures changed too rapidly and those surfaces could not be merged into one surface cell. So, the main geometry was separated into 8 parts.

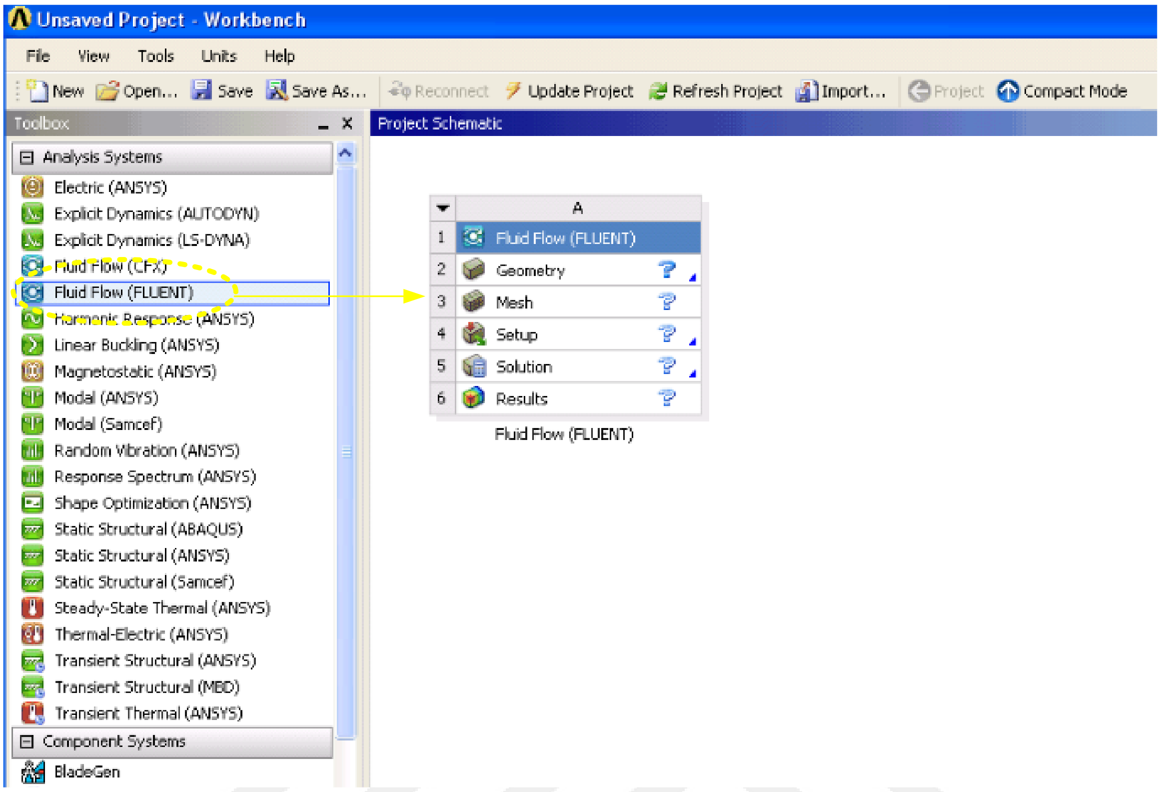

Figure 34. Opening Fluent Flow in Ansys Fluent [3]

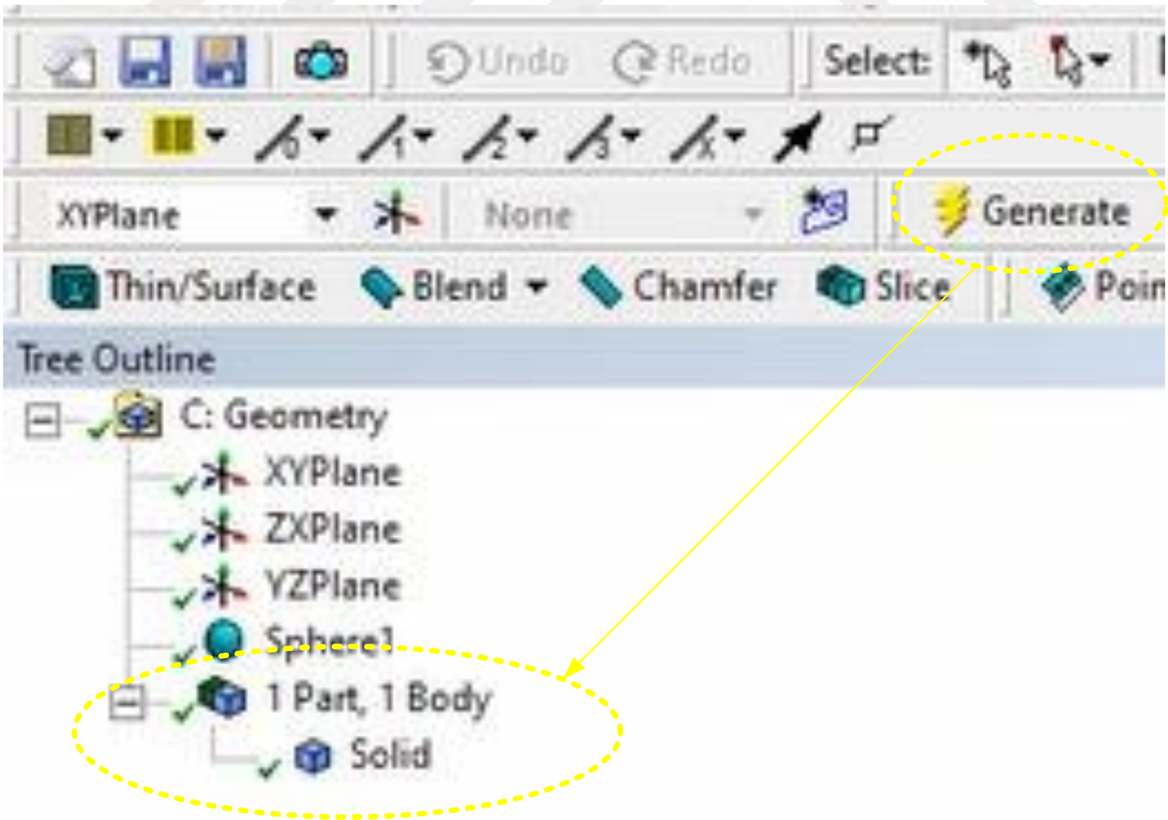

Figure 35. The Generate command in the Geometry section [3]

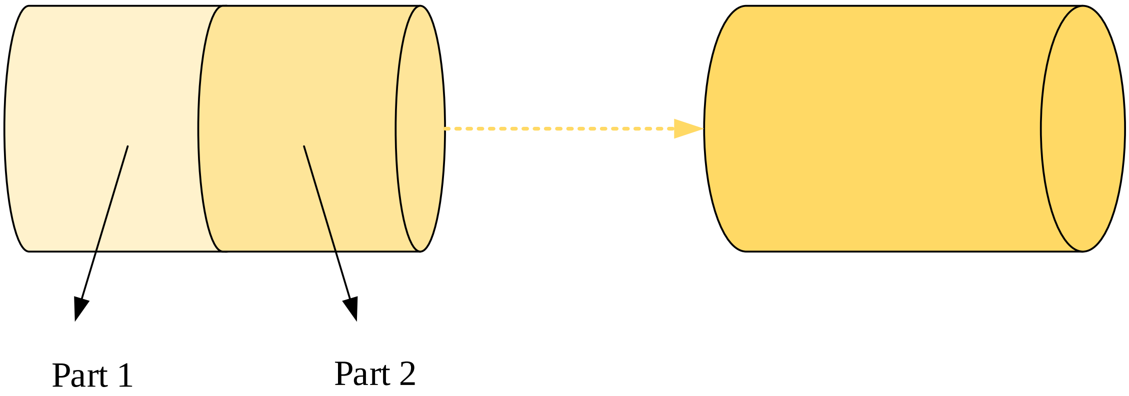

Figure 36. A virtual topology example

There are some very important points to consider in this step. When choosing surfaces, it is necessary to make sure that inlets and outlets are not selected. Otherwise, the inlet and outlet ports of the blood will mix during the analysis, preventing the analysis give correct results and even errors forcing to analysis to stop. After all the necessary surfaces have been selected, virtual cells have been injected into the model. Although it was time-consuming progress, it was a necessary step to make it much easier for the program to calculate the mesh. Afterward, the surface mesh created by the computer was previewed. The purpose of previewing the surface mesh was to see how the mesh goes so that we could add more constraints to it to make the mesh more reliable. To preview the mesh, these steps have been followed: Toolbar > Tools >Options > Mechanical> Graphics> Mesh Visibility > Automatic to Manual. The Mesh button is used to show the mesh or return the mesh off. On geometries, there were some regions where the mesh was extremely dense, these regions represent the boundaries between the virtual topology cells. For this reason, some adjustments have been made to make it less dense on the constructed bodies. An instance of these boundaries is demonstrated in Figure 37.

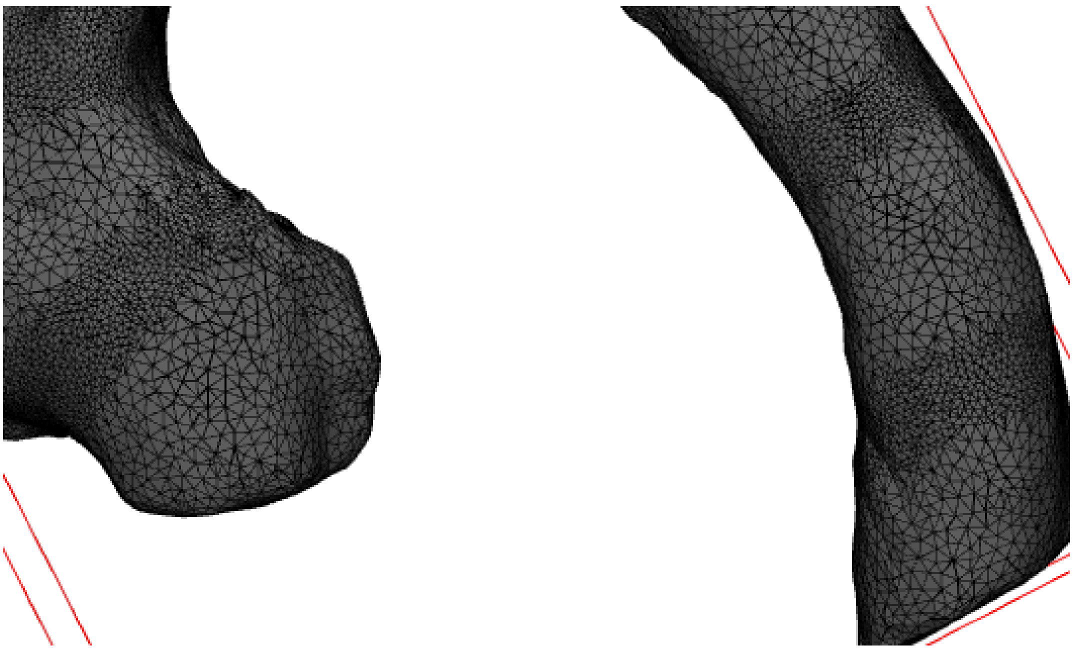

Figure 37. The border areas with different mesh density [3]

However, in the currently formed geometries (at the region near the vessel walls), there were no dense cells at the inlet and outlet boundaries, making it difficult to understand what was going on at those points. This is an important detail if we want accurate results in fluid dynamics. So body sizing and inflation were applied to fix this problem. Inflation details are given in Figure 38. The whole geometry entity was selected for both the inflation and body sizing (Figure 40) in the body selection option.

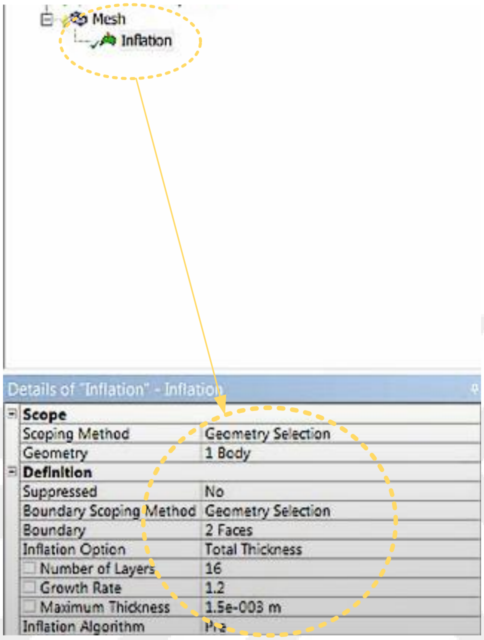

Figure 38. The inflation details [3]

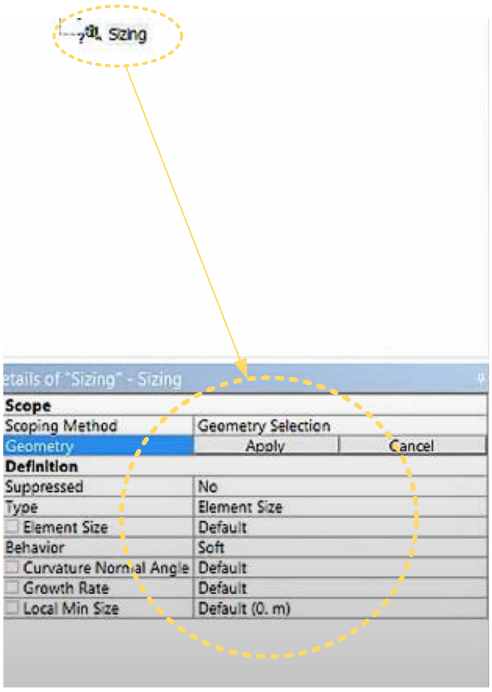

Figure 39. The sizing details [3]

Element size was adjusted to 0,001 meters for the examined vessels. The named selections were chosen for the body selection method in inflation. The advantage of using named selection in the preparation step of analysis is the program lets you pick the whole area instead of picking the little areas one by one. Plus, the walls of the arteries were picked as the boundaries. The total inflation thickness was decided to be 0,0006 meters using the trial and error method for the aortic vessels depending on their thickness. The following steps have been implemented for the purpose: inflation mesh>inflation option>total thickness. Subsequently, the inflation preview was checked. When all these steps were completed, the actual mesh generation was started. Correspondingly, section planes were added to see the mesh more clearly. The progress during the meshing of geometries is shown in Figure 40.

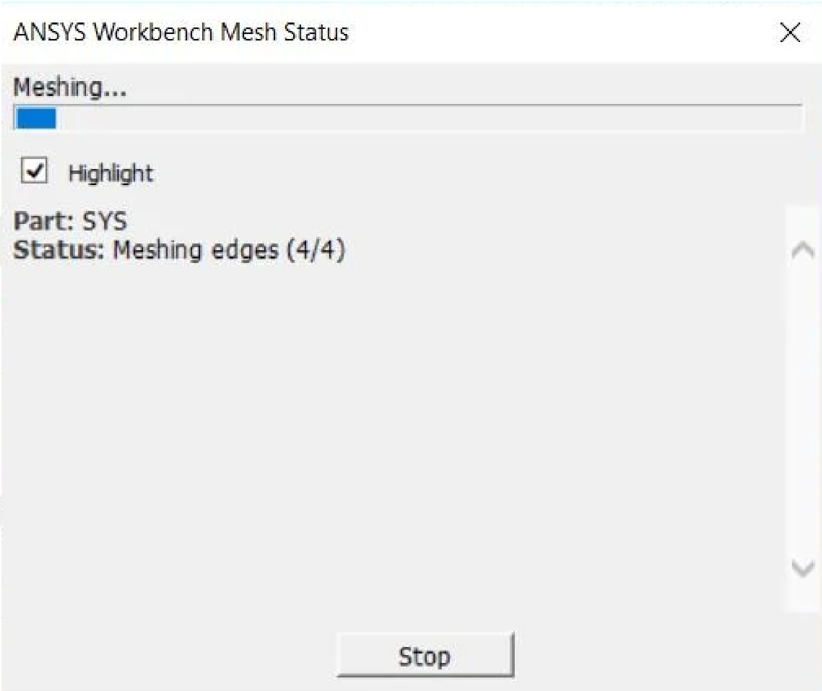

Figure 40. The meshing progress [3]

Then, mesh was updated on ansys workbench to turn that yellow lighning sign into a green tick to perform analysis. When the mesh can not be formed properly or there are errors in the geometries, the yellow lightning part does not turn into a green tick and the analysis cannot be performed. Since the geometries were prepared with great care in this thesis, such errors were not encountered. A full mesh image of one of the vessels prepared for analysis is shown in Figure 41. After all meshing processes were completed, the analysis details were determined. The setup tab is opened, double precision is selected and a fluent window is expected to appear (Figure 43). These initial settings are just as important as the other steps because a decision has been made on how accurate the results were desired. Under the General tab (Figure 44), the time was arranged as transient since our velocity profile changes through time and it is not a steady solution. As additional information, if a steady solution is going to be made in ANSYS, there is no need to make any changes to the models.

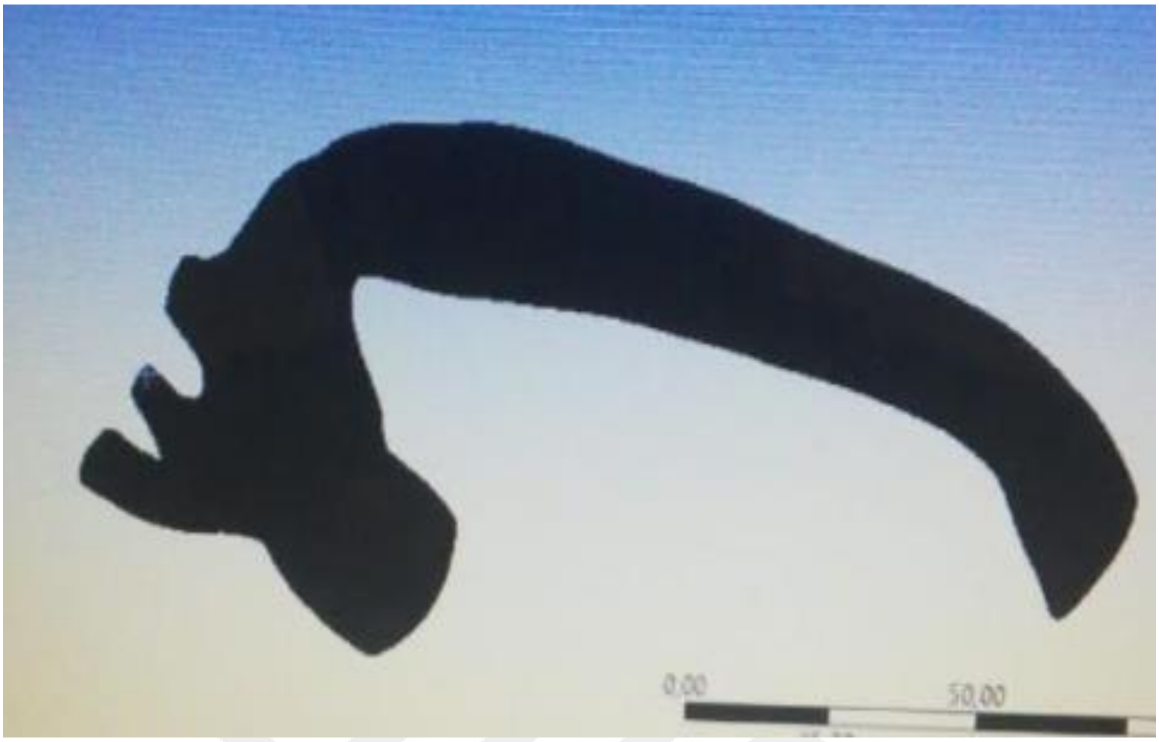

Figure 41. One of the aortic vessels prepared for analysis after meshing is completed [3]

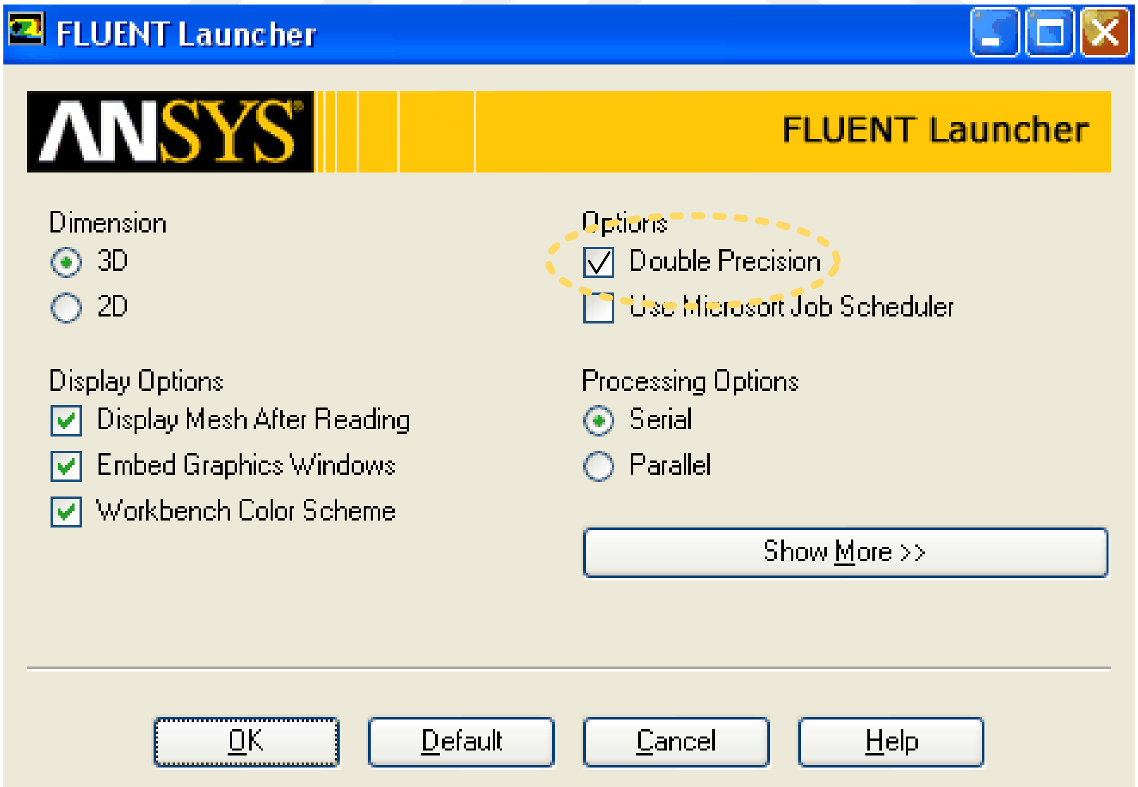

Figure 42. The Fluent Launcher of ANSYS [3]

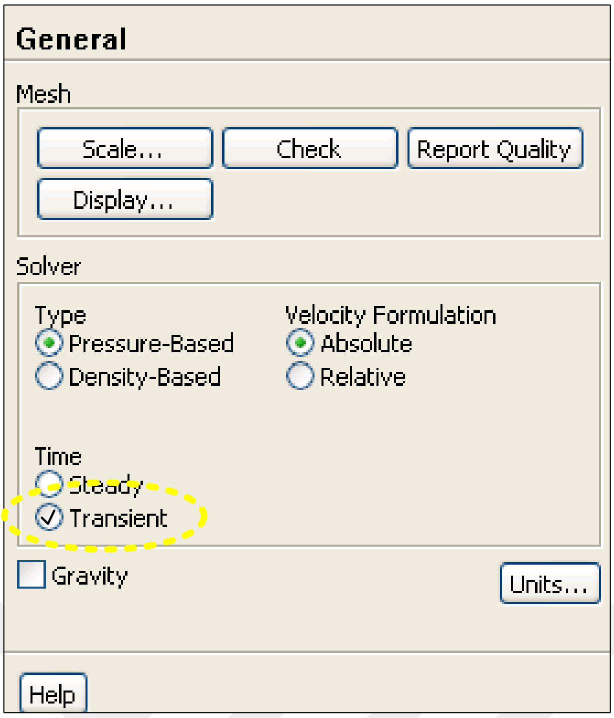

Figure 43. Transient time option [3]

In the next step, the properties of the fluid to be used during the analysis were determined. First of all, under the materials section, the fluids option was opened and both the name and properties of the fluid defined in the system were redefined (Figure 45). Here, the density was set to 1051 kilograms per cubic meter, which is equivalent to the density of blood and the name of the fluid is set as blood. Then, the Carreau model, which is suitable for non-newtonian flows, was chosen as the viscosity model since the flow properties of blood change in time so the constant viscosity option is not suitable for correct results. The point to be noted here is that the flows are turbulent by default in Ansys, so the Carreau model does not appear when the viscosity model is selected. Carreau model becomes visible when Viscous Model -> Laminar selection is applied. Furthermore, the boundary conditions were defined. Dynamic. Outlets were set to 100 millimeters of mercury above the gauge pressure and the operation conditions were checked. After setting the input coordinates of the starting point for the injection, the particles were injected into the fluid. The particles selected for this process were determined in the following order: injections>create>massless particles (Figure 47). At that time, the input coordinates of the starting point for the injection were decided. As the next step, after reopening the geometric model in the design modeler, necessary information such as the area and volume of the desired vessel was obtained in the reference values section and the relevant parts were filled with this information. The sequence followed until this step is done is DM>Tools>Analysis Tools>Entity Information>Click on Geometry>Body Area and Volume (Figure 48).

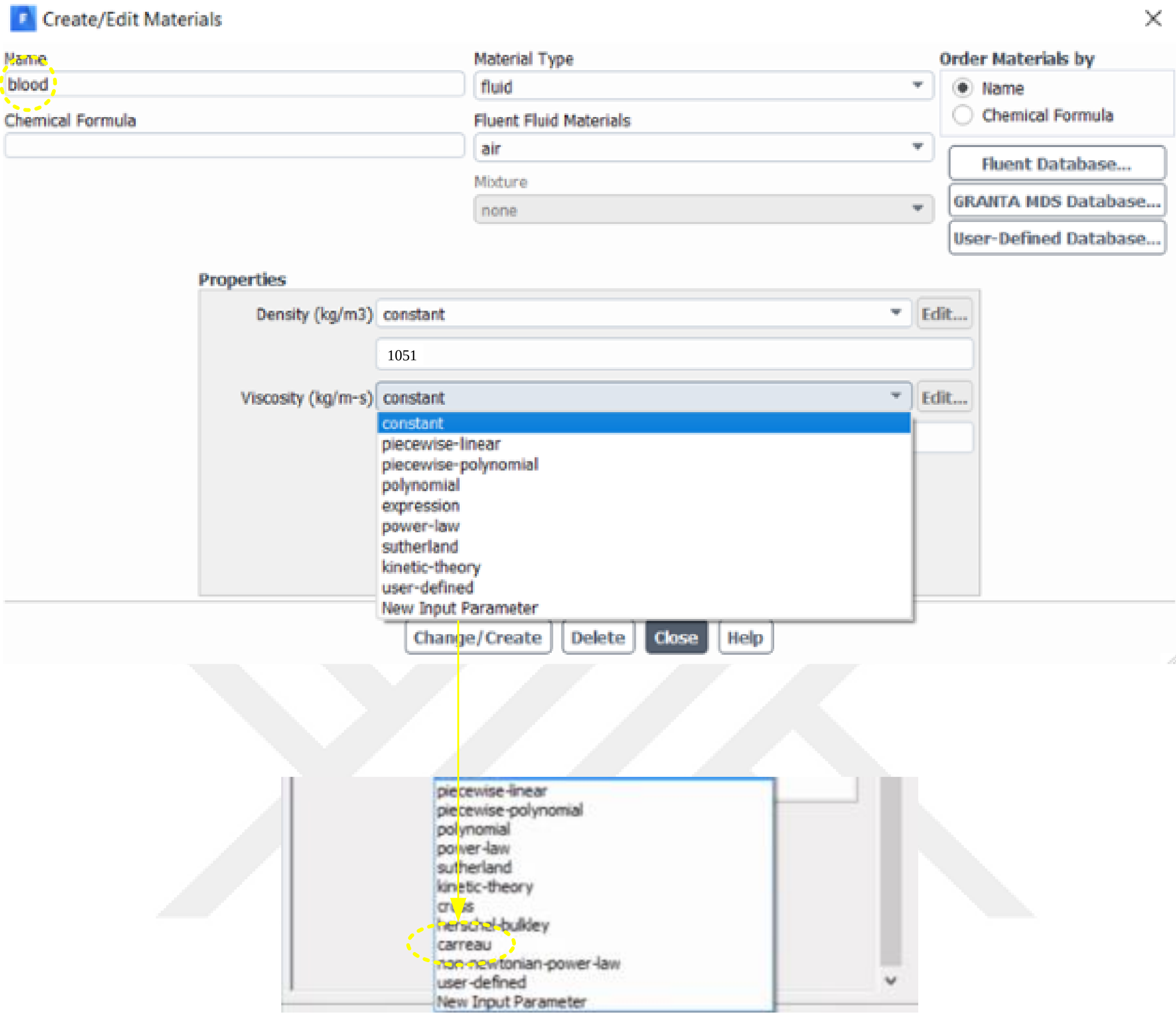

Figure 44. Enabling the Carreau model in ANSYS [3]

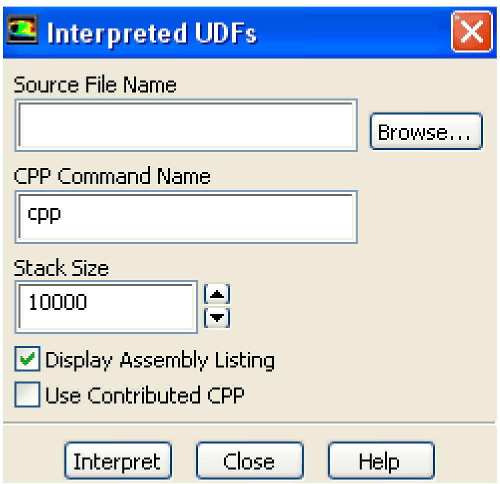

Figure 45. Interpretation of UDFs [3]

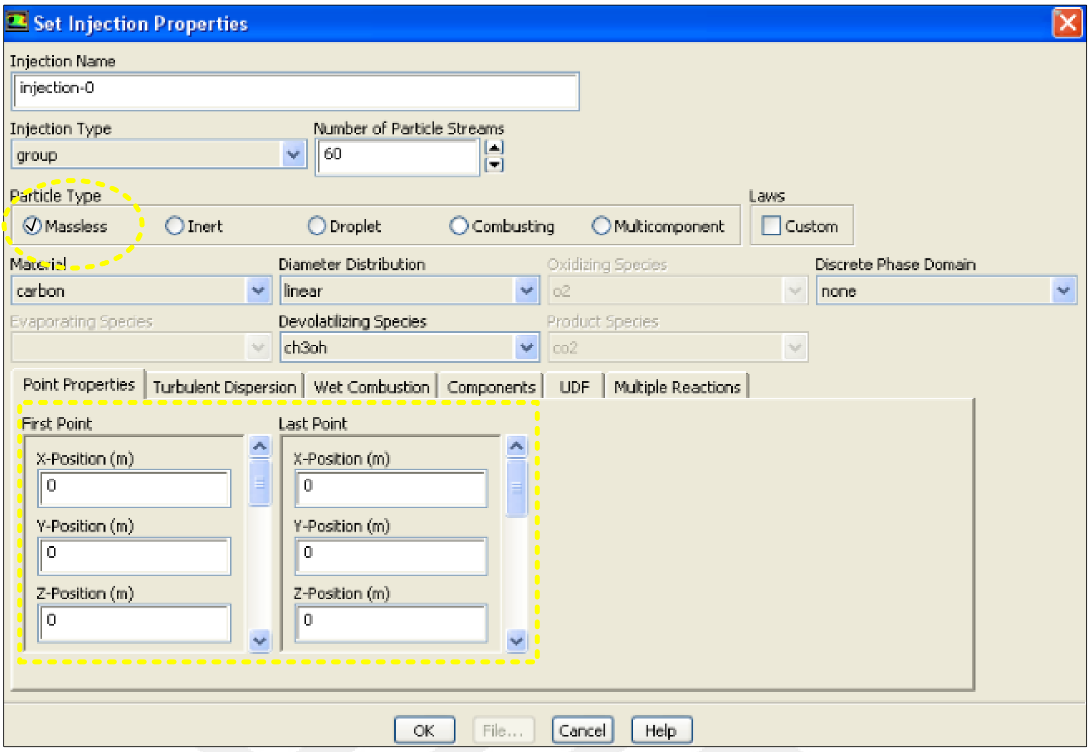

Figure 46. Injection options in ANSYS [3]

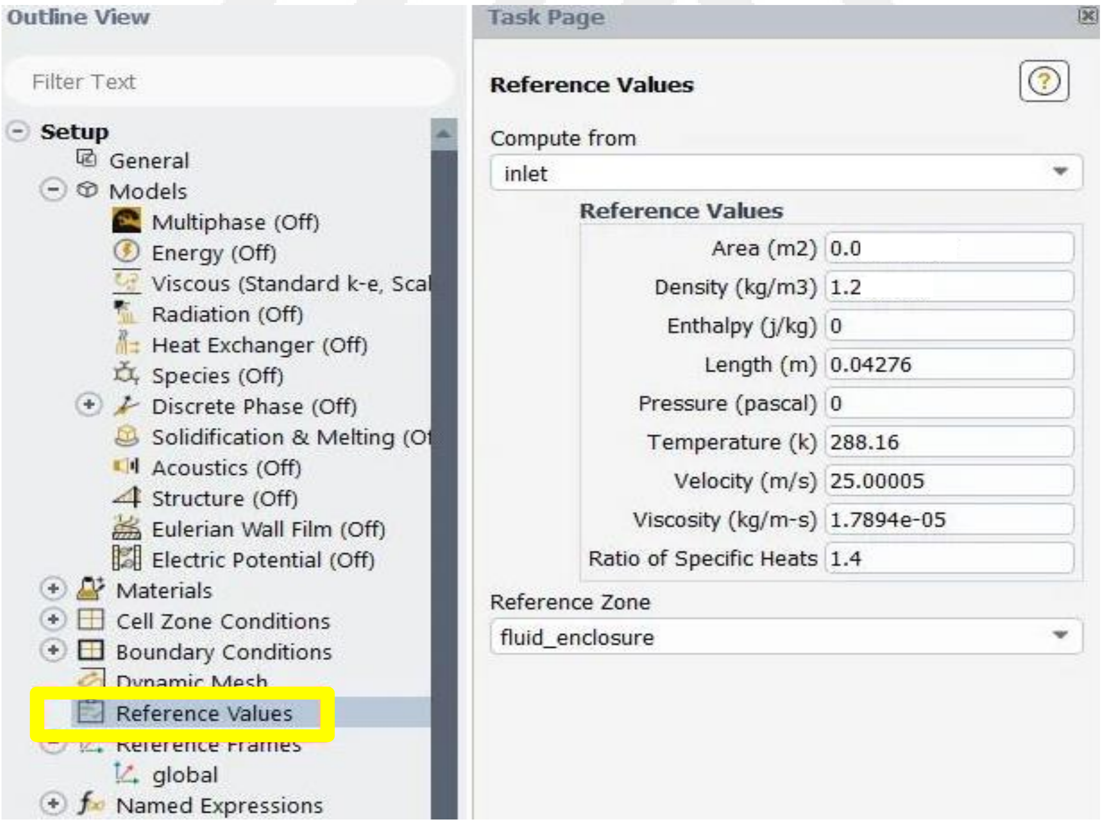

Figure 47. Reference values section [3]

Additionally, monitors were created in the monitors' area (Figure 49) following Monitors>Create a monitor. Print to console was checked and wall zones were chosen.

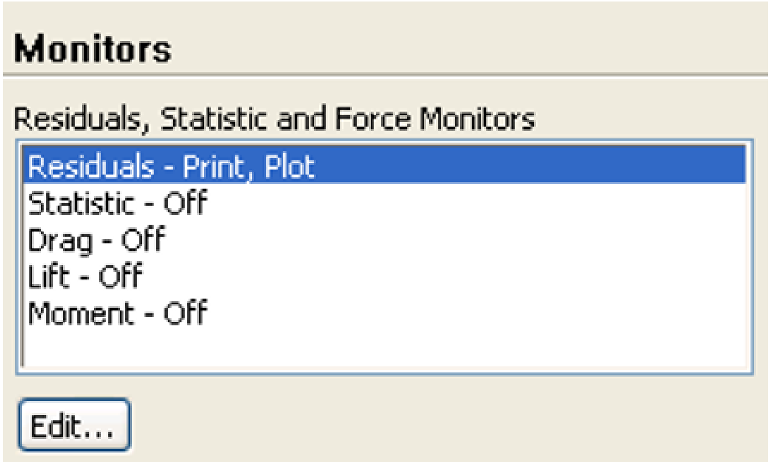

Figure 48. Monitor types in Ansys [3]

Hybrid initialization was checked and initialization was started for the solution (Figure 50). A preliminary answer is formed by the initialization that the solver iteratively enhances. Typically, the identical converged solution is reached regardless of the initialization, however, convergence is quicker when the start line is greater sensible. Fundamental initialization imposes equal values in all cells. The aid of patching one-of-a-kind values into exceptional zones can be given as an instance. Numerous capabilities, consisting of patching and submit-processing, aren't available till after initialization. The hybrid initialization technique is a good technique for initializing the answer primarily based on simple terms at the setup of the simulation without more statistics required. This technique produces a pace field that conforms to complicated area geometries and a strained area that easily connects excessive and occasional stress values.

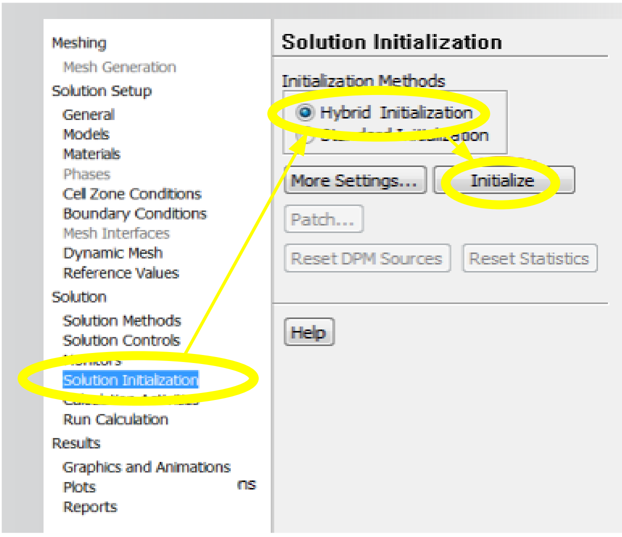

Figure 49. Solution initialization [3]

The parameters that would be calculated, the results that would be stored, and other details (Figure 51) were decided in the calculation activities section.

Figure 50. Calculation activities section [3]

5. RESULTS AND DISCUSSIONS

Stream structure in the aortic vessel for patients having an aortic aneurysm and having Covid-19 has been thought about in this examination, which generally is very critical. The consequences of the investigation have been checked by considering the progressions that essentially happened in 5 unique boundaries, in particular, pressure, wall shear stress, cell volume change, bloodstream speed, and mass stream entering and leaving in this study.

5.1. Wall Shear Stress Distributions and Vectors

Wall shear stress has an essential impact in the deformation of vessel walls. Extremely high stresses cause irreparable tears in the vessel, which results in the death of the person since blood cannot be pumped to the organs. Distribution of the wall shear stresses along the aortic vessels has been demonstrated for both aortas in Figures 56, 57, 58, 59, 60 including their side views. When the animations created after the analysis have been checked, it has been seen that the repaired part behind the operated aorta, and the area between the left carotid and left subclavian in the vessel affected by Covid-19 had the highest WSS. It has been seen that the wall shear stresses of the small vessels above the ascending aorta have been higher in the covid-affected aorta. The maximum value of wall shear stress in the repaired aorta has been found as 6,02 Pa whereas it has been around 1,2 Pa in the other regions of it. The shear stress values of the patient with covid have been higher than the repaired aorta and the shear stress distribution is approximately 20 Pa throughout the covid-affected vessel and reached 25 Pa in smaller vessels. Furthermore, the formulation of WSS vectors is summarized in Figures 54 and 55 and as follows.

$$\vec{\tau} = 2\eta\dot{\varepsilon}.\vec{n} \tag{3}$$

''$\vec{\tau}, \eta, \dot{\varepsilon}$ and $\vec{n}$ '' are used for wall shear stress, dynamic viscosity, deformation rate, and orthogonal vessel wall vector respectively in equation 3.

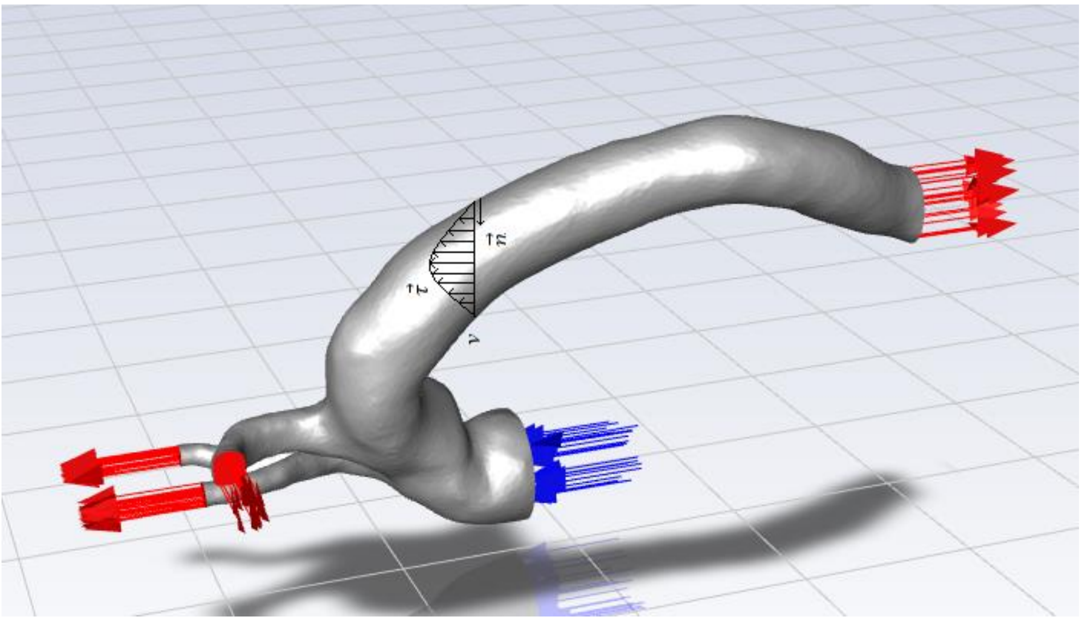

Figure 51. Vector distribution on the aorta of the female patient [3]

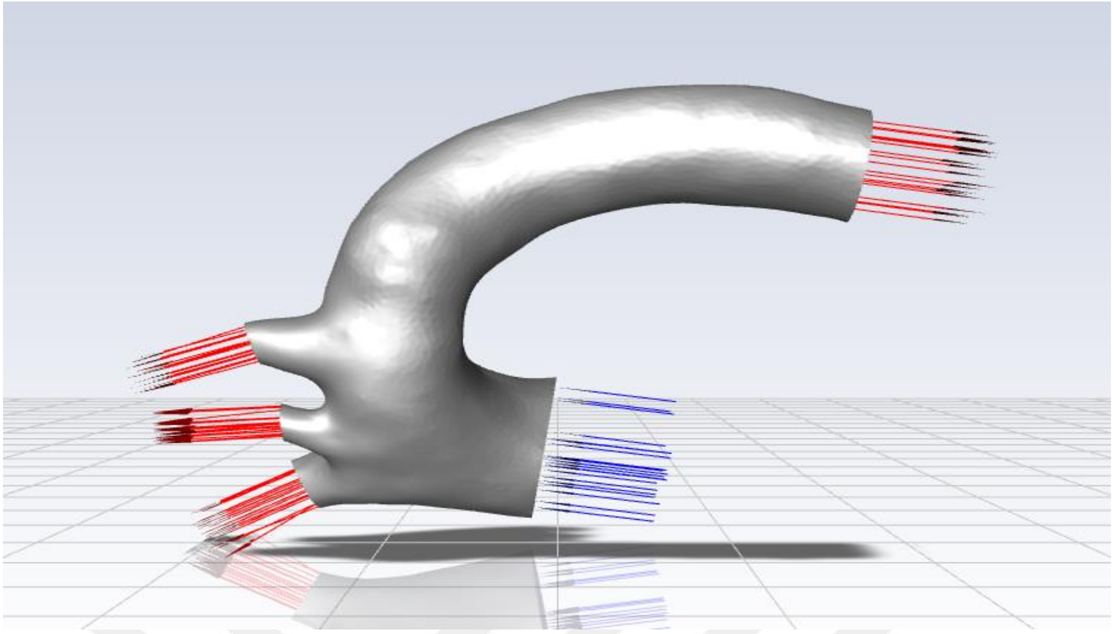

Figure 52. Vector distribution on the aorta of the male patient [3]

Cardiac cycle times have been chosen to indicate the variety of cross-section locations in space so that aortic movement and the differences that occur in areas can be analyzed. The calculation of the total mass of the blood incoming and departing during the cardiac cycle (0s – 0,734s for female and 0s-0,6836s for the male patient) has been made by the expression in the fourth equation below for both aortas as also stated in Novak's study [26].

$$\int_0^{0.734} \dot{m}(t)dt \quad and \quad \int_0^{0.6836} \dot{m}(t)dt \tag{4}$$

where the entry mass stream for the mass passing through and leaving out the blood domain is represented by ''$\dot{m}$'' during the time ''t''. Integrals have been computed utilizing the parabolic interpolating numerical method of the function $\dot{m}$ (t). The mass entering and exiting the blood domain has been acquired to be nearly 0,045 kg/cycle in the operated aorta and 0,056 kg/cycle in the covid-affected aorta during the cardiac cycle.

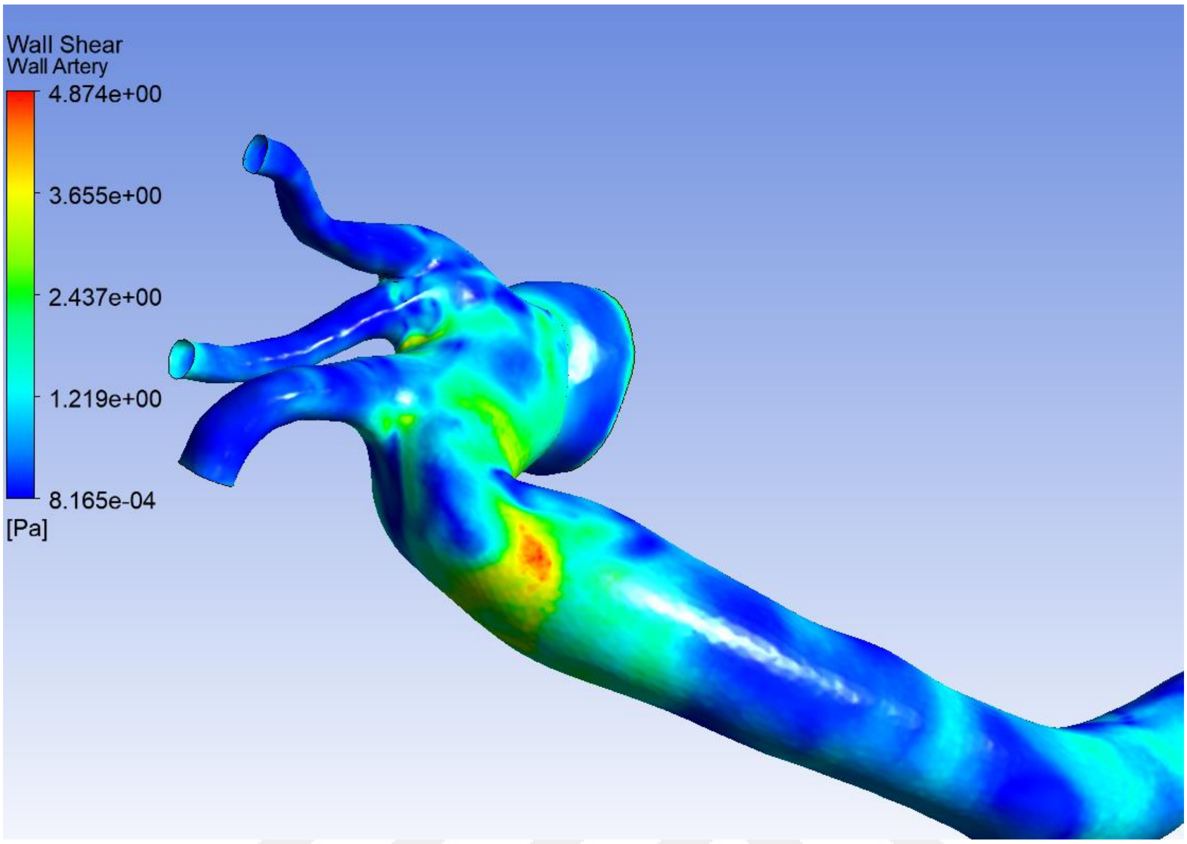

Figure 53. An overlook on the problematic area

The problematic areas here in Figure 54 are the red-colored regions collected in a certain area. This is the area where the tear occurred before the vessel is repaired. The risk continues even after the vessel is repaired. These analyses aim to warn about these problematic areas and remind paying attention to prevent health problems. When generally overlooked, it was seen that the stresses are different in every region and the high-risked areas occur only in small parts

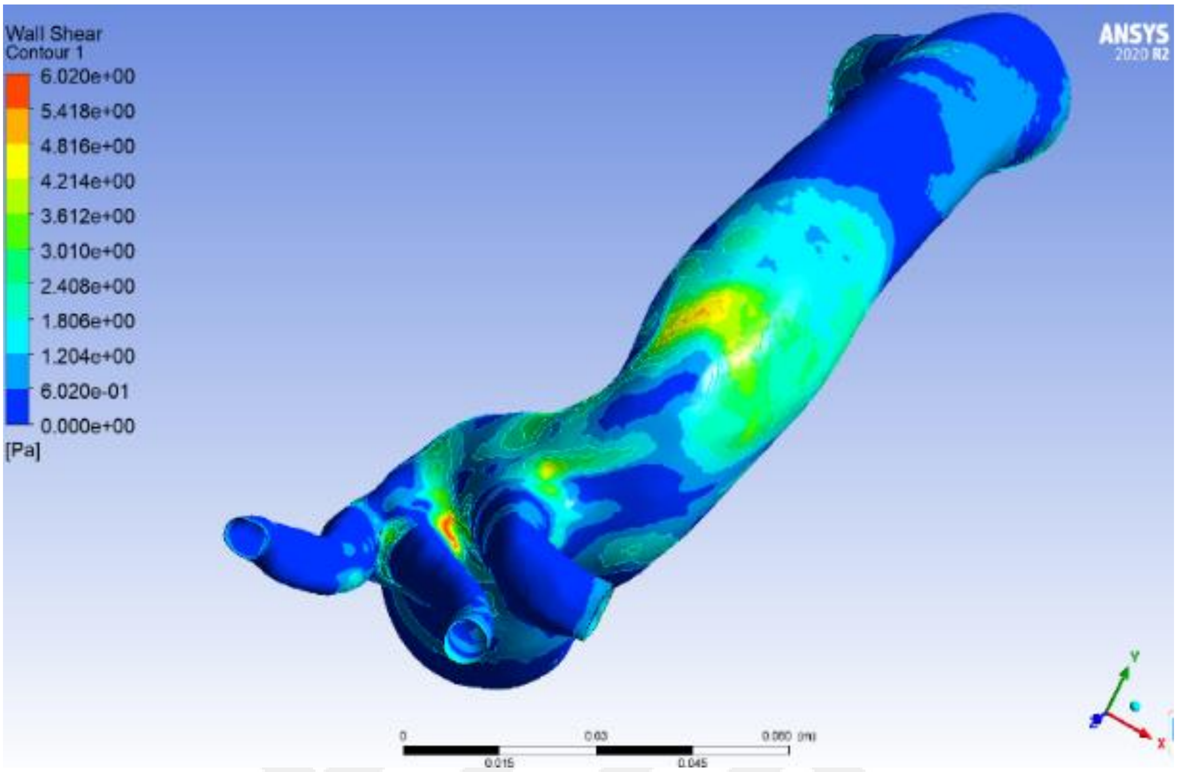

Figure 54. Top view of the female patient's vessel

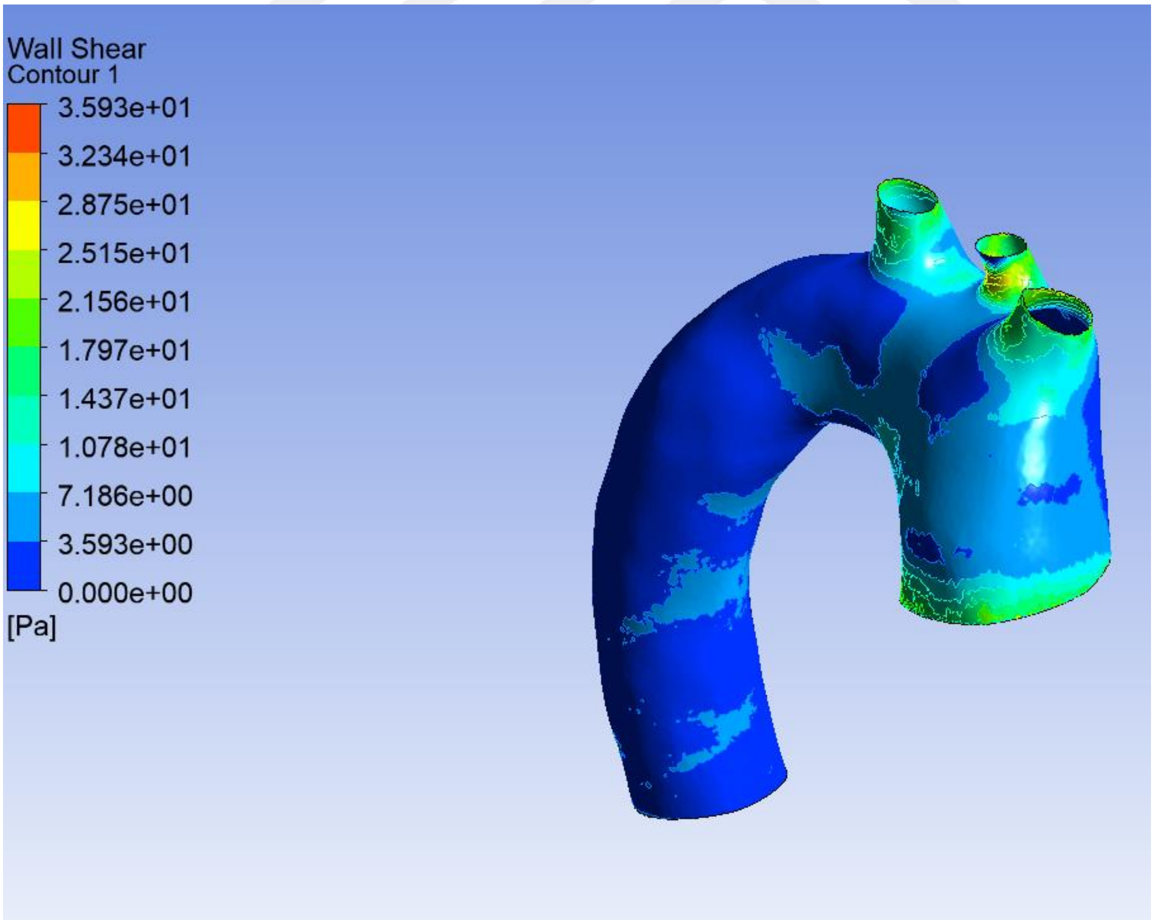

Figure 55. A detailed look of the wall shear stress distribution on the male patient's vessel

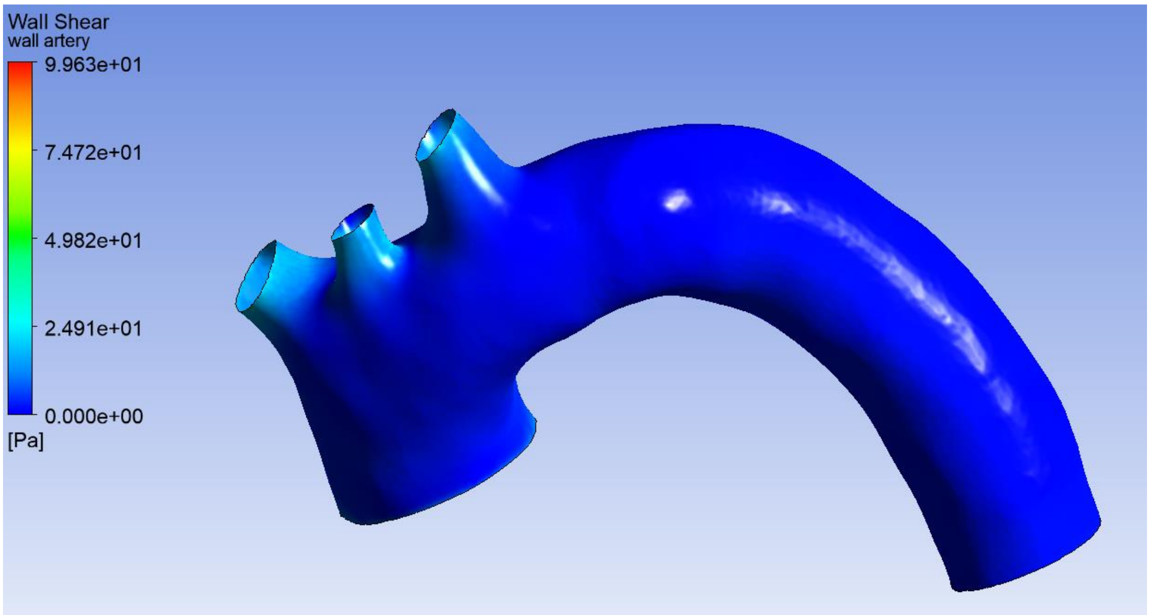

Figure 56. Left side view of the male patient's vessel

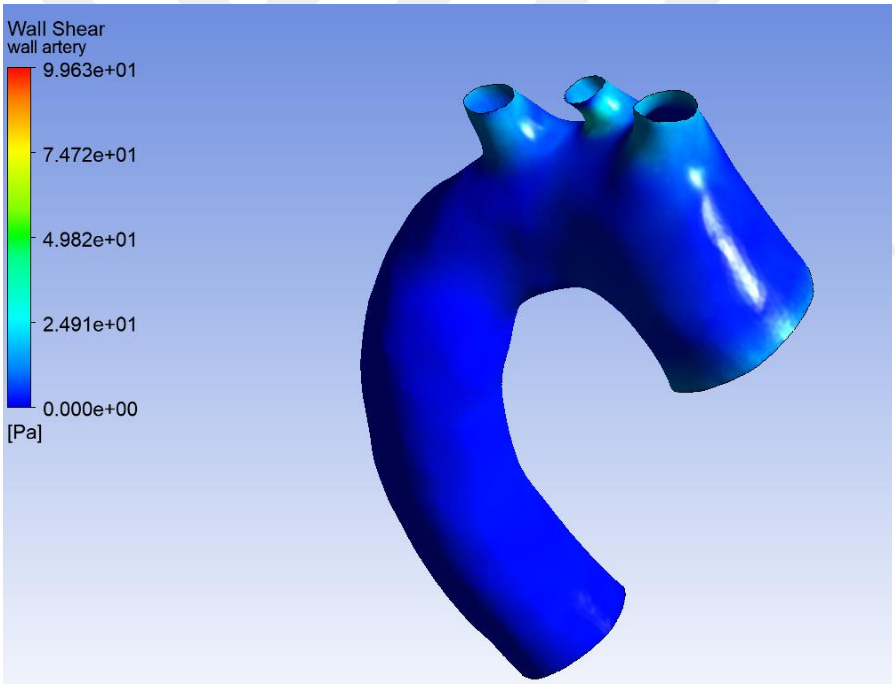

Figure 57. Right side view of the male patient's vessel

5.2. Velocity Profiles

Changes in blood flow rate for each vessel throughout a cardiac cycle and also the elements on the vessel walls laid low with this alteration are illustrated in the following Figures 61, 62, 63, 64, 65. The highest velocity has been ascertained as 0,86 m/s at the point where the blood splits into smaller vessels for the feminine patient as illustrated in Figure 59. Therefore, the maximum value of velocity is found 1,135 m/s at the point where the blood flows in subclavian and carotid arteries for the male patient.

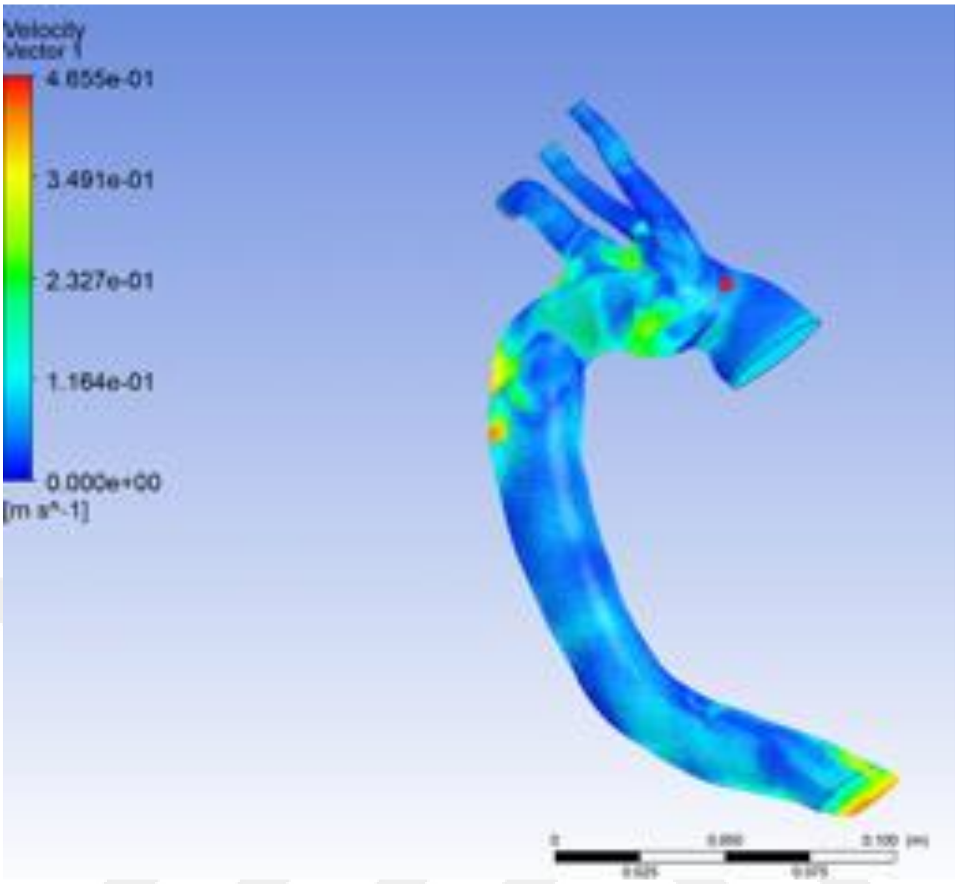

Figure 58. Velocity distribution of the aorta of the feminine patient from the right side

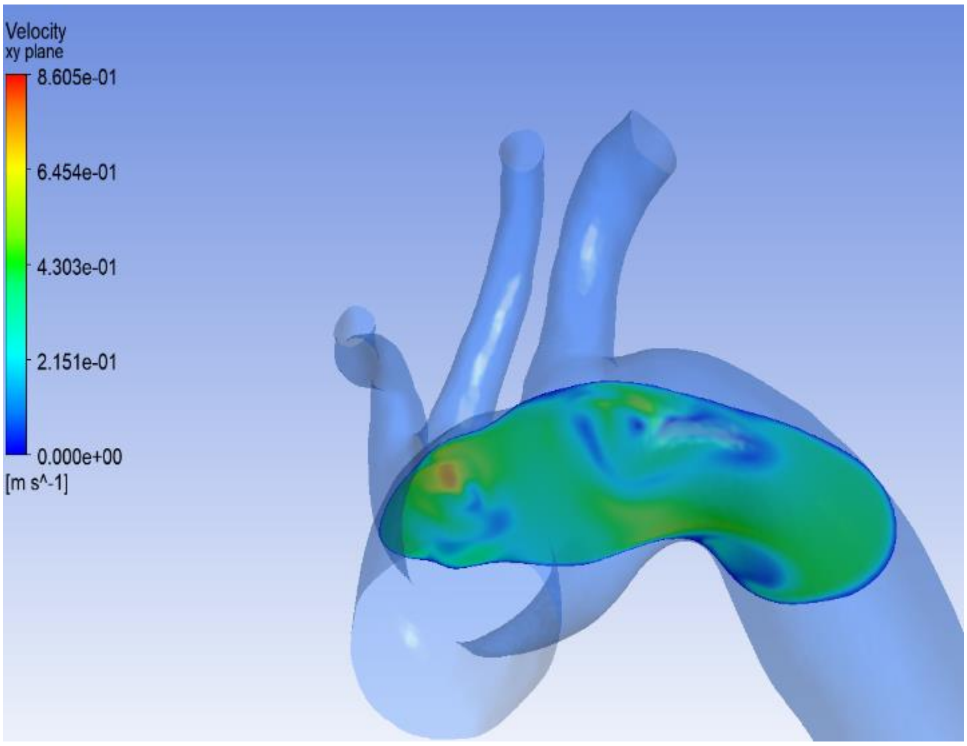

Figure 59. An inside overview of the velocity profile

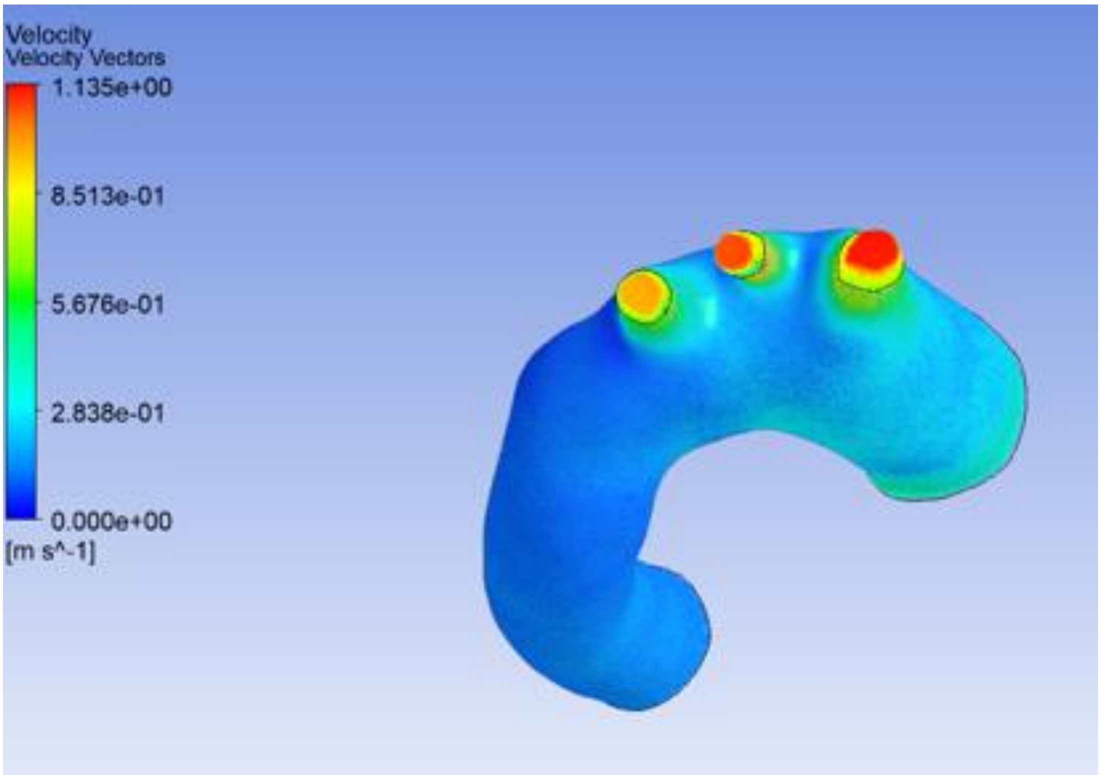

Figure 60. Top view of the velocity distribution of the aorta of the male patient

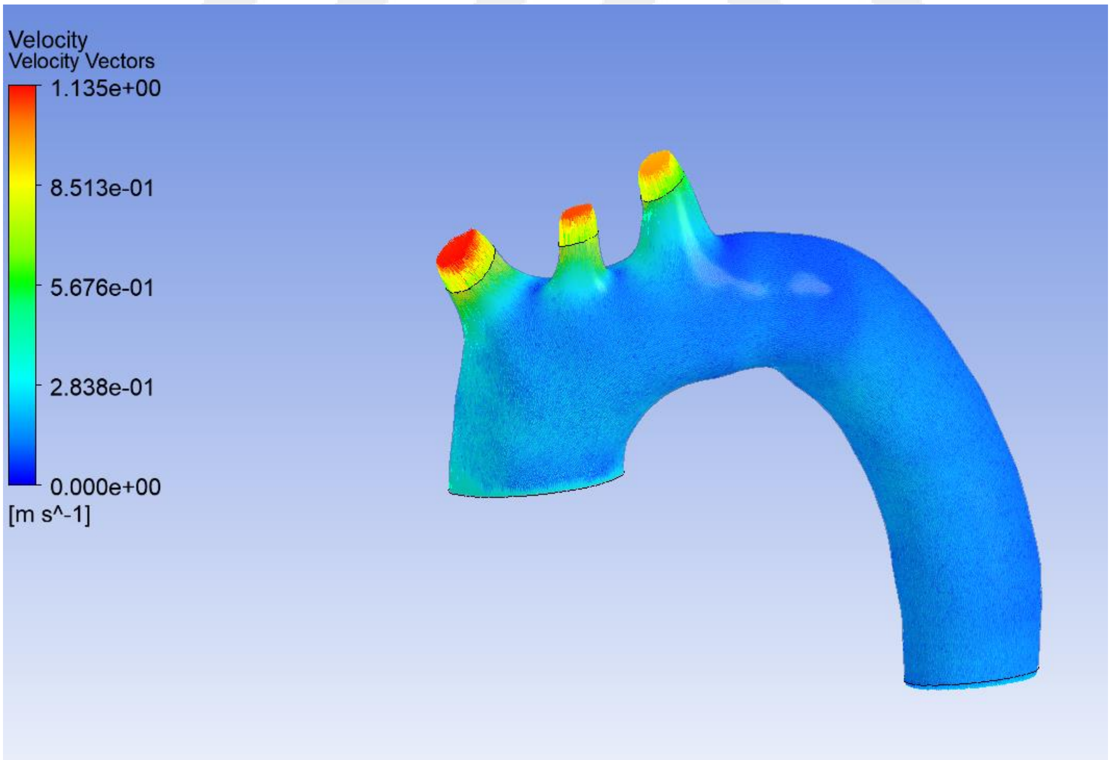

Figure 61. Velocity distribution of the aorta of the male patient from the left side

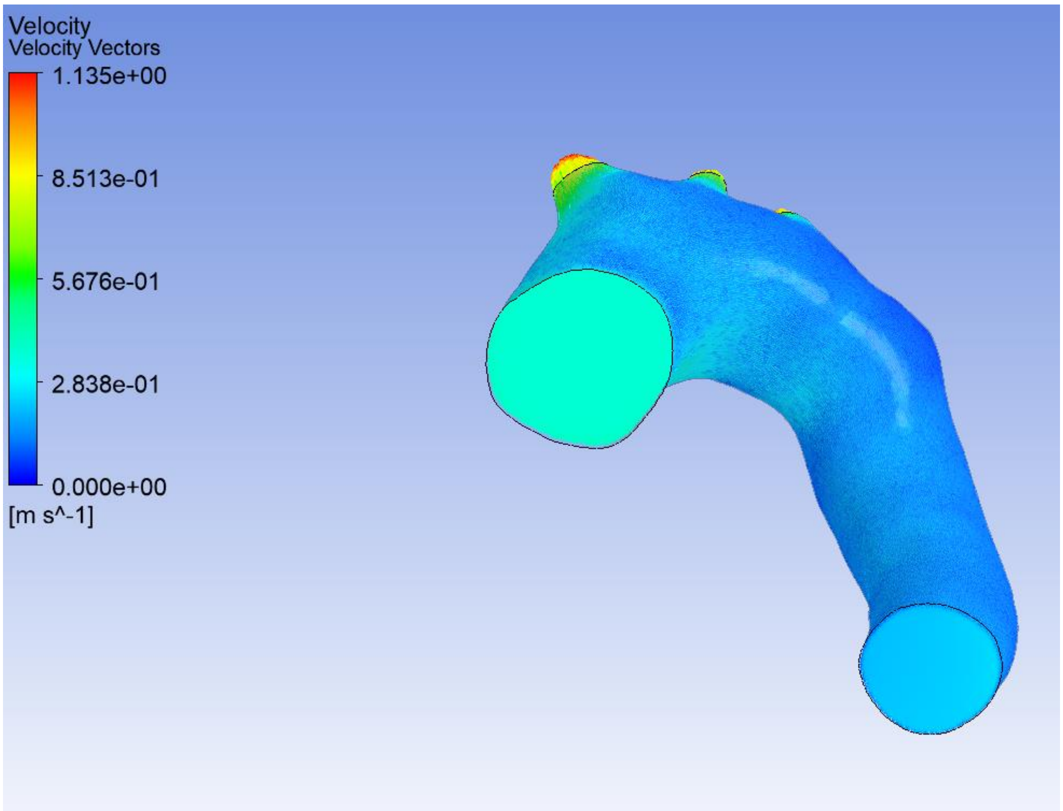

Figure 62. Another side view of the aorta

Consistent with the results in research of (Nowak et al., 2019), it is noticed that there are some reflux regions for both vessels in the descending aorta zone when the velocity distribution animations are controlled after the analysis. In addition, when the changes in blood volume during the cardiac cycle have been analyzed, it is concluded that this backflow may be due to the expansion of the flexible vessel's volume as a result of the blood accumulation. Other factors are that affect this backflow can also be considered as high Reynolds number or the boundary condition of the outlet pressure which is 13332 Pa. The highest Reynolds number of the repaired aorta has been obtained to be 3219, whereas it is 3578 for the covid-affected aorta which exceeded the laminar flow limit (2300) like the result of the study (White, 2010) during the cardiac cycle. But for the period of the analysis, the Reynolds number has been mostly less than 2300 meaning that the flow could be considered laminar in the vast majority of the study.

5.3. Pressure Differences

The pressure zones formed on the outer walls of the aortic vessel that fundamentally has gone through thoracic aortic aneurysm activity and the vessel affected by Coronavirus infection are displayed in Figure 52 and Figure 53 in order, considering the compression (0.18s) and unwinding (0.6s) times. These times are the moments during the cardiac cycle that indicate the lowest and highest rates of the heart. At the point when the vessels were generally inspected exhaustively after the pressure change investigation (Figure 64, 67, 68, 69), some high-pressure regions were found in the female patient's aorta (Figure 64), where the analyzed piece of the vessel was fixed, and at the left subclavian and near the descending aorta. Moreover, high-pressure regions have been acquired at the inlet and exit of the male patient's aorta (Figure 66). The calculation system is indicated in Figure 66.

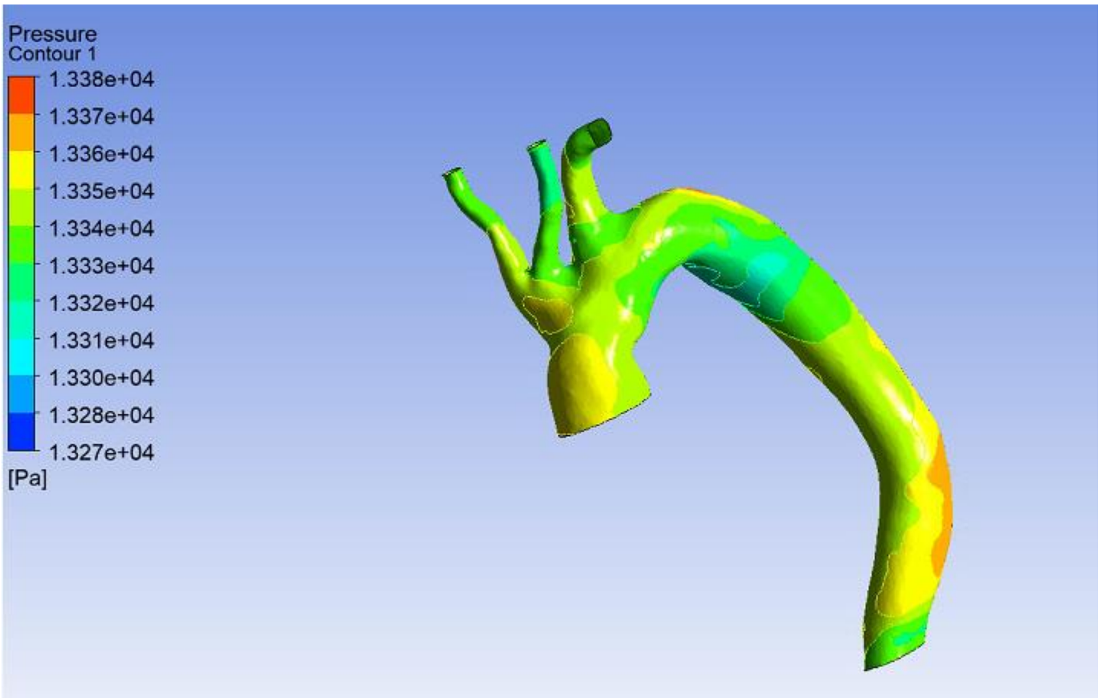

Figure 63. Pressure zones on the aorta of the female patient

Figure 64. Back view of the aorta

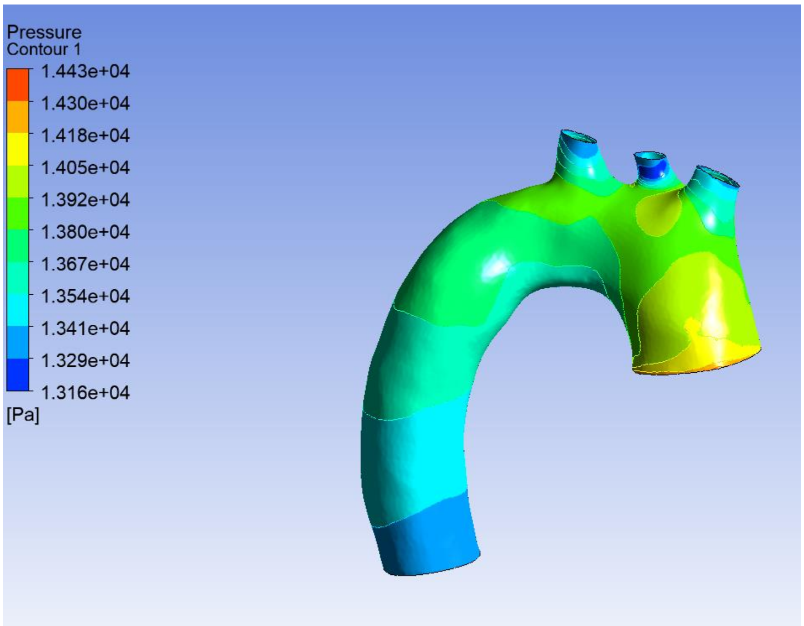

Figure 65. Pressure contribution on the male patient’s aorta

After the pressure factor investigation, the color distributions framed on the vessel show the regions from less hazardous to exceptionally risky. What is implied by risk here is that after the pressure in the vessel becomes too high, the red areas will be affected first. The color representation of the hazard dimensions in the system, from largest to smallest, is as follows: Red>Orange>Yellow>Light Green>Bright Green>Matte Green>Light Blue>Blue>Dark Blue. The kind of the biggest amount of the pressure factor has been gotten as 13380 Pa behind the artery for the moment of systole and the littlest amount, generally, has been seen as 13270 in diastole in the operated aorta in a significant way. For the male patient (influenced by Covid-19), the most noteworthy pressure especially has been determined as 14430 Pa at the inlet region in the rising aorta through the least one has been found as 13160 Pa at the passageway in the dropping aorta. Additionally, the distinction in pressure esteems can be recovered exogenously utilizing FSI strategies or computational fluid elements. Areas with the most pressure values virtually indicate high-risk areas where these elements of the vessels can be primarily affected once health issues are encountered in a major way. Therefore, it reasonably is vital to require some precautions to forestall health problems within these zones. Pressure values in the remaining parts of the vessel surfaces for both vessels are in an acceptable range that the health of the patients won't specifically be affected adversely, which essentially is significant.

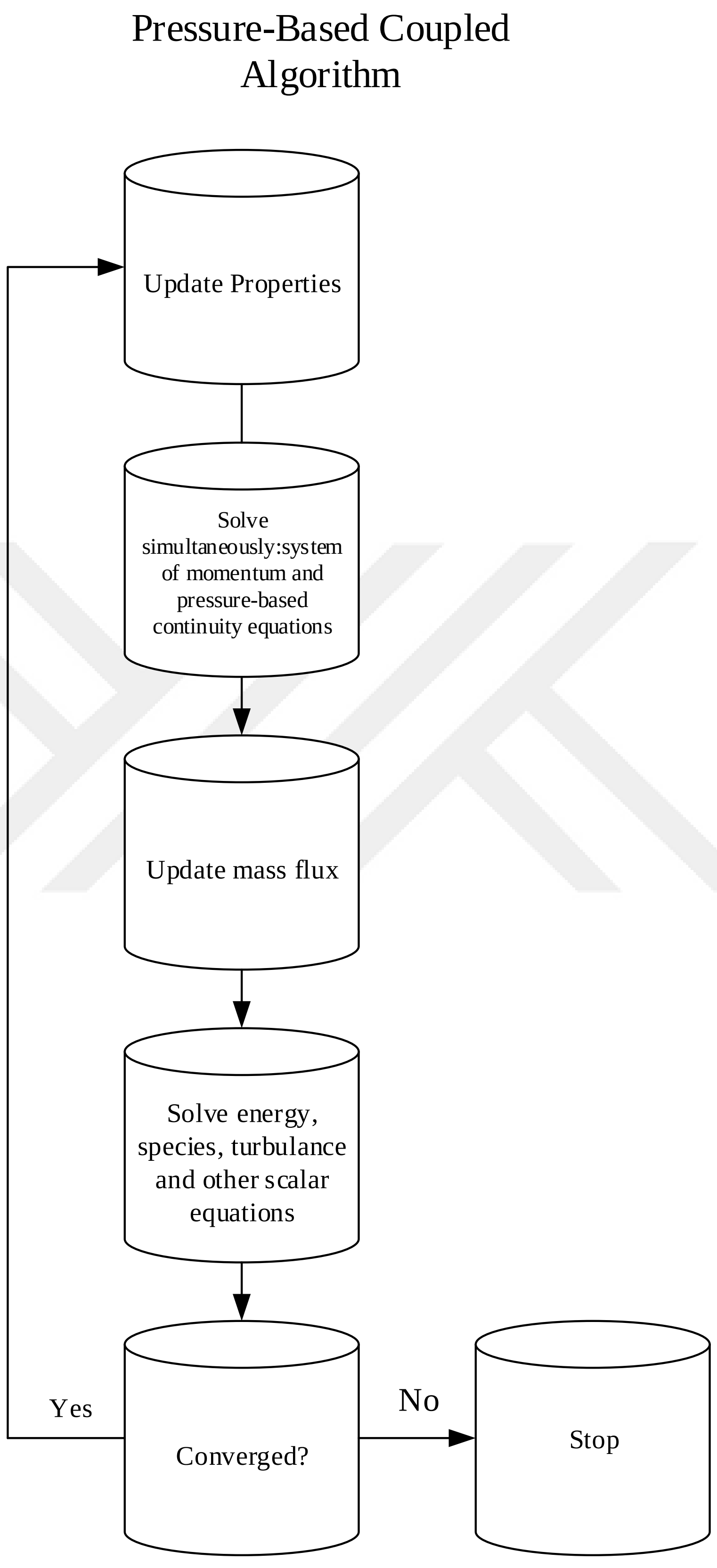

Figure 66. Pressure contribution calculation system

5.4. Cell Volume Change

The change in cell volumes across the aortas during a cardiac cycle has been investigated as the differences in the volume of the cells may initiate or modulate many variations such as cell death and migration. The volume change has been found to occur between 1,013 and 1,710 (Figure 68) percent along the operated aorta and around 3 percent in the other vessel. It can be concluded that such a change in cell volumes is not dangerous for the vessels, considering the elasticity of the vessels.

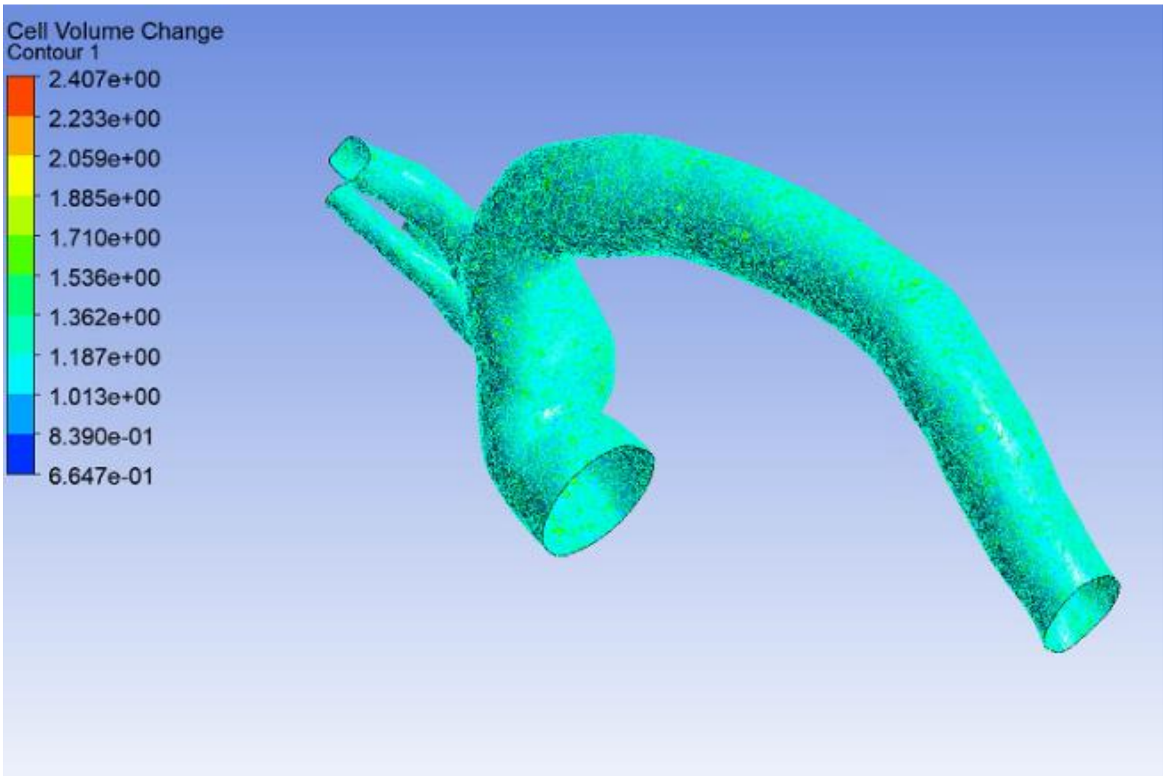

Figure 67. An example of cell volume change on the aorta of the female patient

6. CONCLUSIONS

Aorta aneurysms and the covid-19 virus may threaten human lives as a tear in the artery wall could result in reduced blood flow to organs or the rupture of the aorta. Regarding the obtained values and colour zones after the analysis, a conclusion can be made as to the virus influences some parts of vessel walls and their properties negatively. Numerical values, especially on wall shear stress, have been higher in the infected patient. These values give a warning for the investigated vessels since some of the values acquired are found higher than the recommended values in the literature. High-pressure areas have been encountered in the posterior part of the aorta, that is, in the repaired part of the female patient's vessel, whereas they have been encountered in the inlet and outlet sections for the male patient's vessel. In other parts of both vessels, pressure values have been within the acceptable range. Additionally, it has been seen that blood flowed faster in the infected patient. The outcomes of the study demonstrate that computational fluid dynamics is useful to model blood flow and make investigations due to the examination ability of change in the parameters such as wall shear stress, blood flow velocity, and pressure.

7. RECOMMENDATIONS

Later on, in addition to parameters such as wall shear stress, pressure contrast, cell volume change, and blood flow speed, new techniques can be developed to calculate various other parameters with high exactness in a more limited time. After the utilization of these strategies, the prior and then afterward condition of the vessel can be made 3D with the assistance of a 3D printer, and so substantial models can be created.

REFERENCES

[1] Abdulla, M. (n.d.). Tee or transesophageal echo. Heartsite. https://www.heartsite.com/html/tee.html

[2] Akıncı Ç. (2020, May 27). *Ansys'teki modüllerin kısaca tanıtılması.* Makine Mühendisliği ve Yazılım Blogu. https://cagatayakinci.com/

[3] Ansys® Academic Research Mechanical, Release 18.1.

[4] Barber, D.C., Oubel, E., Frangi, A.F., Hose, D.R., 2007. Efficient computational fluid dynamics mesh generation by image registration. Medical Image Analysis 11, 648–662.

[5] Begic, N., Karahusic, A.B., Kostic, T. 3D Simulation Of Blood Flow Through New Designed Stent Graft In Abdominal Aorta, Atherosclerosis, Volume 287, 2019, Page e160, ISSN 0021-9150.

[6] Benli M. (2020, September 20). *Bilgisayarlı tomografi nedir? Nasıl çekilir?* Grup florence nightingale hastaneleri. https://www.florence.com.tr/bilgisayarli-tomografi

[7] Bhuyan, R.R. (2021, December 8). *Did you know what a thoracic aortic dissection is?* Cardiac Surgery Online. https://www.cardiacsurgeryonline.com/category/cardiovascular/

[8] Biglarian, M., Larimi, M.M., Afrouzi, H.H., Moshfegh, A., Toghraie, D., Javadzadegan, A., Rostami, S., 2020. Computational investigation of stenosis in curvature of coronary artery within both dynamic and static models. Computer Methods and Programs in Biomedicine 185, 105170.

[9] Botar-Jid, C.C., Agachi, P.S., Clichici, S., 2009. Computational fluid dynamics applied to study the hemodynamics in sangvin vessels. Case study - the portal system. Computer Aided Chemical Engineering 26, 677-682.

Bounty, one thousand nine hundred first ed. Bounty Books, ABD

[10] Brown, A.G., Shi, Y., Marzo, A., Staicu, C., Valverde, I., Beerbaum, P., Lawford, P.V., Hose, D.R., 2012. Accuracy vs. computational time. Translating aortic simulations to the clinic. Journal of Biomechanics 45, 516–523.

[11] Bruening, J., Hellmeier, F., Yevtushenko, P., Kelm, M., Nordmeyer, S., Sündermann, S.H., Kuehne, T., Goubergrits, L. Impact of patient-specific LVOT inflow profiles on aortic valve prosthesis and ascending aorta hemodynamics, Journal of Computational Science, Volume 24, 2018, Pages 91-100, ISSN 1877-7503.

[12] Bulut D. (2020, June 24). *Emar (MR) nedir?* Medicalpark. https://www.medicalpark.com.tr/emar/hg-2048

[13] Cadsay (n.d.). *Ansys nedir?* Retrieved August 10, 2021 from https://cadsay.com/ansys-nedir

[14] Caimi, A., Sturla, F., Pluchinotta, F.R., Giugno, L., Secchi, F., Votta, E., Carminati, M., Redaelli, A. Prediction of stenting related adverse events through patient-specific finite element modelling, Journal of Biomechanics, Volume 79, 2018, Pages 135-146, ISSN 0021-9290.

[15] Canè, F., Selmi,M., Santis, G.D., Redaelli, A., Segers, P., Degroote, J. Mixed impact of torsion on LV hemodynamics: A CFD study based on the Chimera technique, Computers in Biology and Medicine, Volume 112, 2019, 103363, ISSN 0010-4825.

[16] Capellini, K., Gasparotti, E., Cella, U., Costa, E., Fanni, B.M., Groth, C., Porziani, S., Biancolini, M.E., Celi, S. A novel formulation for the study of the ascending aortic fluid dynamics with in vivo data, Medical Engineering & Physics, Volume 91, 2021, Pages 68-78, ISSN 1350-4533.

[17] Chi, Q., He, Y., Luan, Y., Qin, K., Mu, L. Numerical analysis of wall shear stress in ascending aorta before tearing in type A aortic dissection, Computers in Biology and Medicine, Volume 89, 2017, Pages 236-247, ISSN 0010-4825.

[18] Cilla, M., Casales, M., Peña, E., Martínez, M.A., Malvè, M., 2020. A parametric model for studying the aorta hemodynamics by means of the computational fluid Dynamics. Journal of Biomechanics 103, 109691.

[19] Circulation Foundation The Vascular Charity. *What is endovascular aneurysm repair?* https://www.circulationfoundation.org.uk/help-advice/abdominal-aortic-aneurysm/endovascular-aneurysm-repair-evar

[20] Condé Nast Traveler (n.d.). Medical or surgical masks. https://www.cntraveler.com/story/best-disposable-face-masks-n95-kn95-surgical

[21] Çayıroğlu, İ. (n.d.). Ansys mesh yapma teknikleri. http://www.ibrahimcayiroglu.com/Dokumanlar/BilgisayarDestekliTasarim/BilgisayarDestekliTasarimVeAnaliz-6-hafta.pdf

[22] Dassault Systemes (n.d.). *Mesh kalitesi denetimleri.* Retrieved August 10, 2021 from http://help.solidworks.com/2018/turkish/SolidWorks/cworks/c_Mesh_Quality_Checks.htm

[23] Dolcourt, J. (2020, May 1). *Will homemade face masks keep you from getting sick with coronavirus? What to know.* Cnet. https://www.cnet.com/how-to/will-homemade-face-masks-keep-you-from-getting-sick-with-coronavirus-what-to-know/

[24] Eagleton M.J. (n.d.). *Thoracic aortic aneurysm.* Society for vascular surgery. Retrieved August 10, 2021 from https://vascular.org/patient-resources/vascular-conditions/thoracic-aortic-aneurysm

[25] Elmekawy, A.N. (n.d.). Global mesh controls. https://drahmednagib.com/CAD_2018/Lecture_3_Meshing_2.pdf

[26] Fedorov, A., Beichel, R., Kalpathy-Cramer, J., Finet, J., Fillion-Robin, J-C., Pujol, S., Bauer, C., Jennings, D., Fennessy, F.M., Sonka, M., Buatti, J., Aylward, S.R., Miller, J.V., Pieper, S., Kikinis, R. 3D Slicer as an Image Computing Platform for the Quantitative Imaging Network. Magnetic Resonance Imaging. 2012, Nov;30(9):1323-41. PMID: 22770690. PMCID: PMC3466397.

[27] Fitzgerald G. (2018, December 12). *The aorta.* Teach me anatomy. https://teachmeanatomy.info/abdomen/vasculature/arteries/aorta/

[28] Fukui, T., Parker, K.H., Tsubota, K., Wada, S., Yamaguchi, T. The effect of wall motion on arterial wall shear stress, Journal of Biomechanics, Volume 39, Supplement 1, 2006, Page S445, ISSN 0021-9290.

[29] Gerçekoğlu, H. (n.d.). *Aort anevrizmaları ve diseksiyonları.* https://drhakangercekoglu.com/hastaliklar/aort-anevrizmalari-diseksiyonlari

[30] Gören M.T. (2005, January 1). *Intravascular ultrasonography*. Türkiye Klinikleri Dahili Tıp Bilimleri Dergisi. https://www.turkiyeklinikleri.com/article/tr-intravaskuler-ultrasonografi-42017.html
[31] Hameed, M., Prather, R., Divo, E., Kassab, A., Nykanen, D., Farias, M., DeCampli,W.M. Computational fluid dynamics investigation of the novel hybrid comprehensive stage II operation, JTCVS Open, Volume 7, 2021, Pages 308-323, ISSN 2666-2736.
[32] Hansen, K.L., Møller-Sørensen, H., Kjaergaard, J., Jensen, J.A., Nielsen, M.P. Vector Flow Imaging of the Ascending Aorta in Patients with Tricuspid and Bicuspid Aortic Valve Stenosis Treated with Biological and Mechanical Implants, Ultrasound in Medicine & Biology, Volume 46, Issue 1, 2020, Pages 64-72, ISSN 0301-5629.
[33] Health Images (n.d.). Medical Imaging. https://www.healthimages.com/can-you-get-an-mri-with-a-tattoo/
[34] Hochstuhl, J., Kassi, M., Elias, S., Ruhparwar, A., Karmonik, C., Chang, S. Computational Fluid Dynamics (CFD) - A Reliable Basis for Therapy and Surgical VAD Strategy? The Journal of Heart and Lung Transplantation, Volume 37, Issue 4, Supplement, 2018, Pages S268-S269, ISSN 1053-2498.
[35] Honeywell International Inc. (n.d.). N95 masks explained. https://www.honeywell.com/us/en/news/2020/03/n95-masks-explained
[36] Hope, T.A., Herfkens, R.J., 2008. Imaging of the Thoracic Aorta with Time-Resolved Three-Dimensional Phase-Contrast MRI. A Review. Thoracic and Cardiovascular Surgery 20, 358-364.
[37] İpci D. (n.d.). *Karmaşık mühendislik problemlerinin çözümünde mesh'in önemi.* Retrieved August 10, 2021 from https://slideplayer.biz.tr/slide/14760959/
[38] Jayendiran, R., Nour, B., Ruimi, A. Computational fluid–structure interaction analysis of blood flow on patient-specific reconstructed aortic anatomy and aneurysm treatment with Dacron graft, Journal of Fluids and Structures, Volume 81, 2018, Pages 693-711, ISSN 0889-9746.
[39] Jensen, J., Hoyos, C.A.V., Traberg, M.S., Olesen, J.B., Tomov, B.G., Moshavegh, R., Holbek, S., Stuart, M.B., Ewertsen, C., Hansen, K.L., Thomsen, C., Nielsen, M.B., and Jensen. J.A., 2018. Accuracy and a Precision of a Plane Wave Vector Flow Imaging Method in the Healthy Carotid Artery. Ultrasound in Medicine & Biology 44, 1727-1741.
[40] Johns Hopkins Medicine (n.d.). *Health.* Retrieved August 10, 2021 from https://www.hopkinsmedicine.org/health/conditions-and-diseases/thoracic-aortic-aneurysm
[41] Kamada, H., Ota, H., Nakamura, M., Imai, Y., Ishida, S., Sun, W., Sakatsume, K., Saiki, Y., Yoshioka, I., Takase, K., 2020. Perioperative hemodynamic changes in the thoracic aorta in patients with aortic valve stenosis. A prospective serial 4D-flow MRI study. Seminars in Thoracic and Cardiovascular Surgery 32, 25-34.
[42] Karimi, S., Dabagh, M., Vasava, P., Dadvar, M., Dabir, B., Jalali, P., 2014. Effect of Rheological Models on the Hemodynamics within Human Aorta. CFD Study on CT Image-based Geometry. Journal of Non-Newtonian Fluid Mechanics 207, 42-52.

[43] Klomp, W.J., Bruinsma, G.J.B.B., Hof, A.W., Grandjean, J.G., Nierich, A.P. "Imaging Techniques for Diagnosis of Thoracic Aortic Atherosclerosis", *International Journal of Vascular Medicine*, vol. 2016, Article ID 4726094, 6 pages, 2016

[44] Koganti, S., Kotecha, T., Rakhit, R.D. Interventional Cardiology Review, 2016;11(1):11–6.

[45] Kostic, T., Begic, N., Botonjic, A., Begić, E. CFD simulation of blood flow through new designed stent graft in abdominal aorta, Atherosclerosis, Volume 275, 2018, Page e144, ISSN 0021-9150.

[46] König, C.S., Long, Q. The influence of the endothelial surface layer on the prediction of wall shear stress in small arteries. Journal of Biomechanics, Volume 39, Supplement 1, 2006, Page S445, ISSN 0021-9290.

[47] Lee, W., Allahwala, U., Bhatia, K., Bhindi, R. TCT CONNECT-142 CFD Analysis to Figure Out a Relationship Between Aortic Valve Calcification and Hemodynamic Factors, Journal of the American College of Cardiology. Volume 76, Issue 17, Supplement, 2020, Page B61, ISSN 0735-1097.

[48] Liang, L., Mao, W., Sun, W., 2020. A Feasibility Study of Deep Learning for Predicting Hemodynamics of Human Thoracic Aorta. Journal of Biomechanics 99, 109544.

[49] Lo, E.W.C., Menezes, L.J., Torii, R., 2020. On outflow boundary conditions for CT-based computation of FFR. Examination using PET images. Medical Engineering and Physics 76, 79-87.

[50] Lopes, D., Puga, H., Teixeira, J., Lima, R. Blood flow simulations in patient-specific geometries of the carotid artery: A systematic review, Journal of Biomechanics, Volume 111, 2020, 110019, ISSN 0021-9290.

[51] Medicana (n.d.). *Aort anevrizması nedir, belirtileri nelerdir?* Retrieved August 10, 2021 from https://www.medicana.com.tr/haber-detay/3016/aort-anevrizmasi-nedir-belirtileri-nelerdir

[52] Memorial Tıbbi Yayın Kurulu (2021, May 11). *Trans özofageal ekokardiyografi (TEE) nedir? Hangi hastalıklarda uygulanır?* Memorial. https://www.memorial.com.tr/tani-ve-testler/trans-ozofageal-ekokardiyografi-tee-nedir-hangi-hastaliklarda-uygulanir

[53] Mendez, V., Di Giuseppe, M., Pasta, S. Comparison of hemodynamic and structural indices of ascending thoracic aortic aneurysm as predicted by 2-way FSI, CFD rigid wall simulation and patient-specific displacement-based FEA. Comput Biol Med. 2018 Sep 1;100:221-229.

[54] Mojarab, A., Kamali, R., 2020. Design, optimization and numerical simulation of a MicroFlow sensor in the realistic model of human aorta. Flow Measurement and Instrumentation 74, 101791.

[55] Mousavi, S.J., Jayendiran, R., Farzaneh, S., Campisi, S., Viallon, M., Croisille, P., Avril, S. Coupling hemodynamics with mechanobiology in patient-specific computational models of ascending thoracic aortic aneurysms, Computer Methods and Programs in Biomedicine, Volume 205, 2021, 106107, ISSN 0169-2607.

[56] Nakamura, M., Wada, S., Yamaguchi, T., 2007. Computational Analysis of Blood Flow in an Integrated Model of the Left Ventricle and the Aorta.

[57] Neidlin, M., Corsini, C., Sonntag, S.J., Schulte-Eistrup, S., Schmitz-Rode, T., Steinseifer, U., Pennati, G., Kaufmann, T.A.S. Hemodynamic analysis of outflow grafting positions of a ventricular assist device using closed-loop multiscale CFD simulations: Preliminary results, Journal of Biomechanics, Volume 49, Issue 13, 2016, Pages 2718-2725, ISSN 0021-9290.

[58] Nowak, M., Melka, B., Rojczyk, M., Gracka, M., Nowak, A.J., Golda, A., Adamczyk, W.P., Isaac, B., Białecki, R.A., Ostrowski, Z., 2019. The protocol for using elastic wall model in modeling blood flow within human artery. European Journal of Mechanics / B Fluids 77, 273-280.

[59] Oechtering, T.H., Sieren, M.M., Hunold, P., Hennemuth, A., Huellebrand, M., Scharfschwerdt, M., Richardt, D., Sievers, H-H., Barkhausen, J., Frydrychowicz, A., 2016. Time-resolved 3-dimensional magnetic resonance phase contrast imaging (4D Flow MRI) reveals altered blood flow patterns in the ascending aorta of patients with valve-sparing aortic root replacement. J Thorac Cardiovasc Surg. 152, 418-427.

[60] Ong, C.W., Wee, I., Syn, N., Ng, S., Leo, H.L., Richards, A.M., Choong, A.M.T.L, 2020. Computational Fluid Dynamics Modelling of Hemodynamic Parameters in the Human Diseased Aorta – A Systematic Review. Annals of Vascular Surgery 63, 336-381.

[61] Opal Mühendislik (n.d.). *CFD analizi nedir?* Retrieved August 10, 2021 from https://www.opalmep.com/cfd-analizi-nedir/

[62] Özgün. (2021, April 4) *Global mesh control in ansys workbench.* Mechead. https://www.mechead.com/global-mesh-control-in-ansys-workbench/

[63] Paul-Ehrlich-Institut (n.d.). *Coronavirus and covid-19*. https://www.pei.de/EN/newsroom/dossier/coronavirus/coronavirus-content.html

[64] Perinajová, R., Juffermans, J.F., Westenberg J.J.M., Palen R.L.F.V.D., Boogaard, P.J.V.D., Lamb, H.J., Kenjereš, S, 2021. Geometrically induced wall shear stress variability in CFD-MRI coupled simulations of blood flow in the thoracic aortas. Comput Biol Med.

[65] PerklabResearch. (2017, December 26). Whole heart segmentation from cardiac CT in 10 minutes. https://www.youtube.com/watch?v=BJoIexIvtGo&t=757s

[66] Su, B., Zhang, J-M., Zou, H., Ghista, D., Le, T.T., Chin, C., 2020. Generating wall shear stress for coronary artery in real-time using neural networks. Feasibility and initial results based on idealized models. Computers in Biology and Medicine 126, 104038.

[67] Tawfik, A.M., Sobha, D.M., Gadelhaka, B., Sobhb, H.M., Batouty, N.M., 2019. The effect of age and gender on tortuosity of the descending thoracic Aorta. European Journal of Radiology 110, 54-59.

[68] This, A., Morales, H.G., Bonnefous, O., Fernández, M.A., Gerbeau, J.F. A pipeline for image based intracardiac CFD modeling and application to the evaluation of the PISA method, Computer Methods in Applied Mechanics and Engineering, Volume 358, 2020, 112627, ISSN 0045-7825.

[69] Tse, K.M., P., Lee, H.P., Ho, P., 2011. Investigation of hemodynamics in the development of dissecting aneurysm within patient-specific dissecting aneurismal aortas using computational fluid dynamics (CFD) simulations. Journal of Biomechanics 44, 827-836.

[70] Ucla Health (n.d.). *Types of imaging tests at the ucla aortic center*. Retrieved August 10, 2021 from https://www.uclahealth.org/heart/aortic/imaging

[71] White, F.M., 2010. Fluid Mechanics, fourth ed. McGraw- Hill, New York.

[72] Wu, Z., Yi, J., Guo, H.X.W., Wang, L., Chen, D., Xiong, J., 2017. The Significance of the Angle between Superior Mesenteric Artery and Aorta in Spontaneous Isolated Superior Mesenteric Artery Dissection. Annals of Vascular Surgery 45, 117-126.
[73] Zakaria, M.S., Ismail, F., Tamagawa, M., Aziz, A.F.A, Wiriadidjaja, S., Basri, A.A., Ahmad, K.A. A Cartesian non-boundary fitted grid method on complex geometries and its application to the blood flow in the aorta using OpenFOAM, Mathematics and Computers in Simulation, Volume 159, 2019, Pages 220-250, ISSN 0378-4754.
[74] Zhang, X., Luo, M., Fang, K., Li, J., Peng, Y., Zheng, L., Shu, C., 2020. Analysis of the formation mechanism and occurrence possibility of Post-Stenotic Dilatation of the aorta by CFD approach. Computer Methods and Programs in Biomedicine 194, 105520.
[75] Zhang, Y., Gao, B., Yu, C., 2016. The hemodynamic effects of the LVAD outflow cannula location on the thrombi distribution in the aorta. A primary numerical study. computer methods and programs in biomedicine, 133, 217–227.
[76] Zhuo, C., He, Y., GW26-e2137 Characterization of hemodynamics in Great Arteries of Wild-type Mouse using CFD based on Ultrasound Images, Journal of the American College of Cardiology, Volume 66, Issue 16, Supplement, 2015, Page C253, ISSN 0735-1097.
[77] Ziganshin, B.A., Rajbanshi, B.G., Tranquilli, M., Fang, H., Rizzo, J.A., Elefteriades, J.A. Straight deep hypothermic circulatory arrest for cerebral protection during aortic arch surgery: Safe and effective, The Journal of Thoracic and Cardiovascular Surgery, Volume 148, Issue 3, 2014, Pages 888-900, ISSN 0022-5223.

SBÜ ADANA ŞEHİR EĞİTİM VE ARAŞTIRMA HASTANESİ - SBÜ ADANA ŞEHİR EĞİTİM VE ARAŞTIRMA HASTANESİ
17/12/2021 18:04 - E-95134008 - 929 - 35904
00154760732

T.C.
ADANA VALİLİĞİ
İl Sağlık Müdürlüğü
Sağlık Bilimleri Üniversitesi Adana Şehir Eğitim ve Araştırma Hastanesi

Sayı : E-95134008-929
Konu : "845" Nolu Etik Kurul Kararına Yardımcı Araştırmacı Eklenmesi Talebi hk.

Doç.Dr. Naime Filiz ÖZDİL

İlgi : 17/12/2021 tarihli ve 48048 sayılı yazınız.

İlgi yazıda 06.05.2020 tarihli ve 845 karar numaralı "Farklı Geometrilerdeki Stenoz ve Anevrizmaların, Aort Atar Damar Disseksiyonu (Yırtılması) Oluşumuna Etkileri" başlıklı çalışmaya Onur Miran ÖZTEKİN isimli yardımcı araştırmacının katılması talebiniz 16.12.2021 Tarihli Etik Kurul Toplantısında görüşülmüş ve uygun bulunmuştur.

Bilgilerinize rica ederim.

Prof.Dr.Süleyman ÇETİNKÜNAR
Başhekim

Bilgi için: Ufuk KARAVELİOĞLU
SÜREKLİ İŞÇİ
Telefon No: (0 322) 455 90 00
Telefon: Faks No:
e-Posta: ufuk.karavelioglu@saglik.gov.tr İnternet Adresi:

T.C
ADANA VALİLİĞİ
İl Sağlık Müdürlüğü
Adana Şehir Eğitim ve Araştırma Hastanesi
Klinik Araştırmalar Etik Kurulu

Toplantı Sayısı: 56
Tarih: 06.05.2020
Karar No: 845

Adana Alparslan Türkeş Bilim ve Teknoloji Üniversitesi'nde **Doç.Dr. Naime Filiz ÖZDİL'in sorumlu araştırmacı**, Uzm.Dr. Tolga Onur BADAK, Öğr. Mehmet Emin TAŞKIRAN'ın yardımcı araştırmacı olarak yürütmesi öngörülen, **"Farklı Geometrilerdeki Stenoz ve Anevrizmaların, Aort Atar Damar Disseksiyonu (Yırtılması) Oluşumuna Etkileri"** başlıklı Retrospektif araştırma projesi, hastanemiz Klinik Araştırmalar Etik Kurulunda görüşüldü ve ilgili projenin etik açıdan bir sakınca içermediği tespit edildiğinden, projenin yapılmasının **UYGUN** olduğuna oybirliğiyle karar verildi. Çalışmanızın sonucu hakkında Etik Kurulumuzu bilgilendirmenizi rica ederiz.

BAŞKAN	**Doç.Dr. Ganiye Begül KÜPELİ** Çocuk Sağlığı ve Hastalıkları
BAŞKAN YARDIMCISI	**Doç.Dr. Banu KARA** Gastroenteroloji
DEĞERLENDİRİCİ ÜYE	**Doç.Dr. Talih ÖZDAŞ** Kulak Burun Boğaz Hastalıkları
ÜYELER	**Doç.Dr. Yarkın ÖZENLİ** Ruh Sağlığı ve Hastalıkları
	Doç.Dr. Sefa ARLIER Kadın Hastalıkları ve Doğum
	Uzm.Dr. Havva KUBAT Tıbbi Farmakolog
	Uzm.Dr. Saliha Dilek ÖZTOPRAK HACIOĞLU Halk Sağlığı
	Hande AYCAN TÜFEKCİ Biyomedikal Mühendis
	Tahsin ERKILINÇ AVUKAT
	Pelin DALKAVRIYAN Sivil